

**UNIVERSIDADE FEDERAL DE SÃO CARLOS**

CENTRO DE CIÊNCIAS EXATAS E DE TECNOLOGIA

PROGRAMA DE PÓS-GRADUAÇÃO EM CIÊNCIA DA COMPUTAÇÃO

**APRENDIZADO DE MÁQUINA APLICADO AO AUXÍLIO  
DO DIAGNÓSTICO DA DOENÇA DE PARKINSON**

**CLAYTON REGINALDO PEREIRA**

**ORIENTADOR: PROF. DR. JOÃO PAULO PAPA**

São Carlos – SP

Julho/2017

**UNIVERSIDADE FEDERAL DE SÃO CARLOS**

CENTRO DE CIÊNCIAS EXATAS E DE TECNOLOGIA

PROGRAMA DE PÓS-GRADUAÇÃO EM CIÊNCIA DA COMPUTAÇÃO

**APRENDIZADO DE MÁQUINA APLICADO AO AUXÍLIO  
DO DIAGNÓSTICO DA DOENÇA DE PARKINSON**

**CLAYTON REGINALDO PEREIRA**

Tese apresentada ao Programa de Pós-Graduação em  
Ciência da Computação da Universidade Federal de  
São Carlos, como parte dos requisitos para a obten-  
ção do título de Doutor em Ciência da Computação,  
área de concentração: Metodologias e Técnicas de  
Computação

Orientador: Prof. Dr. João Paulo Papa

São Carlos – SP

Julho/2017

# FOLHA DE APROVAÇÃO

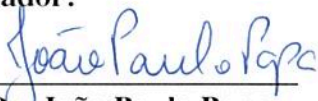
**CLAYTON REGINALDO PEREIRA**

## **APRENDIZADO DE MÁQUINA APLICADO AO AUXÍLIO DO DIAGNÓSTICO DA DOENÇA DE PARKINSON**

**Tese apresentada ao Programa de Pós-Graduação, para a obtenção do título de  
Doutor em Ciência da Computação, Área de concentração: Metodologias e  
Técnicas de Computação**

**Universidade Federal de São Carlos, São Carlos, 26 de Julho de 2017**

**Orientador:**



**Prof. Dr. João Paulo Papa**

**Universidade Estadual Paulista Júlio de Mesquita Filho – UNESP**

**Prof. Dr. João Paulo Papa**  
Departamento de Computação/FC  
Unesp/Bauru



# UNIVERSIDADE FEDERAL DE SÃO CARLOS

Centro de Ciências Exatas e de Tecnologia  
Programa de Pós-Graduação em Ciência da Computação

## Folha de Aprovação

Assinaturas dos membros da comissão examinadora que avaliou e aprovou a Defesa de Tese de Doutorado do candidato Clayton Reginaldo Pereira, realizada em 26/07/2017:

Prof. Dr. João Paulo Papa  
UFSCar

Prof. Dr. Ricardo Cerri  
UFSCar

Prof. Dr. Alexandre Luis Magalhães Levada  
UFSCar

Prof. Dr. Kelton Augusto Pontara da Costa  
Fatec

Profª. Dra. Silke Anna Theresa Weber  
FMP-UNESP

*Quero dedicar essa conquista primeiramente a DEUS e Nossa Senhora Aparecida, muito obrigado por me dar saúde por todo esse período. Dedicar à toda minha família, em especial, minha esposa Keila, meus filhos Lucas e Letícia por serem peças fundamentais neste processo, muito obrigado pela compreensão em minhas ausências e mau humor, não tenho dúvidas que sozinho, não conseguiria. Aos meus Pais, sempre presente acompanhando bem de perto cada etapa, enfim, meu amor e minha eterna gratidão a todos vocês, amo muito cada um!*

## AGRADECIMENTOS

Por fazer parte de uma equipe com pessoas maravilhosas, quero agradecer em geral ao Grupo **Recogna**<sup>1</sup>, cada componente pela ajuda e companheirismo ao longo desses anos, em especial, meus grandes amigos *Danilo Pereira* (o Cotô), *Luis Sugi* (o Luis Japa) e *Leandro Passos* (o Lélis), que não mediram esforços em momento algum no processo de desenvolvimento de nossos trabalhos (*e muitas vezes até financeiros!*), meu eterno agradecimento... MUITO OBRIGADO!

Agradecer a Universidade Federal de São Carlos - UFSCAR e seus professores pela qualidade de ensino, bem como, os auxílios a mim prestados durante meu Doutorado... MUITO OBRIGADO!

Minha família, diversas dificuldades desde minha faculdade, o mestrado, hoje ainda mais difícil, com 42 anos terminando o que até eu jamais imaginaria se quer começar, conseguir o que jamais imaginaria conseguir, um *Doutorado*. O que seria de mim sem vocês? Sem a compreensão de cada necessidade que tivemos em nossa casa durante todo esse período... Não existem palavras que possam agradecer tudo o que já tiveram que suportar por essa minha escolha Keila, Lucas e Letícia, poderia agora, escrever um livro contando cada situação que passamos, mas nesse momento só posso lhes dizer que essa conquista é NOSSA... MUITO OBRIGADO!

Meu Pai, minha mãe, meus irmãos, quanto apoio já me deram pra chegar até aqui, ainda tenho um longo caminho, em nome de Jesus, mas para chegar até aqui, vocês foram fundamentais, agradeço cada um de vocês... MUITO OBRIGADO!

De forma alguma poderia deixar de agradecer uma pessoa mais que especial, meu grande amigo... irmão... Pai e orientador *Professor Dr. João Paulo Papa*, não tenho palavras para descrever toda a gratidão e respeito que tenho por você, por acreditar em mim, por me ouvir, me ajudar da forma que sempre ajudou, sempre cobrando (cobrando forte heim! rs), delegando, discutindo técnicas e resultados, mas também, sempre apoiando, consolando, ajudando de ma-

---

<sup>1</sup><http://wwwp.fc.unesp.br/recogna/members.html>

neira impar meus problemas profissionais e pessoais, pessoa sempre presente nos momentos mais difíceis e que mais precisei. São muitos anos de companheirismo, pode ter total certeza João, está e sempre será para mim como um membro da minha família.... sempre presente em minhas orações... MUITO OBRIGADO MESMO!

## RESUMO

Atualmente, não é uma tarefa trivial apontar um exame que possa diagnosticar com precisão suficiente um paciente com mal de Parkinson, tendo como ponto importante também, após a constatação da enfermidade, a análise do nível da mesma. Especialistas recomendam a aplicação de diferentes tipos de exames, muitos deles baseados em sinais e imagens biomédicas, tais como eletroencefalograma, tomografia computadorizada e ressonância magnética para auxiliar no processo de detecção da doença, já que a faixa etária elevada e sintomas como cansaço e fraqueza podem ocultar o diagnóstico. Com o intuito de prover informações mais eficazes propiciando aos médicos um diagnóstico com maior confiança, metodologias para realizar a fusão entre diferentes modalidades de imagens tem se tornado cada vez mais populares e promissoras. Recentemente, a utilização de formulários contendo algumas atividades utilizando como ferramenta para o seu preenchimento uma caneta biométrica com multi-sensores tem sido aplicada para detecção do mal de Parkinson, efetuando o registro adquirido para análise da escrita. Entretanto, as informações oriundas da própria imagem digitalizada do formulário, bem como as mesmas obtidas pela caneta, ainda não foram utilizadas em conjunto para este fim. Desta forma, a presente proposta de tese de doutorado objetiva a utilização de técnicas de reconhecimento de padrões e processamento de imagens visando utilizar as diferentes informações provenientes do preenchimento do formulário em conjunto com dados provenientes da caneta, visando uma possível melhora no processo de auxílio ao diagnóstico médico do mal de Parkinson. Uma outra contribuição do trabalho é a criação de uma base de dados multimodal para o auxílio ao diagnóstico do mal de Parkinson.



## ABSTRACT

Currently, it is not a trivial task to point out a test that can diagnose accurately enough a patient with Parkinson's Disease, as well as it is quit difficult to assess the level of the disease. Experts recommend the application of different types of tests, many of them based on signs and biomedical imaging, such as electroencephalogram, computed tomography and magnetic resonance to aid the detection of the disease process, since as the age ranges, symptoms such as fatigue and weakness can hide diagnosis. In order to provide a more effective clinical information to doctors aiming at diagnosis with greater confidence, methodologies to perform the fusion of different imaging modalities have become increasingly popular and promising. Recently, the use of forms containing some activities using a biometric pen with multi-sensors have been applied for the detection of Parkinson's Disease by means of handwriting analysis. However, information derived from the scanned image of the form itself, and the one obtained by same pen have not been used together for this purpose. Thus, this proposal aims using pattern recognition techniques and image processing aimed at using the information from the form together with data from the pen. We believe a possible improvement in the medical diagnosis of Parkinson's Disease can be archived. Another contribution of this proposal, is the design of a multimodal database to aid in the diagnosis of Parkinson's Disease.

## LISTA DE FIGURAS

|     |   |    |
|-----|---|----|
| 2.1 | Handwriting exams filled out by a 56-years old PD patient. Extracted from (PEREIRA et al., 2015).   | 43 |
| 2.2 | Template used as an example by the PaHaw dataset. The image has been takes from the home-page of the dataset.   | 44 |
| 2.3 | Voice sample of a healthy individual (top), and the waveform of a voice sample belonging to a patient (down). Extracted from (SAKAR et al., 2013).            | 45 |
| 2.4 | A subject wearing the system used to design the CuPid dataset, with focus on the IMUs attached on the wrists. Extracted from (MAZILU; BLANKE; TRÖSTER, 2015). | 46 |
| 2.5 | Summarization of the works considered in this review.   | 47 |
| 3.1 | Handwriting exams: (a) filled out by a 56-years old PD patient, and (b) an empty exam with the templates.   | 53 |
| 3.2 | Image processing steps concerning ET extraction.  | 54 |
| 3.3 | Image processing steps concerning HT extraction.  | 55 |
| 3.4 | Spiral and meander images and their corresponding HT and ET extracted using the proposed methodology for a (a) spiral and a (b) meander.                      | 56 |
| 3.5 | Thinning of HT and ET using Zhang-Suen algorithm.   | 56 |
| 3.6 | Sampling process: (a) a certain region with discontinuities, and (b) the proposed fair sampling process.  | 57 |
| 3.7 | Some random points and the straight lines representing their connections with the spiral's and meander's center point.  | 58 |
| 3.8 | Spirals from control group (a)-(b), and from the patients group (c)-(d).  | 63 |
| 3.9 | Meanders from control group (a)-(b), and from the patients group (c)-(d).   | 63 |

|     |   |     |
|-----|---|-----|
| 4.1 | Form used to assess the handwritten skills of a given individual. . . . .   | 67  |
| 4.2 | Signals recorded by the pen from a control individual when drawing a spiral. . . . .  | 68  |
| 4.3 | Signals recorded by the pen from a PD patient when drawing a spiral. . . . .  | 69  |
| 4.4 | Meander samples from: (a) control and (b) PD patient, and their respective time series-based images in (c) and (d). . . . .   | 70  |
| 4.5 | Spiral samples from: (a) control and (b) PD patient, and their respective time series-based images in (c) and (d). . . . .  | 70  |
| 4.6 | Time series-based images pattern considering a patient (first and third row) and a healthy individual (second and fourth row): (a) "Exam 1" (circle in the paper), (b) "Exam 2" (circle in the air), (c) "Exam 3" (spiral), (d) "Exam 4" (meander), (e) "Exam 5" (diadochokinesis with the right hand) and (f) "Exam 6" (diadochokinesis with the left hand). . . . .   | 72  |
| 4.7 | Proposed combination approach to evaluate CNNs in the context of PD identification. . . . .   | 73  |
| 4.8 | Examples of meander (first and second row) and spiral (third and fourth row) images obtained by some patients in the early stages of the disease. . . . .   | 79  |
| 4.9 | Time series concerning the patient group: (a) Figure 4.8a, (b) Figure 4.8c, (c) Figure 4.8e, (d) Figure 4.8i, (e) Figure 4.8k, and (f) Figure 4.8m. . . . .   | 80  |
| 5.1 | Architecture of an $l^{\text{th}}$ -layered dOPF. . . . .   | 87  |
| 5.2 | Proposed approach based on BoW and dOPF for computer-aided PD diagnosis. The main workflow is indicated by the light blue arrows: local descriptors are extracted and clustered in order to build the dictionary. The dictionary is used for the quantization of both training and testing signals that is the process of computing the feature vectors (flow indicated by purple arrows). Similarly to the training phase, testing signals have their descriptors computed and the signals are quantized (flow indicated by yellow arrows). Finally, a classifier is fed by the resulting training and testing feature vectors. Notice the two depicted dictionaries are the same. . . . . | 88  |
| 5.3 | Biometric pen. Extracted from (PEREIRA et al., 2016b). . . . .  | 89  |
| 5.4 | Form used to assess the handwritten skills. Extracted from (PEREIRA et al., 2016b). . . . .   | 89  |
| 6.1 | Form used to assess the handwritten skills. Extracted from (PEREIRA et al., 2015). . . . .  | 100 |

|     |  |     |
|-----|--|-----|
| 6.2 | Evolution of the Mean-Squared Error considering: (a) Meander $64 \times 64$ , (b) Meander $128 \times 128$ , (c) Spiral $64 \times 64$ , and (d) Spiral $128 \times 128$ . . . . .     | 104 |
| 6.3 | An "RBM's mind": random weight matrices extracted from (a) Meander $64 \times 64$ , (b) Meander $128 \times 128$ , (c) Spiral $64 \times 64$ and (d) Spiral $128 \times 128$ . . . . . | 105 |

## LISTA DE TABELAS

|     |   |    |
|-----|---|----|
| 3.1 | Experimental results considering the spiral-based dataset. . . . .  | 60 |
| 3.2 | Experimental results considering the meander-based dataset. . . . .   | 60 |
| 3.3 | Average results considering the spiral-based dataset and a cross-validation with 20 runnings. . . . .   | 61 |
| 3.4 | Average results considering the meander-based dataset and a cross-validation with 20 runnings. . . . .  | 61 |
| 3.5 | Average results considering the combination process between spirals and meanders using the constrained 4-fold approach. . . . .                             | 62 |
| 4.1 | Average overall accuracy over the test set considering the six exams, different image resolutions and classification/feature extractor techniques . . . . . | 76 |
| 4.2 | Average class accuracy over the test set considering the six exams, different image resolutions and classification/feature extractor techniques . . . . .   | 77 |
| 4.3 | Average overall accuracy over the test set considering the combined-assessment approach. . . . .  | 78 |
| 4.4 | Average class accuracy over the test set considering the combined-assessment approach. . . . .  | 79 |
| 4.5 | Average accuracy over the early stage (selected) images. . . . .  | 81 |
| 5.1 | Number of descriptors extracted from the training set and number of words computed by each technique. . . . .   | 91 |
| 5.2 | Overall accuracies. . . . .   | 93 |
| 5.3 | Average accuracy rate for each class. . . . .   | 94 |
| 5.4 | Dictionary learning computational load [s] required by each technique. . . . .  | 95 |

|     |   |     |
|-----|---|-----|
| 6.1 | Mean accuracy results considering Meander $64 \times 64$ dataset. . . . .   | 102 |
| 6.2 | Mean accuracy results considering Meander $128 \times 128$ dataset. . . . . | 102 |
| 6.3 | Mean accuracy results considering Spiral $64 \times 64$ dataset. . . . .    | 103 |
| 6.4 | Mean accuracy results considering Spiral $128 \times 128$ dataset . . . . . | 103 |

# SUMÁRIO

|   |           |
|---|-----------|
| <b>CAPÍTULO 1 – INTRODUÇÃO</b>  | <b>17</b> |
| 1.1 Contextualização . . . . .  | 17        |
| 1.2 Objetivos . . . . .   | 21        |
| 1.3 Motivação . . . . .   | 21        |
| 1.4 Principais Contribuições . . . . .                                    | 22        |
| 1.5 Organização . . . . .   | 22        |
| <br>  |           |
| <b>CAPÍTULO 2 – REVISÃO BIBLIOGRÁFICA</b>                                 | <b>24</b> |
| 2.1 Introduction . . . . .  | 24        |
| 2.2 Enabling Technologies . . . . .                                       | 27        |
| 2.2.1 Machine Learning . . . . .  | 27        |
| 2.2.2 Image Analysis . . . . .  | 30        |
| 2.2.3 Signal Analysis . . . . .   | 32        |
| 2.2.4 Smartphone Devices . . . . .  | 36        |
| 2.2.5 Virtual and Augmented Reality . . . . .                             | 37        |
| 2.2.6 Sensors . . . . .   | 38        |
| 2.2.7 Web Applications . . . . .  | 41        |
| 2.3 Dataset description . . . . .   | 42        |
| 2.3.1 HandPD Dataset . . . . .  | 42        |
| 2.3.2 Parkinson’s Progression Markers Initiative Dataset - PPMI . . . . . | 43        |

|       |  |    |
|-------|--|----|
| 2.3.3 | Parkinsonian Disease Handwriting Dataset - PaHaw . . . . . | 44 |
| 2.3.4 | Parkinson Speech Dataset . . . . .                         | 45 |
| 2.3.5 | CuPiD Dataset . . . . .                                    | 45 |
| 2.4   | Discussion . . . . .                                       | 46 |
| 2.5   | Conclusions . . . . .                                      | 48 |

**CAPÍTULO 3 – UMA NOVA ABORDAGEM BASEADA EM VISÃO COMPUTACIONAL APLICADA NO DIAGNÓSTICO DO MAL DE PARKINSON 49**

|       |  |    |
|-------|--|----|
| 3.1   | Introduction . . . . .                               | 49 |
| 3.2   | HandPD Dataset . . . . .                             | 52 |
| 3.3   | Feature Extraction from Visual Description . . . . . | 53 |
| 3.3.1 | Handwritten Trace and Exam Template . . . . .        | 54 |
| 3.3.2 | Feature extraction . . . . .                         | 56 |
| 3.4   | Experiments and Results . . . . .                    | 59 |
| 3.4.1 | Experiment 1 . . . . .                               | 59 |
| 3.4.2 | Experiment 2 . . . . .                               | 60 |
| 3.4.3 | Experiment 3 . . . . .                               | 61 |
| 3.4.4 | Discussion . . . . .                                 | 62 |
| 3.5   | Conclusion . . . . .                                 | 63 |

**CAPÍTULO 4 – AUXÍLIO AO DIAGNÓSTICO DA DOENÇA DE PARKINSON UTILIZANDO DINÂMICA DE ESCRITA E APRENDIZADO EM PROFUNDIDADE 64**

|       |  |    |
|-------|--|----|
| 4.1   | Introduction . . . . .                                     | 64 |
| 4.2   | Methodology . . . . .                                      | 66 |
| 4.2.1 | HandPD Dataset . . . . .                                   | 66 |
| 4.2.2 | Modeling Time Series in CNNs . . . . .                     | 69 |
| 4.2.3 | Assessment Through Convolutional Neural Networks . . . . . | 71 |
| 4.3   | Experiments . . . . .                                      | 72 |



|       |                                 |    |
|-------|---------------------------------|----|
| 4.3.1 | Experimental Setup . . . . .    | 72 |
| 4.3.2 | Single-Assessment . . . . .     | 75 |
| 4.3.3 | Combined-Assessment . . . . .   | 77 |
| 4.3.4 | Early Stage Detection . . . . . | 78 |
| 4.4   | Conclusions . . . . .           | 81 |

**CAPÍTULO 5 – AUXÍLIO AO DIAGNÓSTICO DA DOENÇA DE PARKINSON UTILIZANDO DINÂMICA DE ESCRITA E APRENDIZADO EM PROFUNDIDADE 83**

|       |   |    |
|-------|---|----|
| 5.1   | Introduction . . . . .                          | 83 |
| 5.2   | Optimum-Path Forest Clustering . . . . .        | 85 |
| 5.2.1 | Deep-Hierarchical Optimum-Path Forest . . . . . | 86 |
| 5.3   | Proposed Approach . . . . .                     | 88 |
|       | Data acquisition . . . . .                      | 88 |
|       | Local descriptor extraction . . . . .           | 90 |
|       | Dictionary formulation . . . . .                | 90 |
|       | The new representation . . . . .                | 90 |
| 5.4   | Experiments and Results . . . . .               | 90 |
| 5.5   | Conclusions . . . . .                           | 92 |

**CAPÍTULO 6 – IDENTIFICAÇÃO DA DOENÇA DE PARKINSON USANDO MÁQUINAS RESTRITAS DE BOLTZMANN 96**

|       |   |     |
|-------|---|-----|
| 6.1   | Introduction . . . . .                  | 96  |
| 6.2   | Restricted Boltzmann Machines . . . . . | 98  |
| 6.3   | Methodology . . . . .                   | 100 |
| 6.3.1 | Dataset . . . . .                       | 100 |
| 6.3.2 | Experimental Setup . . . . .            | 101 |
| 6.4   | Experiments . . . . .                   | 101 |
| 6.5   | Conclusions . . . . .                   | 104 |

|                                      |            |
|--------------------------------------|------------|
| <b>CAPÍTULO 7 – CONCLUSÃO</b>        | <b>106</b> |
| 7.1 Trabalhos Publicados . . . . .   | 107        |
| 7.2 Trabalhos em Avaliação . . . . . | 108        |
| <b>REFERÊNCIAS</b>                   | <b>109</b> |

# Capítulo 1

## INTRODUÇÃO

---

---

Este capítulo discorre sobre o contexto do trabalho, seus objetivos, motivação, e as principais contribuições, bem como sua organização geral.

### 1.1 Contextualização

Descrita pela primeira vez pelo médico inglês James Parkinson (PARKINSON, 1817a) e classificada como uma doença degenerativa, crônica e progressiva, a doença de Parkinson (ou mal de Parkinson, do inglês *Parkinson's Disease* - PD) é uma enfermidade neurológica, que afeta os movimentos da pessoa, causando tremores, lentidão de movimentos, rigidez muscular e desequilíbrio, além de alterações na fala e escrita (BURKE, 2010a).

Em nosso cérebro, existe uma área do sistema nervoso central conhecida como substância negra, a qual produz um neurotransmissor conhecido por dopamina (NAVAILLES et al., 2013), que é responsável pelo controle dos movimentos musculares. O mal de Parkinson ocorre quando as células nervosas que produzem a dopamina são destruídas, processo este que é realizado lentamente, caracterizando a progressividade dessa enfermidade. Com a ausência de tal substância, as células nervosas não podem mais enviar mensagens corretamente, ocasionando diversos outros sintomas, tais como depressão, alterações do sono, diminuição da memória e distúrbios do sistema nervoso autônomo.

No Brasil, uma a cada quinhentas pessoas desenvolve o quadro da doença, estimando-se um total de 200 mil pessoas acometidas pelo mal de Parkinson (CORREA, 2016), sendo que uma a cada cem das pessoas portadoras dessa enfermidade possuem mais de 60 anos de idade. Ela afeta tanto homens quanto mulheres, não é uma doença fatal e tampouco contagiosa, sendo que em alguns casos o mal de Parkinson deve-se a causas hereditárias (BURKE, 2010a).

Recentemente, pesquisas voltadas a encontrar possíveis causas para o surgimento da doença, que ainda continua incurável e progressiva (variável em cada paciente), apontam para a relação da presença de alumínio na água ingerida com o aumento do processo de inflamação dos neurônios, o qual está diretamente associado ao mal de Parkinson (BONDY, 2010). Contudo, o estudo não chega a realizar relações de causa e efeito, porém evidencia que o alumínio pode causar danos aos neurônios. Pesquisadores afirmam que a doença de Parkinson afeta hoje aproximadamente 5 milhões de pessoas em todo o mundo, é um mal complexo e heterogêneo que, em 2030, deverá atingir até 10 milhões de indivíduos. Como ainda o diagnóstico depende dos sintomas para detectar tal doença, geralmente, no momento da avaliação médica, o paciente já perdeu cerca de 70% dos neurônios dopaminérgicos.

Com o rápido desenvolvimento da tecnologia e o avanço de modernas instrumentações, técnicas baseadas em aprendizado de máquina e processamento de imagens tornaram-se um componente vital para um grande número de aplicações médicas. Diversas são as técnicas de análise e processamento de imagens voltadas à Medicina, tais como a termografia por imagem infravermelha (*Infra-Red - IR*), que é utilizada para diagnósticos não invasivos permitindo a avaliação e quantificação de variações de temperatura na superfície da pele. Já a ressonância magnética (*Magnetic Resonance Imaging - MRI*), que também consiste em um exame para diagnóstico por imagem, retrata imagens de alta definição dos órgãos através da utilização do campo magnético dos mesmos. Finalmente, tem-se a tomografia computadorizada (*Computerized Tomography - CT*), a qual utiliza radiação ionizante (raios-X) e produz imagens que representam sessões ou “fatias” do corpo (PIELLA, 2003; ZHU; COCHOFF, 2006).

Apesar de contribuírem com informações significativas para auxiliar o diagnóstico, imagens médicas multimodalidades (imagens oriundas de diferentes técnicas) costumam fornecer informações complementares e, ocasionalmente, conflitantes. Tome o seguinte exemplo: a imagem CT pode evidenciar estruturas densas como ossos e implantes com menos distorção, mas não pode detectar alterações fisiológicas, já MRI, fornece informações de tecidos não rígidos (normais e patológicos), mas não podem detectar a informação proveniente dos ossos. Assim sendo, um tipo de imagem pode não ser suficiente para fornecer os requisitos clínicos necessários para uma boa avaliação médica.

Com o intuito de prover informações clínicas mais eficazes e, conseqüentemente, propiciar aos médicos diagnósticos de maior confiança, metodologias para realizar a fusão entre diferentes modalidades de imagens tem se tornado cada vez mais populares e promissoras (ROSS; JAIN, 2003). Barra et al. (BARRA; BOIRE, 2001), por exemplo, apresentam a fusão de imagens anatômicas e funcionais do cérebro visando o estudo do mal de Alzheimer e Epilepsia. Já Olszewski

et al. (OLSZEWSKI et al., 2000) propuseram a fusão de imagens de raios-X de angiografia com imagens de ultra-som intra-vasculares para aplicação de cateteres. Sanches et al. (SANCHES et al., 2013) aplicaram modelos de imagens tridimensionais combinando informações anatômicas e funcionais com o intuito de detectar variações de temperatura na superfície do corpo, dado que essa informação é bastante utilizada na tomada de decisão em diagnósticos médicos.

Recentemente, um avanço entre as tecnologias CT e tomografia por emissão de pósitrons (*Positron Emission Tomographs* - PET) tem possibilitado a fusão das imagens anatômicas geradas através da CT às imagens metabólicas do tipo PET. Neste sentido, tem-se a associação da alta sensibilidade metabólica e resolução de imagens PET à uma correlação anatômica até então inconcebível, possibilitando, assim, a detecção precoce e a localização precisa de uma lesão cancerígena (CAMARGO, 2005). Já o laboratório UCLA<sup>1</sup> Health (COHEN; GLASPY; PALMER, 2013), uma empresa voltada ao uso dos avanços tecnológicos na saúde, introduziu aperfeiçoamentos à biopsia de próstata, melhorando consideravelmente a capacidade de distinguir os homens que devem ter tratamento daqueles que poderiam adiá-lo. Tal avanço pôde ser obtido por meio da fusão de imagens tridimensionais derivadas da técnica MRI, permitindo, assim, uma rápida intervenção de forma apropriada.

No contexto da doença de Parkinson, trabalhos voltados a auxiliar o seu diagnóstico tem apresentado cada vez mais resultados positivos. Spadoto (SPADOTTO et al., 2010b, 2011) propuseram uma aplicação baseada em técnicas evolutivas buscando maximizar a precisão e taxa de acerto no diagnóstico dessa enfermidade por meio do classificador Floresta de Caminhos Ótimos (*Optimum-Path Forest* - OPF) (PAPA; FALCÃO; SUZUKI, 2009; PAPA et al., 2012). Gharehchopogh et al. (GHAREHCHOPOGH; MOHAMMADI, 2013a) utilizaram redes neurais artificiais (*Artificial Neural Networks* - ANNs) com perceptron multicamadas (*Multi-Layer Perceptron* - MLP) para diagnosticar os efeitos causados pelo mal de Parkinson. Já Panet et al. (PAN et al., 2012a) analisaram o desempenho de máquinas de vetores de suporte (*Support Vector Machines* - SVMs), ANN-MLP e redes neurais de função de base radial para comparar o início do tremor em pacientes com mal de Parkinson. Estudos realizados por Watters et al. (WATTERS; PATEL, 1999) por meio de ANNs evidenciaram a degradação das vias dopaminérgicas do cérebro, indicando que o sistema semântico é o que sofre o maior prejuízo, ocasionando, assim, respostas mais lentas com uma quantidade maior de erros em tarefas de avaliação semântica em um paciente com mal de Parkinson.

Haller et al. (HALLER et al., 2012) propuseram um sistema de auxílio ao diagnóstico do mal de Parkinson utilizando SVM e imagens de ressonância magnética por difusão. Esse tipo de

---

<sup>1</sup>UCLA - University of California at Los Angeles

imagem pode fornecer informações importantes sobre o processo de conexão entre diferentes regiões do cérebro. O trabalho em questão partiu do pressuposto de que pacientes com PD possuem regiões do cérebro que são afetadas e, conseqüentemente, podem ser identificadas visualmente. Já Gadav et al. (YADAV; KUMAR; SAHOO, 2011) apresentaram um modelo para identificação de pessoas com PD por meio de sinais da fala, dado que o trato vocal também é atingido por essa doença. Na ocasião, os pesquisadores também fizeram uso do classificador SVM. Vários outros trabalhos objetivaram a detecção do mal de Parkinson utilizando redes neurais, tais como Wu et al. (WU et al., 2010), os quais aplicaram redes neurais com função de base radial na identificação de tremores, e Manap et al. (MANAP; TAHIR; YASSIN, 2011) que utilizaram redes neurais para identificação de padrões no modo de andar de pessoas saudáveis e pacientes com PD.

Pesquisas realizadas pelo Prof. Dr. Christian Hook (PEUEKER; SCHARFENBERG; HOOK, 2011) (Departamento de Matemática, Faculdade de Ciências de Regensburg - Alemanha) e sua equipe resultaram no projeto de uma caneta biométrica inteligente<sup>2</sup> visando a identificação de pessoas por meio de sua assinatura. Tal dispositivo registra as sutilezas com que um indivíduo realiza a tarefa de escrita, sendo que a análise computacional desses dados define uma informação única para cada pessoa. Essa característica somente é possível por meio de seus sensores, os quais detectam a pressão com a qual uma pessoa segura a caneta, bem como sua inclinação e possíveis tremores durante o processo de escrita. Posteriormente, os pesquisadores envolvidos notaram que essa caneta poderia auxiliar no diagnóstico do mal de Parkinson devido às informações extraídas por meio de seus sensores.

Esta constatação deu início a um projeto de pesquisa coordenado pela professora e pesquisadora Dra. Silke Anna Theresa Weber, médica otorrinolaringologista da Faculdade de Medicina de Botucatu (FMB) da Universidade Estadual Paulista “Júlio de Mesquita Filho”, o qual objetivou a viabilidade da utilização da caneta em diagnósticos do mal de Parkinson, dado que tais diagnósticos hoje em dia são realizados por meio de preenchimento de formulários pelos pacientes. Neste caso, é requisitado aos mesmos que executem algumas operações neste formulário (contornar algumas figuras, por exemplo), o qual será processado posteriormente no intuito de revelar o nível da doença (EICHHORN et al., 1996a; ÜNLÜ; BRAUSE; KRAKOW, 2006).

A análise desses formulários é ainda amplamente utilizada por médicos e pesquisadores para um diagnóstico precoce do mal de Parkinson. Muito embora essa metodologia seja bastante eficaz, a mesma é dependente da interpretação de cada profissional, bem como o grande número de exames a serem analisados podem levar a diagnósticos cada vez menos precisos,

---

<sup>2</sup>Biometric Smart Pen - BiSP®

principalmente, devido à fadiga causada pelo excesso de trabalho.

Apesar desses formulários serem ainda muito utilizados no processo de detecção do mal de Parkinson, não se tem evidências sobre a fusão das informações oriundas do formulário (informações visuais) com as provenientes da caneta. Alguns poucos trabalhos apresentam a fusão de informações recebidas por diferentes sensores espalhados pelo corpo no contexto deste trabalho. Bahrepour et al. (BAHREPOUR et al., 2011), por exemplo, utilizam sensores sem fio anexados ao corpo do paciente com o intuito de monitorar, física e psicologicamente, suas condições, enviando, assim, os sinais a um receptor encarregado pelo processo de fusão dos dados dos sensores visando o diagnóstico do mal de Parkinson. Long et al. (LONG et al., 2012) propuseram um sistema para auxiliar o processo de identificação de pacientes com PD por meio de imagens obtidas por duas diferentes fontes: imagens de ressonância magnética funcionais por estado de descanso (*Resting state functional MRI - rsfMRI*) em conjunto com imagens MRI convencionais. O processo de classificação foi realizado por meio da técnica SVM.

## 1.2 Objetivos

Diversas são as técnicas utilizadas na área médica que visam encontrar um diagnóstico preciso que possa, trazer benefícios ao paciente, ou até mesmo a cura de sua enfermidade. Após um estudo detalhado sobre a doença de Parkinson e, através dos resultados obtidos por diversas publicações, a seguinte tese apresenta uma nova proposta baseada em análise de resultados obtidos através do uso de processamento de imagens e sinais, tendo para tal, dois principais objetivos: (i) a extração de informações baseada em características obtidas através do preenchimento de formulários desenvolvidos especialmente para a análise de pacientes com mal de Parkinson, (ii) a criação de uma base de dados de imagens e sinais obtidos através de uma caneta inteligente, sobre a qual serão aplicadas técnicas de aprendizado de máquina com o intuito de analisar as informações extraídas auxiliando, assim, no processo de decisão levando a um possível diagnóstico mais preciso da doença.

## 1.3 Motivação

Embora a motivação principal dessa pesquisa tivesse seu foco voltado à análise das informações obtidas através das extrações de características realizadas nas imagens, bem como os sinais obtidos com a caneta visando um melhor resultado para o diagnóstico do mal de Parkinson, outra contribuição de grande importância para a comunidade científica será o desenvolvimento de

uma nova base de dados de imagens e seus respectivos sinais (estes obtidos através da caneta), **estando a mesma já disponível para a comunidade científica.**

Dado o contexto apresentado, a presente tese foi motivada em prover um método automático baseado na utilização de técnicas de reconhecimento de padrões e processamento de imagens, visando extrair informações visuais através de formulários utilizados para o diagnóstico do mal de Parkinson. Foram também utilizadas técnicas de mineração de dados para esse processo, bem como o emprego da metodologia de processamento de sinais utilizando informações provenientes de uma “caneta inteligente”<sup>3</sup>.

## 1.4 Principais Contribuições

Geralmente uma pesquisa é dividida em três etapas, sendo: (i) fundamentação da proposta (revisão da literatura), (ii) desenvolvimento, e por fim, (iii) validação, podendo estas serem conduzidas paralelamente. Para essa tese, na etapa (i) que compreende o Capítulo 2, foi efetuado um levantamento minucioso entre as técnicas adotadas no processo de diagnóstico do mal de Parkinson, onde uma revisão bibliográfica abordou a utilização de diversas técnicas, tanto na área médica quanto na área tecnológica, trazendo os principais trabalhos e abordagens aplicados na atualidade, bem como os resultados obtidos por meio deles.

Já na etapa (ii), contida na seção 3.2 do Capítulo 3, foi realizado o processo de coleta de dados em conjunto com as pessoas portadoras da doença, bem como indivíduos saudáveis, sendo essa coleta realizada diversas vezes com o intuito de obter uma maior robustez na qualidade dos dados, o que nos motivou através das características adquiridas com essa coleta, disponibilizar dois formatos de base de dados para trabalhos futuros. Por fim, na etapa (iii) é apresentado ao final de todos os Capítulos dessa tese, os resultados obtidos durante o processo de experimentos realizados por meio das bases de dados desenvolvidas.

## 1.5 Organização

Esta tese de doutorado está organizada em sete capítulos. Neste capítulo apresentamos o contexto no qual a proposta da pesquisa está inserida, bem como sua motivação e as principais contribuições para o tema abordado. No Capítulo 2, é apresentada uma revisão bibliográfica dos temas que estão relacionados à esta pesquisa, bem como as técnicas utilizadas e seus resultados. Já no Capítulo 3, é apresentada a metodologia utilizada para aquisição dos dados, as

---

<sup>3</sup>(*Biometric Smart Pen - BiSP*<sup>®</sup>)



---

técnicas aplicadas e os resultados obtidos com os experimentos realizados no processamento das imagens. No Capítulo 4 é realizado um diagnóstico por meio da dinâmica de escrita, e o Capítulo ?? apresenta um trabalho semelhante ao apresentado no capítulo anterior, porém, aplicado agora em sinais e não mais em imagens. No Capítulo 6 são apresentados os resultados da técnica de Máquinas Restritas de Boltzmann aplicadas em imagens para auxiliar no diagnóstico do Mal de Parkinson. Finalmente, no Capítulo 7 são apresentadas as conclusões e limitações de pesquisa, assim como as lições aprendidas e oportunidades futuras. Também neste Capítulo, são apresentados os trabalhos aceitos para publicação na Seção 7.1, bem como, trabalhos que se encontram no processo de avaliação na Seção 7.2.

# Capítulo 2

## REVISÃO BIBLIOGRÁFICA

---

---

Este capítulo apresenta uma coletânea de artigos voltados ao assunto abordado nesta tese. O mesmo foi realizado visando apenas trabalhos recentes (publicados em 2015 e 2016), e teve sua submissão realizada para a revista *Artificial Intelligence in Medicine* - (AIIM) <sup>1</sup>, onde encontra-se no aguardo dos pareceres de seus revisores.

### 2.1 Introduction

Parkinson's Disease, firstly described by the English and physician James Parkinson (PARKINSON, 1817b) in 1817, is a chronic, progressive and neuron-degenerative illness that affects people worldwide. Although there is a number of possible symptoms, PD is often related to progressive bradykinesia, i.e. the slowness of movement, as well as tremors and muscle stiffness, which can worsen over time. Also, PD patients usually feature changes in speech and writing skills (BURKE, 2010b).

Currently, approximately 60,000 Americans are diagnosed with PD (FOUNDATION, ). However, such statistics may be underestimated, since thousands of potential individuals remain uncovered by exams or any sort of clinical diagnosis. As a matter of fact, around 7 to 10 million people might be living with PD nowadays, which turns out to be a problem of public health that deserves a considerable attention.

The main cause of Parkinson's Disease is related to the degeneration of a small part of the brain, the so-called *substantia nigra*. As soon as the cells from this region start to die, the brain becomes deprived of a chemical substance known as *dopamine*, which allows the brain cells to get involved in the control of movement. Therefore, the lower the levels of dopamine, the

---

<sup>1</sup><https://www.journals.elsevier.com/artificial-intelligence-in-medicine>

higher the probability of being affected by Parkinson's Disease (BURKE, 2010b). As such, with the absence of such substance, the brain cells can no longer send messages properly, causing depression, sleep disturbances, memory impairment and disorders related to the autonomic nervous system. Additionally, PD also may be triggered by hereditary causes (BURKE, 2010b). Since it has no cure, several chemical methods have been used to treat Parkinson's Disease in its early stages, being the *Levodopa* (L-dopa) one of the most widely used for such purpose.

In order to better manage such disease and to increase the life quality of PD patients, a bundle of researchers from different areas have worked together. As such, the literature is rich in a number of different works, that range from chemical- and behavioral-driven studies to computer-assisted diagnosis. The main contribution of this work relies on the latter approaches, which make use of computer tools to help researchers when handling the diagnosis of Parkinson's Disease in a faster and more effective way. In this survey, we tried to compile the most prominent works related to computer methods to automatic identify PD, as well as to help its diagnosis.

In order to give you a taste of what is going on concerning this research field, most works make use of artificial intelligence (i.e. machine learning) to learn the most important features that can be considered when diagnosing some individual. Spadotto et al. (SPADOTTO et al., 2010b), for instance, introduced the Optimum-Path Forest (OPF) (PAPA; FALCÃO; SUZUKI, 2009; PAPA et al., 2012) classifier to aid the automatic identification of Parkinson's Disease, and later on the same group of authors proposed an evolutionary-based approach to select the most discriminative set of features that help improving PD recognition rates (SPADOTTO et al., 2011). The OPF classifier seemed to be a suitable tool, since it is parameterless and easy-to-manage.

Pan et al. (PAN et al., 2012b) analyzed the performance of Support Vector Machines with Radial Basis Function (SVM-RBF) in order to compare the onset of tremor in patients with Parkinson's disease. Gharehchopogh et al. (GHAREHCHOPOGH; MOHAMMADI, 2013b) used Artificial Neural Networks with Multi-Layer Perceptron to diagnose the effects caused by Parkinson's disease. One year later, Hariharan et al. (HARIHARAN; POLAT; SINDHU, 2014) developed a new feature weighting method using Gaussian Mixture Models to enrich the discriminative ability of some dysphonia-based features, thus achieving 100% of classification accuracy. Peker et al. (PEKER; SEN; DELEN, 2015) used sound-based features and complex-valued neural networks to aid PD diagnosis as well.

As one can observe, most works that address PD automatic recognition cope with voice-based data. Procedures to identify voiced and unvoiced (silent) periods have been actively pursued to analyze continuous speech samples, since most techniques that quantify periodicity

and regularity in voice signals are applied in the voiced regions only (SHAHBAKHI; FAR; TAHAMI, 2014). Das (DAS, 2010) presented a comparison of multiple classification methods for the diagnosis of PD, among them Neural Networks, and Regression and Decision Trees. Several evaluation methods were employed to calculate the performance of that classifiers, being the experiments conducted in a dataset composed of a range of biomedical voice measurements from 31 people, in which 23 diagnosed with Parkinson's disease. The best results were obtained by Neural Networks (around 92.9% of PD recognition rate). In 2014, Weber et al. (WEBER et al., 2014) used a biometric pen together with SVMs to learn handwritten dynamics from PD patients.

Although they are outnumbered when compared to signal-driven applications, image processing-based approaches have been used to detect Parkinson's Disease either. Recently, Pereira et al. (PEREIRA et al., 2015) proposed to extract features from writing exams using visual features learned from drawings the patients were asked to do. The authors also designed and made available a dataset called "HandPD" with all images and features extracted from the handwriting exams<sup>2</sup>.

In regard to enabling technologies to aid patients with PD, we have compiled eight reviews. Bhande and Raut (BIND; TIWARI; SAHANI, 2013), in 2013, presented a brief analysis to illustrate the merits of a number of available research techniques based on neural networks. More recently, in 2015, Oung et al. (OUNG et al., 2015) carried out a review on technologies for the assessment of motor disorders in PD, considering, for example, wearable, audio, and multimodal sensors. In the same year, Bind et al. (BIND; TIWARI; SAHANI, 2015) presented a comprehensive review concerning the prediction of Parkinson's Disease by means of machine learning techniques.

Pasluosta et al. (PASLUOSTA et al., 2015) focused on PD as a representative disease model by evaluating the Internet-of-Things (IoT) platform in the context of healthcare. The authors considered the potential of combining wearable technology with the IoT in the healthcare scenario, as well as the engagement of patients in the assessment of symptoms, diagnosis, and consecutive treatment options. Zhao et al. (ZHAO et al., 2015) also analyzed E-health support in PD, but now with smart glasses.

Harris et al. (HARRIS et al., 2015) carried out a review about the so-called *exergaming* (i.e. the combination of exercising with games) as a viable therapeutic tool to improve static and dynamic balance. Stamford et al. (STAMFORD; SCHMIDT; FRIEDL, 2015), in 2015, assessed the use of different engineering technologies in the context of PD diagnosis. Ekker et al. (EKKER et

---

<sup>2</sup><http://www.fc.unesp.br/~papa/pub/datasets/Handpd/>

al., 2016) conducted a study about visual rehabilitation by means of wearable devices, making use of the telemedicine for neurorehabilitation in PD-affected patients.

As aforementioned, we aim at putting together a number of works that attempt to handle the problem of automatic PD diagnosis, since the literature lacks on a more recent compilation of related works. We present an extensive comparison about different methodologies to deal with Parkinson's Disease using machine learning techniques. The remainder of this paper is organized as follows. Chapter 2.2 presents the methodology employed to conduct this review, as well as the different techniques used in the papers referred in this work. Chapter 2.3 presents several datasets employed in some related works, and Chapter 2.4 discusses the research that have been conducted to cope with PD. Finally, Chapter 2.5 states conclusions and future tendencies.

## **2.2 Enabling Technologies**

In order to select works within the scope addressed in this systematic review, a relevant search in Science Direct, IEEEExplore, PubMed, Plos One, Multidisciplinary Digital Publishing Institute (MDPI), Association for Computing Machinery (ACM), Springer and Hindawi Publishing Corporation databases was carried out. To this end, only two key words were considered for searching purposes: (i) "Parkinson's Disease" and (ii) "Parkinsonian". The main idea is to make the selection of works fairly tiresome, but quite able to cover a total of 84 recent works published in between 2015 (76 works) and early 2016 (8 works). Some works published in 2014 and earlier were briefly discussed in the previous section.

The next sections describe in deeper details the works divided by their main application domain, i.e. web application, sensors, virtual and augmented reality, smartphone devices, signals analysis, image processing and machine learning.

### **2.2.1 Machine Learning**

Machine Learning is a branch of computational intelligence dedicated to the development of algorithms that enable a computer program to improve its performance based on prior (learned) information. Since the very beginning of "Perceptron", new mathematical modelings of the working mechanism of the brain have been pursued daily. Such intense research has motivated a number of works that aimed at using machine learning-oriented techniques to aid Parkinson's Disease recognition.

Drotár et al. (DROTAR et al., 2015), for instance, proposed to study some features based on

entropy, energy and intrinsic measures of the handwriting skills of an individual. The authors also considered applying such measures to in-air movements and pressure to exploit the full potential of the handwriting for the classification of PD over the “Parkinsonian Handwriting” (PaHaw) database. SVM-RBF kernel was used for classification purposes, achieving around 90% of prediction performance. Connolly et al. (CONNOLLY et al., 2015) applied Support Vector Machines upon local field potentials sensed from an implanted deep brain stimulation device. For such analysis, 83 montages were recorded from 15 patients suffering from advanced idiopathic PD, thus obtaining an accuracy rate of 91%.

Wahid et al. (WAHID et al., 2015) presented a study with two main contributions: firstly, they used a multiple regression normalization strategy to identify differences in spatial-temporal gait features between PD patients and control (healthy) individuals. Secondly, they evaluated the effectiveness of machine learning strategies in classifying PD gait after multiple regression normalization. The authors argued the study has important implications for the analysis of spatial-temporal gait data concerning the diagnosis of PD, as well as the evaluation of its severity.

Smith et al. (SMITH et al., 2015) employed evolutionary algorithms to provide clinically relevant and objective measures to identify PD both in humans and animal models. Their work used Cartesian Genetic Programming, thus showing such technique can be successfully applied to the assessment of movements in humans when distinguishing PD patients from healthy controls, as well as to classify severity of dyskinesia in patients. Hirschauer et al. (HIRSCHAUER; ADELI; BUFORD, 2015) presented a comprehensive model for the diagnosis of PD based on motor, non-motor, and neuroimaging features using Enhanced Probabilistic Neural Networks (AHMADLOU; ADELI, 2010), a machine learning technique that make use of local decision circles surrounding training samples to control the spread of the Gaussian kernel. Using the Parkinson’s Progression Markers Initiative (PPMI)<sup>3</sup> dataset, the proposed approach obtained an accuracy of 98.6% when classifying healthy people from PD patients, and 92.5% of recognition rate when dealing with data of six clinical exams and functional neuroimaging data for two regions of interest of the brain.

Segovia et al. (SEGOVIA et al., 2015) demonstrated a new method based on SVMs and Bayesian networks to separate idiopathic Parkinson’s Disease from atypical parkinsonian syndromes. Their methodology achieved an accuracy rate over 78%, a reasonable result between sensitivity and specificity, suggesting the proposed method is suitable to assist the diagnosis of PD. Cook et al. (COOK; SCHMITTER-EDGECOMBE; DAWADI, 2015) proposed to employ a com-

---

<sup>3</sup><http://www.ppmi-info.org/access-data-specimens/download-data/>

combination between smart home and machine learning technologies to observe and quantify the behavioural changes of PD patients. The main focus is to aid the clinical assessment and a better understanding of the differences between healthy older adults (HOA) and older adults with cognitive and physical impairments, also classified by the authors as mild cognitive impairment (MCI). The results indicated that smart homes, wearable devices and ubiquitous computing technologies can be useful for monitoring the activity of PD patients, as well as to pinpoint the differences between HOAs and older adults with PD or MCI. However, the authors described some limitations concerning the devices, such as to operate in settings with multiple residents and interrupted activities.

In 2015, Shamir et al. (SHAMIR et al., 2015) proposed an approach called Clinical Decision Support Systems (CDSS) to examine the results of the incorporation of patient-specific symptoms and medications into three key functions: (i) information retrieval; (ii) visualization of treatment; and (iii) recommendation on expected effective stimulation and drug dosages. In order to fulfil this purpose, the authors used Naïve Bayes, Support Vector Machines and Random Forest to predict the treatment outcomes. The combined machine learning algorithms were able to accurately predict 86% of the motor improvement scores at one year after surgery.

Tucker et al. (TUCKER et al., 2015) proposed a low-cost data mining-driven approach composed of non-wearable multimodal sensors to model and predict a PD patient's adherence to medication protocols based on variations in their gait. Using whole-body movement data readings from the patients, it is possible to discriminate PD patients that are "on" or "off" medication with an accuracy of 97% for some patients using an individually customized model, and an accuracy of 78% considering a generalized model containing multiple patient gait data.

Procházka et al. (PROCHÁZKA et al., 2015) presented a novel method of Bayesian gait recognition using a Kinect sensor (data acquisition and spatial modelling) combined with signal processing techniques and Bayesian classifier for gait feature analysis aiming at recognizing individuals affected by Parkinson's disease (the authors achieved an accuracy of 94.1% in this study). Singh and Samavedham (SINGH; SAMAVEDHAM, 2015a) proposed an innovative and effective approach for monitoring the disease progression and clinical diagnosis, which is based on the combination of Self-Organizing Maps and Least Squares Support Vector Machines. The proposed approach can achieve an accuracy of up to 97% concerning the differential diagnosis of PD using the PPMI dataset. The same group of authors used unsupervised learning techniques to identify reliable biomarkers to aid the diagnosis of neurodegenerative diseases (SINGH; SAMAVEDHAM, 2015b). The authors obtained a classification accuracy of up to 99% for the differential diagnosis of PD.

### 2.2.2 Image Analysis

Zhang et al. (ZHANG et al., 2015) tested the hypothesis that changes in cortical thinning can be detected in PD patients without dementia, as well as these changes are correlated with measured cognitive decline through its relationships to cognitive impairment using high-resolution T1 weighted magnetic resonance images (MRI) of the brain. An advanced hierarchical multivariate Bayesian model to analyze the cortical thickness measurement and thinning pattern was adopted, with suitable results observed. Szymanski et al. (SZYMANSKI et al., 2015) used WEKA (HALL et al., 2009) and Rough Set Exploration System data mining methods to analyze neurological data of PD patients with the local cerebral blood flow (CBF) measured by the Single-Photon Emission Computed Tomography (SPECT). The results were correlated with the Unified Parkinson's Disease Rating Scale, being possible to demonstrate that CBF changes suggest that a general state of PD is stronger related to the CBF than to only motor symptoms.

Paredes et al. (PAREDES et al., 2015) developed the e-Motion Capture System, which is a Kinect-based software to calculate motor (cadence, stride and step length) and spatio-temporal (velocity and acceleration) parameters that affect the quality of life in patients with PD. In order to assess the reliability of the proposed system as a benchmark reference, a multiple-camera 3D motion capture system to track the gait pattern during a walking test was employed. The authors stated the e-Motion Capture System was able to measure the motor and spatial-temporal variables that are sensitive to changes in the timeline of the disease.

Hewavitharanage et al. (HEWAVITHARANAGE et al., 2015) applied a grey-level dependence matrix in order to segment the *rima glottidis*<sup>4</sup> in 4D laryngeal Computed Tomography (CT) scans in PD patients in order to identify vocal impairments. The SVM-based segmentation algorithm showed to be useful in distinguishing the *rima glottidis* area from the remaining tissues of the larynx. Bhalchandra et al. (BHALCHANDRA et al., 2015) used image analysis to segment the high-activity regions of the brain using SPECT images. Such regions correspond to the concentration of the striatal dopamine transporter, which is in charge of transmitting the dopamine substance related to the motor control. An accuracy rate of 99.42% was achieved by means of Discriminant Analysis and Support Vector Machines. In the same year, Wu et al. (WU et al., 2015) analyzed the application of Auto-Regressive (AR) models to describe the stochastic process underlying stride series of idiopathic PD patients, which are used as features to distinguish the PD stride series from the healthy normal cases. The Linear Discriminant Analysis (LDA) and Support Vector Machines were employed, being SVM better than LDA for the separation of both healthy and idiopathic PD groups, with relatively high sensitivity (0.72),

---

<sup>4</sup>An opening between the true vocal cords and the arytenoid cartilages.



specificity (0.89), and area under the curve (0.83) values, showing the autoregressive model parameters could be useful for the classification of stride series.

Rocha et al. (ROCHA et al., 2015) investigated the impact of a recent version of Kinect (version 2) in the context of PD clinical assessment when compared against the former Kinect (version 1) over 3D body data acquired from normal and PD patients treated with deep brain stimulation. In order to validate the methods, the statistical analysis showed it is possible to highlight the gait parameters are useful to distinguish between non-PD and PD patients with 96% of accuracy concerning the new version of Kinect, as well as 72% considering the former Kinect device.

Li et al. (LI et al., 2016) collected data from 10 patients (6 men and 4 women) with Parkinson's Disease acquired by means of sensors implanted with deep brain stimulation devices. Since the literature points the *subthalamic nucleus* (STN) as one of the most important regions of the brain concerning the treatment of PD patients, the authors developed an automated algorithm for MRI data using the Level Set method for image segmentation in order to aid neurosurgeons to better place the electrodes in the brain. In short, this algorithm seeks to facilitate neurosurgeons in the preoperative process and provides clinical guidance for reducing the repeated intraoperative adjustments, as well as the risk of bleeding.

Wabnegger et al. (WABNEGGER et al., 2015) investigated the use of facial emotion recognition in PD to compare brain activation during emotion perception between PD patients and healthy controls. The participants were shown pictures of different facial expressions, while the brain activity was captured by means of functional Magnetic Resonance Imaging (fMRI). The study did not conclude whether PD patients and the control group have enough discrepancies in such context or not. However, other works (CLARK; NEARGARDER; GOLOMB, 2008; SUZUKI et al., 2006) reported the lack of emotions in some group of patients.

Castellanos et al. (CASTELLANOS et al., 2015) analyzed an automated method to segment the *substantia nigra* and *locus coeruleus* volumes based on Neuromelanin-Sensitive MRI (NM-MRI) in patients with idiopathic (when the source of the disease is unknown) and monogenic (genetic inheritance pattern determined by a single gene) PD patients. The authors found evidences that NM-MRI can provide highly accurate diagnosis. Gilat et al. (GILAT et al., 2015) used a virtual reality paradigm in combination with fMRI to explore the neural correlation in 17 PD patients with freezing of gait (FoG), and 10 PD patients without FoG while off their dopaminergic medication. The results state the PD patients with FoG show alterations in the blood oxygen level responses across regions that implicate the prospective recruitment of a stopping network, which may be manifested pathologically as a freeze when the sensorimotor processing

becomes more complex.

Feis et al. (FEIS et al., 2015) introduced a multimodal approach to model symptom sides at disease onset in brain morphology based on different aspects of diffusion MR parameters and multi-kernel support vector classification. They consider these results as a major step in further predictive clinical models of Parkinson's Disease by incorporating the many clinical aspects that determine the progression of the disease.

### 2.2.3 Signal Analysis

Karamintziou et al. (KARAMINTZIOU et al., 2015) presented a novel approach based on closed-loop deep brain stimulation system for PD treatment. The proposed work operates according to an online real-time algorithm that integrates a sensitive biomarker approach together with an improved modification of a stochastic dynamical phase model. The approach is validated as a control parameter, as well as its potential to support on-demand stimulation with enfolded the dynamics of adaptive stimulation and the minimum-energy desynchronizing control of neuronal activity.

Villa-Canãs et al. (VILLA-CANÃAS et al., 2015) analyzed the low-frequency components of continuous speech signals uttered by PD patients using four-time-frequency approaches based on Wigner-Ville distribution. The idea is to determine whether the features associated to changes in the spectrum can be used to identify the tremor in speech signals of PD patients or not. The spectra are characterized based on energy analysis and spectral centroids, and the automatic detection is carried out using Support Vector Machines. The authors achieved around 72% of accuracy when discriminating between PD and healthy speakers.

Restrepo-Agudelo and Roldán-Vasco (RESTREPO-AGUDELO; ROLDÁN-VASCO, 2015) developed a method to simulate the intracranial signals recorded during a deep brain stimulation surgery of a patient with Parkinson's Disease. The method, called Auto-Regressive Parametric Model, allowed the reconstruction of the signal in time-domain with an accuracy nearly to 95% with respect to the real and simulated signals. Su and Chuang (SU; CHUANG, 2015) adopted a fuzzy entropy-based dynamic feature selection approach that showed to be effective to remove insignificant features concerning speech pattern classification of PD patients. The authors used Linear Discriminant Analysis to distinguish voice samples between PD patients and health people, thus obtaining an accuracy rate up to 97.5%.

Handojoseno et al. (HANDOJOSENO et al., 2015) investigated the brain dynamic changes associated with freezing of gait during turning using (electroencephalogram) EEG signals, which

were classified via Levenberg Marquardt and Backpropagation Neural Networks. The authors achieved an accuracy of 71%, showing that gait during turning is associated with significant alterations in the high beta and theta power spectral densities across the occipital and parietal areas, being the visual cortex region an optimal reference location for the detection of a turning freeze. According to the authors, this is the first study that shows cortical dynamic changes associated with freezing of gait during turning.

Smekal et al. (SMEKAL et al., 2015) carried out an acoustic analysis of hypokinetic dysarthria in patients with PD to identify vowels in Czech language, introducing a new speech feature based on empirical mode decomposition that increases global performance when combined with the sequential forward feature selection technique. The authors observed an accuracy rate of 94% concerning different vowels identification in PD patients. Mekyska et al. (MEKYSKA et al., 2015) carried out a complex acoustic analysis of phonation in patients with PD focusing on the estimation of the disease progress, being able to identify vowels whose analysis provides best estimation of particular clinical scores used for assessment. The authors introduced a new concept of PD progress quantification based on acoustic analysis of phonation and Random Forests, achieving a sensitivity of 92.86% and specificity of 85.71%.

Ruonala et al. (RUONALA et al., 2015) investigated the effects of a commonly used antiparkinsonian medication (levodopa) on cardiac autonomic regulation. The functioning of autonomic nervous system during levodopa medication was examined in patients with advanced PD. Resting state electrocardiogram measurements were performed over 11 patients with idiopathic PD 30 minutes before the administration of levodopa, where the heart rate variability measurements show that parasympathetic nervous system activity is decreased and the sympatho-vagal balance is shifted towards sympathetic control. Later on, i.e. 60 minutes after the administration of levodopa, the parasympathetic nervous system activates slightly, thus causing a decrease in the heart rate.

Arnulfo et al. (ARNULFO et al., 2015) characterized and compared the spiking and bursting activity in the dorsolateral and ventral subthalamic nucleus sub-regions using intra operative multi-electrode recordings and highly accurate channel localization techniques in PD patients, suggesting the existing functional difference among subthalamic nucleus regions possibly arises from different network connections rather than intrinsic neuronal properties. Dai et al. (DAI et al., 2015) proposed a novel method based on the empirical mode decomposition to filtered electromyograms (EMG), which makes use of a flexible number of features for PD detection. The signals were preprocessed in three stages by means of a novel bandpass filtering technique in order to show the features are linearly separable. Later, the proposed algorithm was

implemented as a mobile application to be more flexible than the existing methods.

Eftaxias et al. (EFTAXIAS et al., 2015) presented a new hybrid-constrained complex singular spectrum analysis method for the assessment of Parkinson's tremor by the separation of real EMG signals, in which the characteristics of tremor within a subspace of the single channel surface were measured during the prescribed hand movement (including flexion and extension), and further decomposed using singular spectrum analysis. The method showed a great potential for biomedical multichannel signal processing. Mohammed et al. (MOHAMMED et al., 2015) proposed the use of patient-specific dynamic feature extraction via Local field potential signal combined with adaptive Support Vector Machines that uses the selected features when detecting PD or non-PD patients by adjusting its decision boundary until a suitable model is obtained. The authors achieved a classification accuracy greater than 98%.

Belalcazar-Bolanos et al. (BELALCAZAR-BOLANOS et al., 2015) proposed the estimation of the different glottal flow features by means of the Iterative and/or Adaptive Inverse Filtering considering the nonlinear dynamic behavior of the vocal folds (Spanish vowels) to detect PD. The authors obtained accuracy rates of up to 75.3%, sensitivity of 0.79, and specificity of 0.72 when all vowels are considered in the experiments. Iuppariello et al. (IUPPARIELLO et al., 2015) defined a new kinematic index to evaluate the smoothness of the movements based on the minimum-jerk theory. The work aimed at studying the kinematic quality and the motor composition of visually-guided reaching movements from people with PD by applying a sub-movement decomposition method based on a mixture of Gaussian pulses.

Alekhyia and Chakravarthy (ALEKHYA; CHAKRAVARTHY, 2015) developed a 2D spiking network to analyze the cognitive aspects of PD during medication and deep brain stimulation. The authors observed the electrode's position and current spread independently lead to a critical change in performance levels, as well as the work shows that simulated PD "on" medication performed poorly compared to healthy individuals. Thanawattano et al. (THANAWATTANO et al., 2015) developed and analyzed the performance of a novel feature based on the hypothesis that PD patients have more temporal fluctuation of tremor while performing resting tasks than action tasks. The signals were acquired via a gyroscope sensor attached to the subject's finger. The tremor fluctuation was defined as the area of 95% of a confidence ellipse covering the two-dimensional signal considering 32 PD and 20 patients diagnosed with Essential Tremor (ET). The proposed work was able to discriminate PD from ET patients with 100% of accuracy. Camara et al. (CAMARA et al., ) developed an automatic real-time system for resting tremor episode detection in 10 PD patients using fuzzy models. In regard to the classification step, electrophysiological signals obtained from Local field potential (recorded in the STN) and

electromyography were adopted, achieving accuracies of 98.7%.

Recent studies have pointed out that besides the freezing of gait, many people with Parkinson's disease also suffer from freezing in the upper limbs (FoUL). In order to investigate whether upper limb freezing and other abnormalities during writing are provoked by gradual changes in amplitude sustained in patients with and without freezing of gait or not, Heremans et al. (HEREMANS et al., 2015) collected signs of 34 patients with PD, being 17 with and 17 without FoG. The experiments were conducted on a touch-sensitive writing tablet, which confirms the hypothesis that some patients with FoG also suffer from FoUL.

In another paper, Chomiak et al. (CHOMIAK et al., 2015) analyzed patients with FoG by means of a 4<sup>th</sup> generation iPod Touch sensor in order to capture data from hip flexion and step height. The work examined whether stepping-in-place with a concurrent mental task (e.g., subtraction) can be used as a simple method for evaluating cognitive-motor deficits in people with PD or not. The results indicated that during concurrent tasks, the step height of PD patients with FoG was significantly worse than PD patients with non-freezing of gate and control individuals.

Defazio et al. (DEFAZIO et al., 2015) analyzed 48 people with Parkinson's Disease and 37 healthy subjects by means of voice/speech measurements using the Robertson Dysarthria Profile (RDP), which is a clinical-perceptual method to explore all components potentially involved in speech difficulties. The approach used in this work observed that patients with early PD would theoretically express less severe voice/speech symptoms. The conclusions suggested that RDP may be a useful tool to detect speech/voice disturbances in early PD patients, even when these disturbances do not carry a significant level of disability.

Lancioni et al. (LANCIONI et al., 2015) evaluated the use of technology-aided leisure and communication tools (music and videos, verbal statements/requests, reading, text messaging, telephone calls and prayers) on three participants with advanced PD that possessed minimal or unreliable motor responses, being unable to operate conventional interface devices. The obtained results were more promissory and relevant given the limited amount of evidence available on helping persons affected by PD with leisure and communication. Braatz and Coleman (BRAATZ; COLEMAN, 2015) proposed a mathematical model based on the biochemical systems theory to examine the changes that occur over the course of the Parkinson's Disease, as well as identify the processes that would be the most effective targets for treatment. The model predicts that combined tools might be the most effective ones.

### 2.2.4 Smartphone Devices

Mobile devices use features of personal computers that can be extended to cope with profiles of different users. Also, mobile-oriented applications can make use of a number of sensors available at tablets and cell phones, which can measure hand tremors and other movements. Arora et al. (ARORA et al., 2015) evaluated a system based on smartphones in a home and community setting during 35 days to detect and monitor the symptoms of PD. The system was able to assess voice, posture, gait, finger tapping, and response time with mean sensitivity and specificity of 96.2% and 96.9% for the detection of Parkinson's Disease, respectively.

Recently, Ivkovic et al. (IVKOVIC; FISHER; PALOSKI, 2016) presented a study about the movement modulation and motor-cognitive integration effectiveness of smartphone-based tactile cues (TC) from different activities in moderately impaired PD patients and healthy individuals, who performed seated heel tapping and straight line walking tasks with and without a secondary motor task. The smartphone-driven TC showed to be a promissory tool and user-friendly movement modulation aid.

Kostikis et al. (KOSTIKIS et al., 2015) proposed a smartphone-based system to accurately assess upper limb tremor in 25 PD patients using a phone's accelerometer and gyroscope information to compute a set of metrics that can be used to quantify a patient's tremor symptoms. The authors used machine learning techniques to correctly classify 82% of the PD patients and 90% of the healthy volunteers, being possible to remotely evaluate the patient's condition. The proposed tool has low cost, is platform independent, noninvasive, and requires no expertise to be used.

Bai et al. (BAI; CHAN; YU, 2015) developed a friendly mobile system using an open-source platform in smartphones to aid PD patients, which features an interactive interface, a large font, a big button, an intuitive graphical interface, an important feature enhancement and some simplified functions, thus being suitable for the elderly people affected by PD. The proposed application also includes an improved main menu composed of several functions like telephone, SMS, internet, medication calendar, photo gallery, and emergency button, as well as a scrollable full screen containing graphical buttons. The application contains a main menu and a reply message voice button function either.

Kim et al. (KIM et al., 2015) proposed a novel smartphone-based system using inertial sensors to detect FoG symptoms in an unconstrained way. Several motions such as ankle, trouser pocket, waist and chest pocket, were evaluated. Data obtained and pre-processed via discriminative features extracted from accelerometer and gyroscope motion signals of the smartphone

were used to classify FoG episodes from normal walking using AdaBoost.M1 classifier with sensitivity of 86% at the waist, and 84% and 81% in the trouser pocket and at the ankle, respectively.

Ellis et al. (ELLIS et al., 2015) evaluated the performance of smartphone-based gait analysis using the smartphone built-in tri-axial accelerometer and gyroscope to calculate successive step times and step lengths, being validated from heel-mounted foot-switch sensors and an instrumented pressure-driven sensor. The authors stated the proposed method was able to serve as an alternative to conventional gait analysis methods.

### **2.2.5 Virtual and Augmented Reality**

Virtual reality is an advanced interface to computer applications, in which users can navigate and interact with a three-dimensional environment generated by computers from multi-sensory devices. Augmented reality is a mixture of real and virtual worlds at some point of reality/virtuality continuous that connects real and virtual environments, as well as overlay virtual objects.

Yang et al. (YANG et al., 2016) analyzed a home-based virtual reality environment able to improve balance, walking, and quality of life in 23 patients with idiopathic PD. The study did not find any difference between the effects of the home- and the virtual reality-based training, which highlights VR is able to build realistic environments that can help dealing with PD. Waechter et al. (WAECHTER et al., 2015) submitted 16 PD patients to navigation through a customized virtual reality (VR) corridor by stepping in place on a force plate while EEG data was recorded. The VR environment was combined with a cognitive, visual two-stimulus-oddball response task, which was repeated while seated to allow for comparisons to the stepping-in-place condition. The environment proves to be a very efficient and reliable method to induce FoG-like symptoms in a controlled fashion in PD participants with FoG, providing a platform for further experiments on the pathology of freezing of gait. According to the authors, the study was the first of its kind that investigated event-related potential during locomotion in a clinical population. FoG participants demonstrated decreased behavioral performance for the stepping-in-place condition while simultaneously performing a secondary cognitive task.

Khobragade et al. (KHOBRAGADE; GRAUPE; TUNINETTI, 2015) applied a Large-Memory Storage and Retrieval neural network for the prediction of onset of tremor in PD patients. The work demonstrated a fully automated deep brain stimulation system that can be applied on-demand, i.e. only when it is needed, since the usual treatments apply that stimulation continuously. Navarro et al. (NAVARRO; MAGARIÑO; LORENTE, 2015) proposed to employ an augmented

reality-based approach that has been widely used in the field of rehabilitation to aid PD patients. The experiment was tested on 7 PD individuals, and showed that VR is a simple and suitable tool that should be encouraged to be used in PD patients.

Geldenhuys et al. (GELDENHUYS et al., 2015) presented the use of a novel video-based paradigm for analyzing the gait of patients with Parkinson's disease. The idea was to consider the locomotor kinematics, which is capable of detecting subtle changes in gait and analyze the results in a gender-specific manner. In their experiments, a male mice group showed a statistically significant higher propensity towards gait changes than the female mice, suggesting that gait deficits in female-treated mice might be subtler.

### **2.2.6 Sensors**

Jellish et al. (JELLISH et al., 2015) examined the ability of persons with PD when using a real-time feedback (RTFB) system to improve gait and postural impairments, being considered the hypotheses that the patients with PD are able to utilize RTFB to maintain their step length compared to their baseline value, and employ RTFB of their back angle to maintain a more upright posture. As such, it is possible to develop RTFB-based technologies and protocols to manage gait and posture during daily activities in clinics and/or at home.

Yoneyama et al. (YONEYAMA et al., 2015) proposed an accelerometer-based gait analysis considering single trunk-mounted accelerometer and an analytical algorithm for the assessment of gait behavior that may be context-dependent aiming to detect gait peaks from acceleration data. The study also aimed the analysis of multimodal patterns in the relationship between gait cycle and vertical gait acceleration. According to the authors, this was the first work that quantitatively demonstrated that PD patients may make different types of decisions on how to walk in daily environments.

Tay et al. (TAY et al., 2015) developed a wearable wireless PD monitoring and biofeedback system to address the above issues. Each one of the wearable device consists of an accelerometer, gyroscope, compass, flex-sensors, among other sensors, and accompanying communication via bluetooth and wi-fi to transmit data wirelessly to a computer. As such, a wearable gait monitoring system is able to process real-time captured sensory data and FoG events, and then trigger audio and vibration biofeedback to prevent or reduce freezing when FoG has occurred. The system's adaptive gyroscope-based FoG detection algorithm uses automated temporal gait analysis by means of wearable wireless sensors. By using this system, PD patients will be more aware of their risk of falling, and also benefit from the periodic cueing to pace their steps after a FoG occurrence, hence improving their quality of life. The system is mobile and hands-free,



which allows the patient to walk freely for long periods of time and distance.

Mazilu et al. (MAZILU; BLANKE; TRÖSTER, 2015) investigated the correlation between wrist movement (arm movements) and FoG in PD during walking, and analyzed the possibility to detect FoG from wrist-attached wearable sensors. According to the authors, this is the very first time that wrist movements during walking are correlated with FoG in PD. Beyond this, they computed new features to describe FoG from wrist from ETHOS Inertial Measurement Units (IMU) on both wrists (FoG and wrist movement during the rest of walking) of 11 subjects of the CuPiD dataset. Finally, the authors evaluated the feasibility in detecting FoG using wrist-attached IMU in subject-dependent and -independent evaluation schemes using the FoG detection methods based on supervised machine learning. The work showed that FoG episodes can be detected using the wrist movements with a hit-rate of 90% in a subject-dependent evaluation scheme, suggesting that the wrist sensors can be a feasible alternative to the cumbersome placement on the legs.

Mazilu et al. (MAZILU et al., 2015) proposed the use of new sensor modalities to continuously monitor the FoG episodes in PD, being possible to be predicted before it happens by means of physiological data, namely electrocardiography (ECG) and skin-conductance (SC). The authors analyzed the variations of some specific features extracted from both ECG and SC for periods of data right before, during, and right after FoG events. Such features were then compared to normal walking events. Further, the authors deployed an anomaly-based method for predicting gait-freeze events using SC features and multivariate Gaussians, being able to predict 71.3% of FoG episodes with an average of 4.2s right before that event has happened.

Lorenzi et al. (LORENZI et al., 2015) proposed a wireless headset sensing system based on Inertial Measurement Units designed for long-time monitoring of specific movement disorders. The system is composed of a single inertial sensor to be positioned laterally on the head, close to the ear. The headset allows emphasizing signals related to oscillations of the trunk, improving timely detection of the freezing of gait and timely auditory stimulation directly in the ear. With respect to other positions on the body, the headset has the maximum sensitivity to the trunk oscillations made by patients when moving, thus increasing dramatically the risk of falls. The identification of the motion features is performed using an artificial neural network, which obtained excellent results without the need of large number of samples.

Iuppriello et al. (IUPPARIELLO et al., 2015) tested the hypothesis that muscle vibration of splenius muscles can improve step initiation performance in patients with PD. According to the authors, no study has examined the contribution of proprioception to postural control in PD when a bilateral continue vibration train is applied to neck muscle groups. Thought this

study, the authors show that a bilateral continue vibration train, applied to neck muscle groups, reduces postural instability by increasing stepping performance and specific posture related mechanisms, leading to a reduction in hesitation and increasing self-confidence to start walking.

Reinfelder et al. (REINFELDER et al., 2015) evaluated a robust and automated phase segmentation method of the traditional Timed Up-and-Go (TUG) test, providing phase times for PD patients. The recordings were conducted with the Embedded Gait Analysis using a intelligent system consisting of two IMUs placed unobtrusively at the lateral side of each shoe. Also, the work validated a classification approach using SVM for separating the TUG test into resting (before sit to walk), sit to walk (first torso movement), forward walking (start of walking), first turn (end of forward walking), backward walking (end of first turn), second turn (end of backward walking), turn to sit (end of turning), and resting (end of turn to sit), obtaining an accuracy rate of 81.80%.

Dong et al. (DONG et al., 2015) proposed a wireless body area sensor network as a non-intrusive device to measure the activity of individuals with PD in order to understand their spontaneous movement in an un-observed environment. Tiny body sensors attached to lower limbs collect position and acceleration data in a periodic manner, and transmit them to a processing and storage node that can store data and transfer the information to the doctor's office via telecom network or wireless local area network. In order to measure the posture changes in a non-intrusively manner, they used low voltage flex sensors, pressure sensors, accelerometers and gyroscopes to build a networked sensor device that can be worn by a person to detect posture and gait changes. Adaptive fractal and frequency domain analysis for cued and spontaneous movements detection were used either.

Jellich et al. (JELLISH et al., 2015) presented a study about people with Parkinson's disease that have difficulty while walking, and showed an increased variability in step time and step length, which are associated with higher risk of falls. Based on this rationale, the authors developed a treadmill-based rehabilitation system that has the ability to provide real-time feedback. Their results suggested that persons with PD can effectively follow feedback of posture via the presentation of visual feedback of back angle.

Dai et al. (DAI et al., 2015) develop a sensor-based quantitative assessment method to analyze the features of parkinsonian tremors, where the current possibilities of inertial sensor technology and motion-tracking algorithms can be used to implement quantitative assessments of these tremors. The authors adopted a time-frequency signal analysis algorithm to detect tremor states. Trojaniello et al. (TROJANIELLO et al., 2015) proposed a comparative analysis of selected single inertial measurement units for estimating gait temporal parameters in different pathological gait

conditions. The results showed the acceleration signals were filtered before being processed using the Z-method. The Z-method, including a preliminary filtering of the acceleration signals, seems to be preferred when analyzing Parkinson's Disease populations.

Yang et al. (YANG et al., 2016) conducted a study on the correlation of hand tremors using laser signals, i.e. Laser Line Triangulation Measurement (LLTM). The work considered four different modes of hand tremors, being the analysis performed off-line. The results showed a significant correlation among different tremor frequencies. McCandless et al. (MCCANDLESS et al., 2016,) investigated the effect of three different devices of cueing when applied to 20 PD patients with freezing of gait. Also, 10 cameras and 4 force platforms were used in the experimental section. They compared three devices (Laser Cane, sound metronome and vibrating metronome) against the walking stick and no intervention. In the tests, 12 of 20 patients had freezing incidents. The study identified patterns among the devices, being the best improvement obtained by Laser Cane.

Shao et al. (SHAO et al., 2016) introduced a case study of a 77-years old PD patient with hand contracture. The authors submitted the patient to a therapy using the game "Microsoft Fligh Simulator X", where the patient reached significant decreasing in the hand contracture. This work proposed an individualized therapy computer-based either. Volpe et al. (VOLPE et al., 2016) presented a study about the under water gait therapy. The work used a software that performs a 3D analysis of the gait. After three weeks of under water gait therapy, the results showed significant improvement in the gait speed and cadency.

Finally, Qiang and Marra (QIANG; MARRAS, 2015) used the telemedicine to the treatment of PD patients to reduce cost in the travel, as well as to provide a better therapy and patient satisfaction. After the initial treatment, the patients answered a satisfaction questionnaire, and 85% preferred continuing with telemedicine, thus showing the importance of the telemedicine in the patient satisfaction.

### **2.2.7 Web Applications**

Kraepelien et al. (KRAEPELIEN et al., 2016) investigated the feasibility and preliminary effects of internet-based cognitive behavioral therapy for depression and anxiety on 9 patients with PD while exploring the effects on non-motor symptoms. Concerns about some PD-specific health and quality of life, insomnia, plus the participant's involvement, satisfaction, and subjective evaluation of the treatment were also considered. The patients reported lower values of hospital anxiety and depression after internet-based cognitive behavioral therapy, but levels of inactivity were rather high. The participants suggested the treatment can be improved by adding

more therapist support.

Pasluosta et al. (PASLUOSTA et al., 2015) presented a review about some existing wearable technologies and the Internet-of-things applied to Parkinson's disease with an emphasis on how this technological platform may lead to a shift in the paradigm, being mindful the transition that is coming along with the technological revolution. In terms of diagnostics and treatment, they discussed the wearable technologies, their main concepts and applications, as well as the new possibilities using machine learning and artificial intelligence.

Braatz and Coleman (BRAATZ; COLEMAN, 2015) developed a mathematical model based on biochemical systems theory to examine the changes that occur over the course of PD, as well as to identify what processes would be the most effective targets for treatment. The model predicts that combined tools, initiated as early as possible and targeting a wide range of pathways, are the most effective ones.

Ferreira et al. (FERREIRA et al., 2015) identified relevant parameters through assessment tools in six domains (gait, bradykinesia/hypokinesia, tremor, sleep, balance and cognition) using a system to evaluate people with PD at home. Yang et al. (YANG et al., 2015) evaluated a virtual reality system for balance training at home, which seemed to be more effective than the conventional home balance to improve walking and quality of life in PD.

## 2.3 Dataset description

In this section, we introduce some datasets used in the aforementioned works, as well as how they were designed to cope with Parkinson's Disease.

### 2.3.1 HandPD Dataset

The *HandPD Dataset* was designed by Pereira et al. (PEREIRA et al., 2015), being composed of images extracted from handwriting exams of 92 individuals divided in two groups: (i) the first one contains 18 exams of healthy people, named *control group*, with 6 male subjects and 12 female individuals; (ii) the second group contains 74 exams of people affected with Parkinson's disease, named *patients group*, having 59 male subjects and 15 female ones. The images were collected at the Faculty of Medicine of Botucatu, São Paulo State University, Brazil.

In order to compose the dataset, each subject is asked to fill a form in order to fulfil some task, such as drawing circles, spirals and meanders. Figure 2.1 displays an exam of a 56 years-old male patient, in which we can observe the tremor inherent to Parkinson's disease. Note the

patient is required to perform 6 distinct activities (a-f), which consist in the repetition of several operations in accordance with certain drawings.

The image shows a handwritten form with the following content:

- Date: 22/11/2010
- No: [blurred]
- RG: [blurred]
- Diagnosis: *Distonia e Hiperkinesia Medicamentosa*
- Age: *56*
- Hand dominance: *(x) direita ( ) esquerda*
- Field study: Unesp 2010
- Institution: University of Applied Sciences Regensburg, Biometric Smart Pen Project
- Institution: Universidade Estadual Paulista Faculdade de Medicina (FMB), Botucatu
- Task a: *Desenhar circulo 12 vezes no mesmo lugar sem parar.* Response: *TESTE* with a circled 'X' and a circle.
- Task b: *Desenhar circulo no ar 12 vezes no mesmo lugar sem parar.* Response: A circle drawn in the air.
- Task c: *Desenhar espiral após sinal sonoro, de dentro para fora.* Response: Four spirals drawn from the center outwards.
- Task d: *Desenhar meander após sinal sonoro, de dentro para fora.* Response: Four meander patterns drawn from the center outwards.
- Task e: *Diadococinesia: Mão direita 20 segundos.* Response: A small mark.
- Task f: *Diadococinesia: Mão esquerda 20 segundos.* Response: A small mark.

**Figura 2.1: Handwriting exams filled out by a 56-years old PD patient. Extracted from (PEREIRA et al., 2015).**

After filling the forms out, they are digitized for the further extraction of spirals and meanders. Such step is performed by hand, where each drawing is cropped to its minimum bounding box (or close to it). Later, the cropped spiral and meander images are numbered as follows: 1,2,3,4 concerning the spirals from left to right, and 5,6,7,8 concerning the meanders from left to right. Therefore, the entire dataset is composed of 736 images labeled in two groups: patients (296) and control (72). Also, the dataset comprises 368 images from each drawing, i.e. spirals and meanders<sup>5</sup>.

### 2.3.2 Parkinson's Progression Markers Initiative Dataset - PPMI

The Michael J. Fox Foundation (MJFF)<sup>6</sup> has been an essential driver for the PD biomarkers initiative. Such foundation developed a clinical study to verify progression markers in Parkinson's disease, the so-called *Parkinson's Progression Markers Initiative Dataset* - PPMI, which emerged as a model for following multiple cohorts of significant interest, and it is being conducted at a network of clinical sites around the world. The study is designed to establish a comprehensive set of clinical, imaging and biosampled data to be used to define biomarkers

<sup>5</sup><http://www.fc.unesp.br/~papa/pub/datasets/Handpd/>

<sup>6</sup><http://www.ppmi-info.org/fundingpartners>

of PD progression. Once these biomarkers are defined, they can be used in therapeutic studies, which is the ultimate goal of this research work<sup>7</sup>.

### 2.3.3 Parkinsonian Disease Handwriting Dataset - PaHaw

The *Parkinson's Disease Handwriting Database - PaHaW*<sup>8</sup> consists of multiple handwriting samples from 37 parkinsonian patients, being 19 men and 18 women. In regard to the control group, the dataset contains 38 individuals, being 20 men and 18 women. The database was acquired in cooperation with the Movement Disorders Center at the First Department of Neurology<sup>9</sup>, Masaryk University and St. Anne's University Hospital in Brno, Czech Republic.

Each individual was asked to fill a form, and the completed template was shown to the subjects, as well as no restrictions about the number of repetitions of syllables/words in the tasks or their height were given. Figure 2.2 displays an empty template (containing only printed lines and a square box specifying the spiral area). A conventional ink pen was held in a normal fashion, allowing for immediate full visual feedback. The signals were recorded using the Intuos 4M (Wacom technology) digitizing tablet with 200Hz of sampling frequency.



**Figura 2.2: Template used as an example by the PaHaw dataset. The image has been taken from the home-page of the dataset.**

The signals were digitized on-the-fly, since the individual exerts pressure on the writing surface during the movement. The perpendicular pressure exerted on the tablet surface was also recorded. The recordings started when the pen touched the surface of the digitizer, and finished when the task was completed.

<sup>7</sup><http://www.ppmi-info.org/access-data-specimens/download-data/>

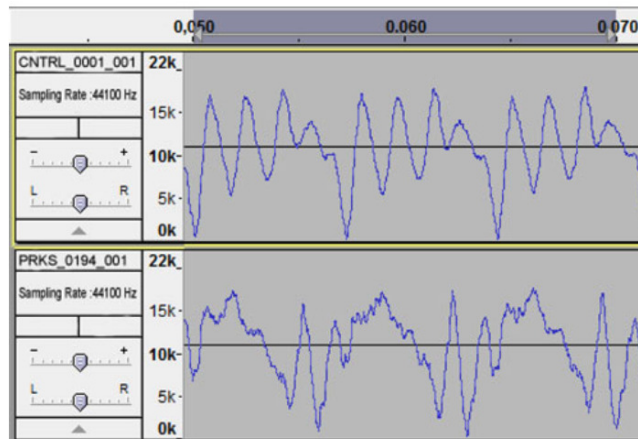
<sup>8</sup>[https://www.researchgate.net/publication/289525377\\_Parkinson's\\_Disease\\_Handwriting\\_Database\\_PaHaW](https://www.researchgate.net/publication/289525377_Parkinson's_Disease_Handwriting_Database_PaHaW)

<sup>9</sup><http://bdalab.utko.feec.vutbr.cz>

### 2.3.4 Parkinson Speech Dataset

The *Parkinson Speech Dataset* database consists of exams performed with 20 PD patients, being 6 female and 14 male. The healthy individuals comprise 20 people, being 10 female and 10 male who appealed at the Department of Neurology in Cerrahpasa Faculty of Medicine, Istanbul University<sup>10</sup>.

From all subjects, multiple types of sound recordings (26 voice samples including sustained vowels, numbers, words and short sentences) are taken. The voice samples are selected by a group of neurologists from a set of speaking exercises that aim at leading to more powerful sound of PD patients (SAKAR et al., 2013). The recording step was achieved by a Trust MC-1500 microphone with a frequency range between 50Hz and 13 kHz, as shown by Figure 2.3.



**Figure 2.3: Voice sample of a healthy individual (top), and the waveform of a voice sample belonging to a patient (down). Extracted from (SAKAR et al., 2013).**

During the collection of data, 28 PD patients were asked to say only the sustained vowels “a” and “o” three times, which makes a total of 168 recordings. The test group consists of patients who are suffering from PD for 0 to 13 years, and individual ages vary between 39 and 79.

### 2.3.5 CuPiD Dataset

The CuPiD dataset contains 24 hours of sensing data collected from Inertial Measurement Units (MAZILU et al., 2013a) attached on both wrists of 18 subjects with Parkinson’s disease, which performed different walking protocols in a laboratory setting designed to provoke FoG, including walking with 360- and 180-degrees turns, walking in straight lines and passing narrow

<sup>10</sup><http://archive.ics.uci.edu/ml/datasets/Parkinson+Speech+Dataset+with++Multiple+Types+of+Sound+Recordings>

corridors, or walking across the crowded hospital halls (MAZILU et al., 2013b). The idea was to analyze whether the hand movements during walking correlate with freezing of gait episodes or not, as shown in Figure 2.4.



**Figure 2.4:** A subject wearing the system used to design the CuPid dataset, with focus on the IMUs attached on the wrists. Extracted from (MAZILU; BLANKE; TRÖSTER, 2015).

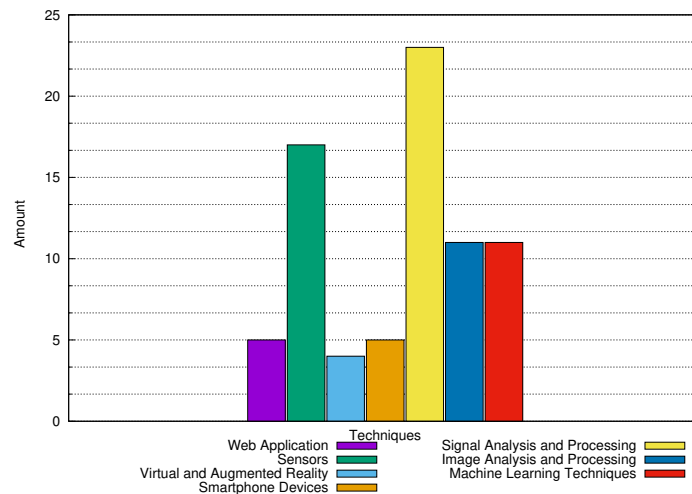
The data collection system contained 9 wearable ETHOS Inertial Measurement Units (HARMS et al., 2010) attached on different parts of the body, one electrocardiogram sensor, a galvanic skin response sensor and a near-infrared spectroscopy sensor. The dataset was designed by collecting data from the IMUs attached on both wrists of the subjects.

## 2.4 Discussion

Figure 2.5 summarizes the amount of works considered in this review separated by area of interest. Clearly, the great majority of works focus on signal analysis and processing, followed by sensor-based studies. Actually, most works are related to speech analysis, which makes sense to find a number of papers that make use of signal analysis to aid PD recognition. Also, a lot of works employ sensors for data acquisition, thus making signal analysis even stronger.

Although machine learning-related papers are outnumbered by others, a considerable number of works related to signal analysis make use of some sort of artificial intelligence either, thus increasing the number of papers that employ machine learning to aid PD recognition. We have observed that image-based data for PD identification do not play a big role, since we have the problem of digitizing the forms for the further application of image processing techniques, which are strongly dependent on the quality of the input images, and thus more prone to errors.





**Figure 2.5: Summarization of the works considered in this review.**

Smartphone devices can contribute to alleviate the errors induced during image acquisition by using applications that use touch-based sensors, which digitize the exams in real-time. However, we did not find many works on this subject. The fewer number of papers refers to virtual and augmented reality. Although such environments are quite suitable, some of them are expensive to design and maintain. However, in-home devices such as Kinect seem to be a game-changing.

Recently, the NPJ/Parkinson's Disease journal <sup>11</sup> pointed out that both sensors- and smartphone device-based applications to aid PD treatment have grown considerably. With such devices, it is possible to monitor the amount of severity of the disease at home, as well as some therapeutic activities and games can be used for the treatment. Nowadays, tablets and smart phones usually contain a lot of sensors, that can measure tremors and orientation. Trister et al. (TRISTER; DORSEY; FRIEND, 2016) claimed that such mobile-oriented systems would ideally evaluate all aspects of the disease through a series of measures captured on activities, thus being able to consider a more detailed view into the day-to-day variability that patients may describe. Bot et al. (BOT et al., 2016) used the ResearchKit provided by Apple to collect data from PD patients using an iPhone. The study interrogated aspects of movement disorders by means of surveys and sensor-based recordings from healthy and PD individuals. The authors stated that such works are in the very early beginning.

Actually, some past works have used technology to handle PD treatment either. In 2011, Nemedi et al. (MEMEDI et al., 2011) presented a web-based system to monitor PD patients remotely. The system was composed of three main parts: (i) a handheld computer to collect data, (ii) a server for information storage, and (iii) an interface to visualize and interpret the results. Westin

<sup>11</sup><http://www.nature.com/articles/npjparkd20166>

et al. (WESTIN et al., 2010) presented a system composed of a touch screen-equipped computer for assessment of PD patients at home. The proposed approach highlighted the treatment has been effective in two patients, both in self-assessments, tapping tests and spiral scores.

In 2014, Hariharan et al. (HARIHARAN; POLAT; SINDHU, 2014), presented a study about PD identification using a hybrid approach composed of Gaussian Mixture Model, Principal Component Analysis, and several other techniques over University of California-Irvine (UCI) machine learning datasets. The experiments showed the combination of feature pre-processing, feature reduction/selection methods and classification leads to an accuracy of 100%.

## 2.5 Conclusions

In the last years, the amount of people with Parkinson's Disease has increased considerably, which turns out to be one of the world's major health problem up to date. The use of artificial intelligence and machine learning techniques have presented promising results, thus becoming a fundamental aid to cope with PD early detection.

In this work, we presented a review concerning Parkinson's Disease detection and monitoring by means of recent technologies. The main contribution of this work is to consider very recent works dating from 2015 and 2016 mostly. Several approaches based on image and signal analysis, smartphone devices, virtual and augmented reality, sensors and web-based application were considered, as well as some datasets widely used in the literature.

We have observed the great majority of works make use of signal analysis, which are often acquired by on-body sensors, thus making both kind of tools the most used ones in the papers considered in this review. Also, machine learning-driven works have been widely referred either, since most works, even using signal- or image-based data, require some sort of decision-making mechanism supported by artificial intelligence. Similarly, we believe the smartphones and tablets will begin to play an important role in the future, since e-health research kits are constantly being developed, and to monitor patients at home seems to be the most promising direction towards Parkinson's Disease understanding.

# Capítulo 3

## UMA NOVA ABORDAGEM BASEADA EM VISÃO COMPUTACIONAL APLICADA NO DIAGNÓSTICO DO MAL DE PARKINSON

---

---

Este capítulo apresenta uma proposta baseada na extração de informações visuais de imagens de formulários utilizadas para o diagnóstico do mal de Parkinson. O capítulo compreende os resultados de dois artigos publicados pelo candidato, *A Step Towards the Automated Diagnosis of Parkinson's Disease: Analyzing Handwriting Movements* (PEREIRA et al., 2015) e *A New Computer Vision-based Approach to aid the Diagnosis of Parkinson's Disease* (PEREIRA et al., 2016a).

### 3.1 Introduction

Parkinson's disease (PD) is a degenerative, chronic and progressive illness that may cause tremors, slowness of movement, muscle stiffness, and changes in speech and writing skills due to the neurological disorder (BURKE, 2010b). PD was first described by the English physician James Parkinson (PARKINSON, 1817b), being its symptoms well-known in the scientific community. However, it is still unheard-of a trivial test to diagnose Parkinson's disease with a reliable recognition rate in its early stages. Moreover, it is not straightforward to establish the PD level soon after its diagnosis.

The Parkinson's disease occurs when nerve cells that produce dopamine are destroyed, a process that is performed slowly, thus characterizing the progression of this disease. With the absence of such a substance, the nerve cells can no longer send messages properly, causing many other symptoms such as depression, sleep disturbances, memory impairment and autonomic

nervous system disorders. In some cases, Parkinson's disease may be triggered by hereditary causes (BURKE, 2010b).

In the last decades, some works attempted at designing solutions to aid PD diagnosis. Expert systems based on machine learning techniques have been employed to this purpose, showing promising results (SAKAR et al., 2013). Generally, these works are signal analysis-oriented, which means one can use the patient's voice to assess the level of the illness (LITTLE et al., 2009; PEREIRA et al., 2006), since the voice capability is gradually compromised by PD. Little et al. (LITTLE et al., 2009), for instance, presented a dataset composed of biomedical voice measurements from 31 male and female subjects, being 23 patients diagnosed with PD and 8 healthy subjects. The authors introduced a new measure of dysphonia called Pitch Period Entropy, which seems to be more robust to identify changes in the speech, since approximately 90% of PD patients exhibit some form of vocal impairment (HO et al., 1998; LOGEMANN et al., 1978).

In the work conducted by Zhao et al. (ZHAO et al., 2014), five patients and seven healthy individuals were used to recognize Parkinson's disease by means of the voice analysis. In order to fulfil this purpose, the individuals' voice were recorded using an Isomax EarSet E60P5L microphone, being the recording sessions lasting around 25 minutes each, and a total of 50 pre-recorded prompts consisting of emotional sentences spoken by a professional actress. Tsanas et al. (TSANAS et al., 2012) evaluated different algorithms based on dysphonia measures aiming at PD recognition. A total of 132 acoustic features were initially used for further feature selection, and the authors concluded the dysphonia information together with existing features end up helping PD recognition. Harel et al. (HAREL; CANNIZZARO; SNYDER, 2004) claimed that PD symptoms are detectable up to five years prior to clinical diagnosis, and symptoms presented in speech include reduced loudness, increased vocal tremor, and breathiness. In their work, the authors used a dataset of the National Center for Voice and Speech, which comprises 263 phonations from 43 subjects (17 females and 26 males, being 10 healthy controls and 33 diagnosed with PD).

Since one of the first manifestation of Parkinson's Disease is the deterioration of handwriting, the micrography (a writing exam) is another approach widely used for the diagnosis of Parkinson's disease (EICHHORN et al., 1996b). This technique is considered an objective measure, since a PD patient possibly features the reduction of calligraphy size, as well as the hand tremors. Nowadays, this procedure is often conducted by filling out some specific forms. Rosenblum et al. (ROSENBLUM et al., 2013) suggested that writing exams can be used to distinguish PD patients from healthy individuals. The authors employed the following methodology to sup-

port their assumption: 20 PD patients and 20 control individuals were asked to write their names and addresses in a piece of paper attached to a digital table. Further, for each stroke, the mean pressure and velocity were measured in order to compute spatial and temporal information. The authors presented very good recognition rates, being 97.5% of the participants classified correctly (100% of the control individuals, and 95% of PD patients). Later on, Drotár et al. (DROTÁR et al., 2014) claimed that movement during handwriting of a text consists not only from the on-surface movements of the hand, but also from the in-air trajectories performed when the hand moves in the air from one stroke to the next. The authors demonstrated the assessment of in-air hand movements during sentence handwriting has a higher impact than the pure evaluation of on surface movements, leading to classification accuracies of 84% and 78%, respectively.

Machine learning-based techniques have also been applied to help the automatic PD recognition. Spadotto et al. (SPADOTTO et al., 2010b), for instance, introduced the Optimum-Path Forest (OPF) (PAPA; FALCÃO; SUZUKI, 2009; PAPA et al., 2012) classifier to the aforementioned context. Later on, Spadotto et al. (SPADOTTO et al., 2011) proposed an evolutionary-based approach to select the most discriminative set of features in order to improve PD recognition rates. Gharehchopogh et al. (GHAREHCHOPOGH; MOHAMMADI, 2013b) used Artificial Neural Networks with Multi-Layer Perceptron to diagnose the effects caused by Parkinson's disease. Pan et al. (PAN et al., 2012b) analyzed the performance of Support Vector Machines with Radial Basis Function in order to compare the onset of tremor in patients with Parkinson's disease. Hariharan et al. (HARIHARAN; POLAT; SINDHU, 2014) developed a new feature weighting method using Model-based clustering (Gaussian mixture model) in order to enrich the discriminative ability of the dysphonia-based features, thus achieving 100% of classification accuracy. Recently, Peker et al. (PEKER; SEN; DELEN, 2015) used sound-based features and complex-valued neural networks to aid PD diagnosis as well.

However, although many works deal with voice- and speech-driven information, there is a large number of writing exams out there that can give us valuable information about the development of Parkinson's Disease, since it is cheaper and easier to acquire such sort of exam. Moreover, most hospitals and clinics have writing exams by hand only, which means they need to be digitized prior to information extraction. Usually, the patients are asked to draw spirals and meanders, which are then compared against the templates. Very recently, Pereira et al. (PEREIRA et al., 2015) proposed to extract features from writing exams using image processing techniques, achieving around 79% percent of recognition rates, which is considered very reasonable. The authors also designed and made available a dataset called "HandPD" with all images and features extracted<sup>1</sup>. However, they employed "spirals" drawings only.

<sup>1</sup><http://www.fc.unesp.br/~papa/pub/datasets/Handpd/>

In this paper, we extended the work of Pereira et al. (PEREIRA et al., 2015) by presenting the following contributions: (i) a deeper analysis and explanation about the feature extraction process, as well as a tremor-based feature is also analyzed; (ii) we considered both spirals and meanders for the classification process; and (iii) we also extended “HandPD” dataset with images and features from meanders. Since we are committed with science, we also made available to the readers this new dataset, and we believe it can serve as a basis for future researches regarding Parkinson’s Disease diagnosis. The proposed approach is innovative in the sense we can extract both the template and drawings of each patient automatically, thus having no user intervention.

The remainder of this paper is organized as follows. Section 3.2 presents the methodology employed to design the dataset, and Section 3.3 describes the methodology used to extract visual features from the handwriting exams. Section 6.4 states the experimental results and discussion, and Section 6.5 states conclusions and future works.

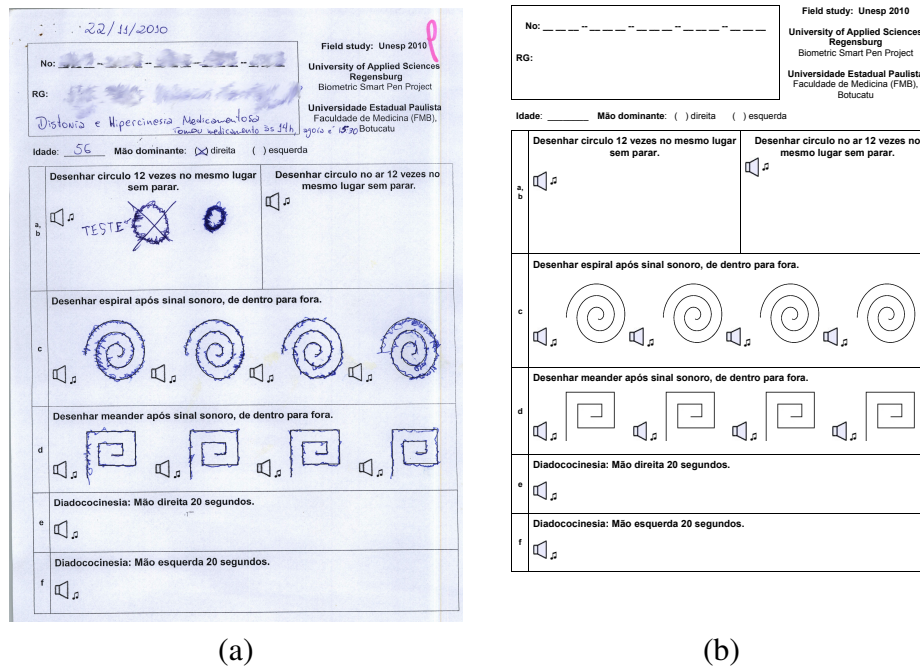
## 3.2 HandPD Dataset

The HandPD dataset was collected at the Faculty of Medicine of Botucatu, São Paulo State University, Brazil, being composed of images extracted from handwriting exams of 92 individuals, being divided in two groups: (i) the first one contains 18 exams of healthy people, named *control group*, with 6 male subjects and 12 female individuals; (ii) the second group contains 74 exams of people affected with Parkinson’s disease, named *patients group*, having 59 male subjects and 15 female ones. Therefore, 80.44% of the dataset is composed of patients, and 19.56% comprises control individuals. Although the dataset is unbalanced, it is easier to achieve similar proportions by adding more control individuals than patients.

The control group is composed of 16 right-handed and 2 left-handed individuals, with an average of  $44.22 \pm 16.53$  years. In regard to the patients group, we have 69 right-handed and 5 left-handed individuals with an average of  $58.75 \pm 7.51$  years. Therefore, one can observe the dataset is not age-biased, which provides an interesting scenario for learning purposes. In fact, most patients are considerably older than 60 years, since Parkinson’s disease usually gets worse within this age group. On the other hand, the dataset is heterogeneous enough to contain a 38-years old male patient as well.

In order to compose the dataset, each subject is asked to fill a form in order to fulfil some task, such as drawing circles, spirals and meanders. Figure 3.1a displays an exam of a 56 years-old male patient, in which we can observe the tremor inherent to Parkinson’s disease. Note the

patient is required to perform 6 distinct activities (a-f), which consist in the repetition of several operations in accordance with certain drawings. However, the analysis of the images will be focused on tasks c and d only, which are related to drawing 4 spirals and 4 meanders according to the template. Figure 3.1b depicts an empty form, in which one can observe the templates regarding spirals and meanders.



**Figura 3.1: Handwriting exams: (a) filled out by a 56-years old PD patient, and (b) an empty exam with the templates.**

After filling the forms out, they are digitized for the further extraction of spirals and meanders. Such step is performed by hand, where each drawing is cropped to its minimum bounding box (or close to it). Soon after, the cropped spiral and meander images are numbered as follows: 1, 2, 3, 4 concerning the spirals from left to right, and 5, 6, 7, 8 concerning the meanders from left to right. Therefore, the entire dataset is composed of 736 images labeled in two groups: patients (296) and control (72). Also, the dataset comprises 368 images from each drawing, i.e. spirals and meanders. The reader can refer to the HandPD home-page for more technical details about organization of the dataset.

### 3.3 Feature Extraction from Visual Description

In this section, we describe the methodology used to extract the features and keypoints from spiral and meander forms. In order to fulfil this task, we split the proposed methodology in two stages: (i) image preprocessing, and (ii) the feature extraction. In the first stage (Sec-

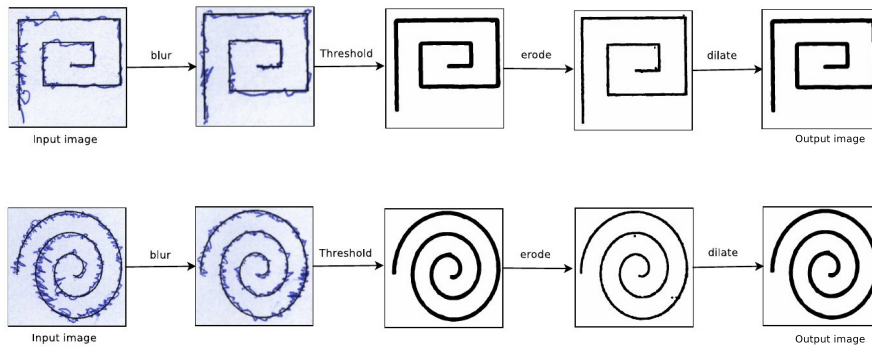
tion 3.3.1), we design an approach to automatically separate the handwritten trace (HT) from the exam template (ET) considering both spiral and meanders, since the images are not registered to each other. Soon after, in the second stage (Section 3.3.2) we used the HD and ET extracted from images to compute the visual features.

### 3.3.1 Handwritten Trace and Exam Template

In order to extract both HT and ET, we merged some classical image processing techniques such as blurring filters and mathematical morphology, being the process of extracting either HT and ET contours performed separately. Since the images were digitized, we applied a preprocessing step to reduce noise and undesirable artefacts by means of a  $5 \times 5$  mean filter<sup>2</sup>. Later on, we extracted the exam template applying a thresholding in the smoothed image aiming to obtain a binary mask  $M_{ET}^i(I)$ . This step is performed as follows:

$$M_{ET}^i(I) = \begin{cases} 0 & \text{if } R^i(I) < 100 \wedge G^i(I) < 100 \wedge B^i(I) < 100 \\ 1 & \text{otherwise,} \end{cases} \quad (3.1)$$

where  $R^i(I)$ ,  $G^i(I)$  and  $B^i(I)$  stand for the value of pixel  $i$  of the input image  $I$  considering the channels "Red", "Green" and "Blue", respectively. If Equation 3.1 is satisfied, the foreground (ET) pixels will be set to 0 ("black" color), and the background pixels will be set to 1 ("white" color), as displayed in Figure 3.3. Since the ET in the original image is supposed to be black or near-black (the original - empty - form is colourless), it is reasonable to assume low brightness values for such pixels when looking for the form itself. Finally, we applied an opening operation (erosion followed by a dilation) to guarantee a fully connected ET. Figure 3.3 shows the proposed pipeline for the ET extraction.



**Figure 3.2: Image processing steps concerning ET extraction.**

In regard to the HT extraction step, we employed a similar methodology to the one used to

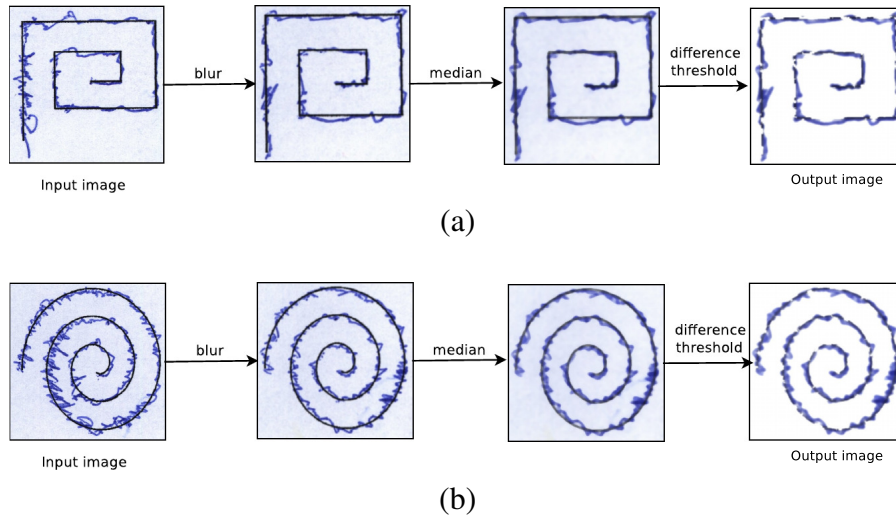
<sup>2</sup>Notice the size of this convolutional kernel was set up empirically.



extract the ET, but now with some additional steps and a different thresholding method, since both HT and the background are blue-coloured due to the digitation process. First, we applied a  $5 \times 5$  mean filter followed by a  $5 \times 5$  median filter to smooth the image in order to reduce noise and small artefacts, mainly those around the HT's borders (once again, both filter sizes were determined empirically). Further, the filtered image  $F$  is thresholded using the following equation:

$$M_{HT}^i(F) = \begin{cases} 255 & \text{if } |R^i(F) - G^i(F)| < 40 \wedge |R^i(F) - B^i(F)| < 40 \wedge \\ & |G^i - B^i| < 40 \\ F^i & \text{otherwise,} \end{cases} \quad (3.2)$$

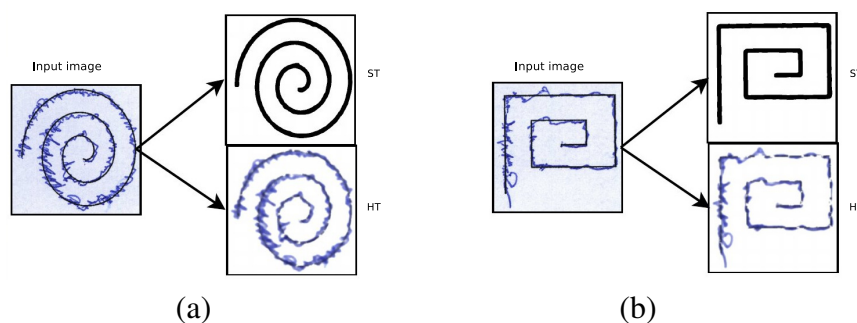
where  $F^i$  represents the brightness of pixel  $i$ . The intuitive idea behind this step is to remove pixels with quasi-similar values for the three channels (i. e., background pixels), and to maintain pixels with considerable differences between the channels (foreground - HT - pixels). Figure 3.3 shows the proposed pipeline for the ET extraction<sup>3</sup>.



**Figure 3.3: Image processing steps concerning HT extraction.**

Figure 3.4 illustrates a spiral and a meander image and their corresponding ET and HT extracted using the proposed methodology. One can observe the quality of both template and trace extracted from the images.

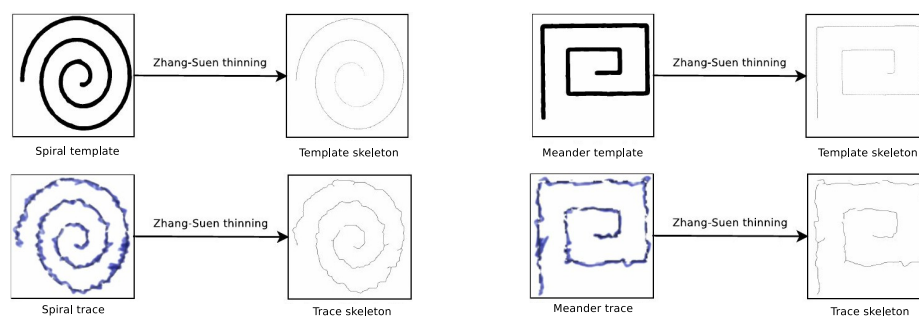
<sup>3</sup>Notice the value 255 in Equation 3.2 stands for the triplet (255, 255, 255), since we have an RGB image as the result of thresholding operation.



**Figure 3.4: Spiral and meander images and their corresponding HT and ET extracted using the proposed methodology for a (a) spiral and a (b) meander.**

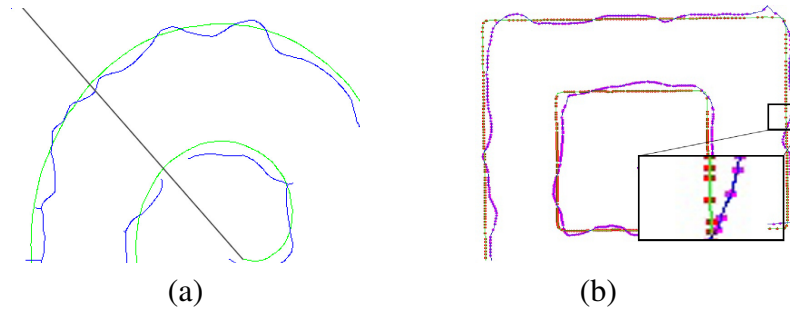
### 3.3.2 Feature extraction

The feature extraction step aims at describing both HT and ET, and then to compare them in order to evaluate the “amount of difference” between both images. In fact, this difference among images is computed over points sampled at the very same positions considering HT and ET images. At each point, we extracted a set of features that will represent the whole template or handwritten trace. First, we need a concise and compact representation of both HT and ET, which is accomplished here by means of the skeleton of the thresholded images. Therefore, we extracted the skeleton of HT and ET images based on the Zhang-Suen thinning algorithm (ZHANG; SUEN, 1984), which consists of two parallel routines: (i) to remove the south-east boundary points and the north-west corner points, and (ii) to remove the north-west boundary points and the south-east corner points. Figure 3.5 depicts the thinning result of the spiral and meander templates, as well as the handwritten trace.



**Figure 3.5: Thinning of HT and ET using Zhang-Suen algorithm.**

Even after the pre-processing step, the template and handwritten images may contain small discontinuities (blue lines in Figure 3.6(a)). Therefore, we need to select the sample points from the template and handwritten spiral/meander very carefully. As such, points in regions that contains discontinuities should be discarded. This phase is crucial, since it has a considerable influence in the feature extraction step, which may affect the learning process as well.



**Figure 3.6: Sampling process: (a) a certain region with discontinuities, and (b) the proposed fair sampling process.**

In regard to the selection of sampled points, we trace 360 rays<sup>4</sup> from the center of the spiral/meander to the image borders. For this task, we created two empty lists: (i) template points, and (ii) handwritten points. The ray tracing process begins from the more external point of the spiral or the meander. For each ray, we capture its intersections with the template and the handwritten trace, and if this ray intercepts only one of the images, this point is discarded; otherwise, the pair of points is inserted in their respective list of points (template or handwritten). Therefore, with the aforementioned procedure, we can guarantee a fair sampling by considering only points presented in both images. Figure 3.6(b) shows a thinned meander with overlapped traces (template and handwritten), as well as the highlighted sampling points obtained by means of the proposed fair sampling process.

Further the sampling process, we then extract nine numeric features from each skeleton (i.e., HT and ET) by measuring the statistical differences between them. However, prior to the feature description, we introduce to the reader the definition of “radius” of a spiral or meander point, which is basically the length of the straight line that connects this point to the center of the spiral or meander, as displayed in Figure 3.7. The “red” point stands for the spiral’s or meander’s center, being some random (“white”) points connected to the thinned spiral (skeleton) through the arrows with straight lines.

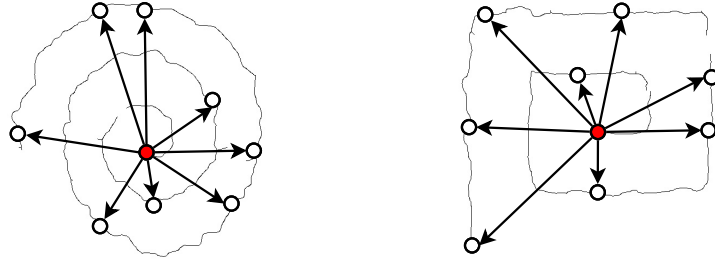
A brief description of each feature is given below:

- $f_1$ : Root Mean Square (RMS) of the difference between HT and ET radius. The RMS is computed as follows:

$$\text{RMS} = \sqrt{\frac{1}{n} \sum_{i=1}^n (r_{HT}^i - r_{ET}^i)^2}, \quad (3.3)$$

where  $n$  is the number of sample points drawn from each HT and ET skeleton, and  $r_{HT}^i$  and  $r_{ET}^i$  denote the HT and ET radius considering the  $i$ -th sampled point, respectively.

<sup>4</sup>the value 360 was obtained empirically, since this amount of sampling points has showed a good trade-off between efficiency and accuracy.



**Figure 3.7: Some random points and the straight lines representing their connections with the spiral's and meander's center point.**

- $f_2$ : the maximum difference between HT and ET radius, i.e.:

$$\Delta_{max} = \operatorname{argmax}_i \{|r_{HT}^i - r_{ET}^i|\}; \quad (3.4)$$

- $f_3$ : the minimum difference between HT and ET radius, i.e.;

$$\Delta_{min} = \operatorname{argmin}_i \{|r_{HT}^i - r_{ET}^i|\}; \quad (3.5)$$

- $f_4$ : the standard deviation of the differences between HT and ET radius;
- $f_5$ : Mean Relative Tremor (MRT): Pereira et al. (PEREIRA et al., 2015) proposed this quantitative evaluation to measure the “amount of tremor” of a given individual's HT, being defined as the mean difference between the radius of a given sample and its  $d$  left-nearest neighbors. The MRT is computed as follows:

$$\text{MRT} = \frac{1}{n-d} \sum_{i=d}^n |r_{ET}^i - r_{ET}^{i-d+1}|, \quad (3.6)$$

where  $d$  is the displacement of the sample points used to compute the radius difference<sup>5</sup>.

The following three features are computed based on the relative tremor  $|r_{ET}^i - r_{ET}^{i-d+1}|$ ;

- $f_6$ : the maximum ET;
- $f_7$ : the minimum ET;
- $f_8$ : the standard deviation of ET values;
- $f_9$ : the number of times the difference between HT and ET radius changes from negative to positive, or vice-versa.

<sup>5</sup>In this work, we used  $d = \{1, 3, 5, 7, 10, 15, 20\}$ , being  $d = 10$  the one that maximized the PD recognition rate.

Finally, the features were normalized as follows:

$$f'_i = \frac{f_i - \mu_i}{\sigma_i}, \quad (3.7)$$

where  $f'_i$  denotes the normalized version of feature  $f_i$ , and  $\mu_i$  and  $\sigma_i$  stand for the average and standard deviation of feature  $f_i$ ,  $i = 1, 2, \dots, 9$ .

## 3.4 Experiments and Results

In this section, we present the experimental results to assess the robustness of the proposed dataset and feature extraction approach<sup>6</sup>. Also, we evaluate three pattern recognition techniques: Naïve Bayes (NB), Optimum-Path Forest (OPF), and Support Vector Machines with Radial Basis Function (SVM-RBF). Note the kernel parameters concerning SVM are optimized through cross-validation. In regard to OPF, we used LibOPF (PAPA; SUZUKI; X, 2014), and with respect to NB and SVM we used scikit-learn (PEDREGOSA et al., 2011).

In order to evaluate the proposed approach, we performed three different rounds of experiments. The first one (Section 3.4.1) uses 75% of the dataset for training purposes, and the remaining 25% for the classification phase. However, instead of to partition the dataset randomly, we created four subsets in order to guarantee that each individual will be represented in the dataset with its 3 spirals/meanders, being the remaining one used for classification purposes. In this experiment, the spiral- and meander-based datasets are used individually. In the second experiment (Section 3.4.2), we decided to conduct a cross-validation procedure with 20 runnings. Now, we no longer guarantee each individual will be represented in both training and test sets. In the third round (Section 3.4.3), we conducted some experiments in order to check whether we can benefit from the learning process over spirals and meanders in one single approach, i.e. by using them together. Finally, we present a discussion about the experiments, as well as some insights about this research.

### 3.4.1 Experiment 1

Since each individual contains four spirals/meanders in the datasets, we employed a constrained hold-out approach to guarantee that each of them will be represented in both training and testing sets concerning both spiral and meander-based datasets. Tables 3.1 and 3.2 display the mean recognition rates considering all four configurations of training and test sets for the

<sup>6</sup>The proposed dataset and the extracted features are available at <http://www.fc.unesp.br/~papa/pub/datasets/Handpd>

spiral- and meander-based datasets, respectively. One can observe NB obtained the best global results concerning Spiral dataset, while SVM achieved the best results over Meander dataset. Notice the global accuracy is the one proposed by Papa et al. (PAPA; FALCÃO; SUZUKI, 2009), which considers unbalanced datasets, while the recognition rates per class (i.e. Control and Patient group) are computed using the standard approach (the ratio between correct classifications and the total number of samples for that specific class). The values in bold stand for the most accurate ones considering the standard deviation only. As aforementioned, in this round of experiments we used a similar approach to a 4-fold cross-validation, but ensuring we have three drawings for the same individual for training purposes. Therefore, we can guarantee all individuals are represented in both training and test sets. However, as we have only four accuracy values to compute the mean recognition rates and their standard deviation, we did not employ any robust statistical evaluation in this experiment.

|               | <b>OPF</b>  | <b>NB</b>          | <b>SVM</b>  |
|---------------|-------------|--------------------|-------------|
| Control group | 31.94%±5.32 | 62.50%±5.32        | 2.78%±5.56  |
| Patient group | 76.35%±3.22 | 69.26%±7.18        | 99.66%±0.68 |
| Global        | 54.15%±3.58 | <b>65.88%±4.57</b> | 51.22%±2.91 |

**Tabela 3.1: Experimental results considering the spiral-based dataset.**

Curiously, a different behaviour considering each classifier and both datasets can be observed. Note OPF obtained better results over meander dataset when compared to the spirals dataset, while NB holds the opposite situation. Such situation motivated us to consider a bag-of-classifiers in order to check whether a combination among all classifiers will make the results better or not (Section 3.4.3).

|               | <b>OPF</b>  | <b>NB</b>    | <b>SVM</b>         |
|---------------|-------------|--------------|--------------------|
| Control group | 34.72%±8.33 | 20.83%±41.67 | 36.11%±9.62        |
| Patient group | 85.81%±4.20 | 79.73%±33.34 | 96.62%±2.59        |
| Global        | 60.27%±4.02 | 50.28%±4.18  | <b>66.37%±4.01</b> |

**Tabela 3.2: Experimental results considering the meander-based dataset.**

### 3.4.2 Experiment 2

In this section, we consider a cross-validation procedure with 20 runnings to assess the robustness of the proposed approach under a different scenario. Therefore, we can no longer guarantee each individual will be represented in both training and test sets, but we can obtain more conclusive results by means of the Wilcoxon signed-rank statistical test (WILCOXON, 1945a). In this work, we used a significance of 0.05. Tables 3.3 and 3.4 present the mean

recognition rates considering spiral- and meander-based datasets, respectively. Once again, we can observe results very similar to the ones obtained in the previous section. The values in bold stand for the most accurate techniques considering the aforementioned statistical evaluation.

|               | <b>OPF</b>  | <b>NB</b>          | <b>SVM</b>  |
|---------------|-------------|--------------------|-------------|
| Control group | 26.39%±9.17 | 65.56%±11.48       | 1.67%±4.07  |
| Patient group | 78.58%±5.02 | 62.91%±12.65       | 98.65%±4.34 |
| Global        | 52.48%±5.32 | <b>64.23%±7.11</b> | 50.16%±1.71 |

**Tabela 3.3: Average results considering the spiral-based dataset and a cross-validation with 20 runnings.**

Since the dataset is dominated by patients, all classifiers achieved better recognition rates for that class, except for NB considering spiral and meander datasets. In fact, with respect to this classifier, the accuracy rates per class were similar to each other considering the spiral dataset, but considerably distinct with respect to meanders. NB seemed to better manage control individuals, but we can also observe the highest standard deviations for this classifier as well.

|               | <b>OPF</b>   | <b>NB</b>    | <b>SVM</b>         |
|---------------|--------------|--------------|--------------------|
| Control group | 32.78%±12.08 | 80.83%±16.37 | 36.94%±10.71       |
| Patient group | 82.30%±3.72  | 37.57%±22.83 | 96.49%±2.50        |
| Global        | 57.54%±6.35  | 59.20%±4.78  | <b>66.72%±5.33</b> |

**Tabela 3.4: Average results considering the meander-based dataset and a cross-validation with 20 runnings.**

### 3.4.3 Experiment 3

In this section, we conducted an experiment to check whether we can benefit from information learned from both drawings. We used a standard majority voting for each classifier, and in case of ties, we opted to use the classification given by the meanders dataset, since it has been the most accurate (Section 3.4.2). Table 3.5 presents the mean accurate rates for each class, as well as the global accuracy. Notice we used the very same sets employed in the first experiment (Section 3.4.1), since we can guarantee that both spiral and meander analyzed at a given time step of the classification algorithm come from the same individual.

The results evidenced one may not benefit from the combined information between spirals and meanders, since the results are now worse than the ones obtained with meanders only. The main problem is related to the inconsistency among samples from control and patients group. That means we can not observe that different drawings can help each other since we have inconsistencies at the very same exam for different patients. In the next section we discuss such statements in more details.

|               | <b>OPF</b>         | <b>NB</b>    | <b>SVM</b>         |
|---------------|--------------------|--------------|--------------------|
| Control group | 64.96%±16.29       | 27.30%±37.36 | 12.50%±25.00       |
| Patient group | 60.23%±4.73        | 70.36%±39.08 | 96.49%±2.50        |
| Global        | <b>55.86%±3.63</b> | 45.79%±4.15  | <b>58.61%±2.84</b> |

**Tabela 3.5: Average results considering the combination process between spirals and meanders using the constrained 4-fold approach.**

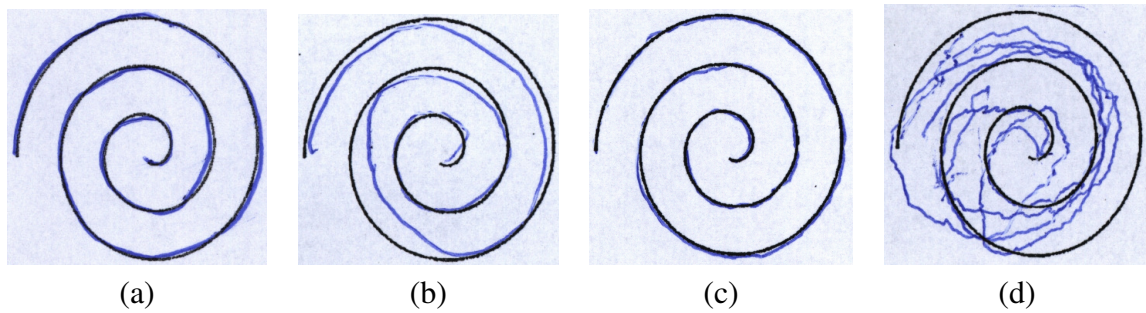
### 3.4.4 Discussion

The experiments conducted in this paper may drive us to three main conclusions: (i) first, to ensure that we have the very same patient in both training and testing sets does not seem to benefit the final classification rates, since the results obtained in Sections 3.4.1 and 3.4.2 were very similar to each other; (ii) second, meanders can provide more reliable recognition rates; and (iii) finally, it seems the combination of information provided by both spirals and meanders does not benefit the final classification rates.

The main problem related to PD automatic recognition concerns with patients in the initial stage of the disease, since they often do not present any symptoms related to tremors. Figure 3.8 depicts some examples of spirals from both control and patients group. If we consider Figures 3.8b and 3.8c, for instance, the former belongs to a control individual, and the latter belongs to a patient. Clearly, the patient exam looks like from someone that is not affected by the disease, i.e. it is very similar to Figure 3.8a. The high variability of the dataset may lead the classifiers to errors as well. However, the main idea in designing such dataset is to capture such sort of problems, which are not straightforward to solve. Obviously, Figure 3.8d is easier to be labeled as patient than Figure 3.8c, but the opposite situation is not true. Actually, the main problem concerns when Figure 3.8c is represented in the training set, not in the test set. In the former situation, this exam has a high probability to be an outlier, thus leading the learning process to mistakes in the classification phase. The latter situation usually only affects that sample only, i.e. it will be probably labeled as control. Although it may decrease the overall classification rate, the major problem is related to the fact that such exam will be a false negative, thus postponing the treatment of the disease.

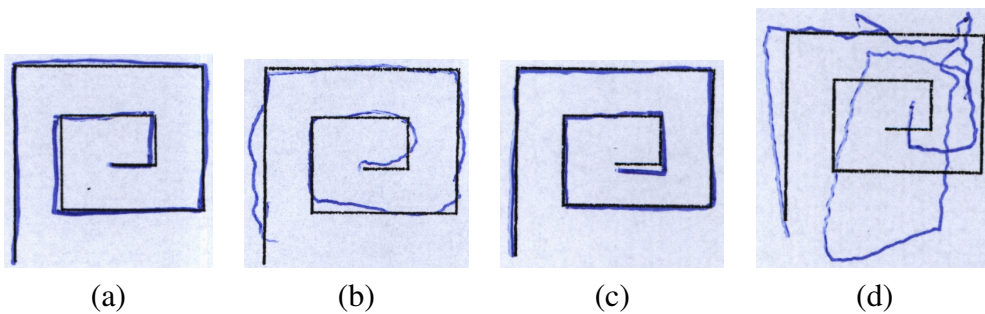
Figure 3.9 displays some meanders from both control and patients group. A similar situation to the one faced with spirals can also be observed with meanders. The high variability of the dataset makes the classifiers more prone to errors, thus turning the problem of identifying PD in the early stages quite complicated. However, the proposed approach obtained  $\approx 67\%$  of recognition rates using meanders, which we consider a very suitable result. As aforementioned, we have not noticed any particular image-based dataset available in the internet, as well as with





**Figure 3.8: Spirals from control group (a)-(b), and from the patients group (c)-(d).**

the proposed pipeline for feature extraction adopted in this work.



**Figure 3.9: Meanders from control group (a)-(b), and from the patients group (c)-(d).**

## 3.5 Conclusion

In this paper, we dealt with the problem of Parkinson's Disease recognition by combining machine learning and computer vision techniques. The main contributions are related to the design of a new dataset that contains images from both spirals and meanders, which are cropped out from digitized handwritten exams, as well as we proposed a pipeline that can deal with the problem of learning from non-registered images. The proposed approach can automatically extract both the template and handwritten trace from each exam for further feature extraction and classification.

The experimental results can lead us to conclude that meanders are more informative than spirals, since the latter pose a greater challenge due to the contours inherent to their shape. Also, the combination of both approaches did not seem to improve the results. The main problem is related to the high variability of the dataset, which comprises patients at the very early stages of the disease, thus being very difficult to be diagnosed. In regard to future works, we intend to increase the dataset with more samples from the control group, as well as to design new features that can better distinguish between control individuals and patients.

# Capítulo 4

## AUXÍLIO AO DIAGNÓSTICO DA DOENÇA DE PARKINSON UTILIZANDO DINÂMICA DE ESCRITA E APRENDIZADO EM PROFUNDIDADE

---

---

Este capítulo apresenta duas principais contribuições: (i) o uso da técnica de Redes Neurais por Convolução para classificação das imagens contidas no conjunto de dados HandPD, e (ii) o uso e disponibilização de um conjunto de dados composto por seis tipos diferentes de sinais adquiridos com um caneta *smart pen* baseado em séries temporais. O artigo contido neste capítulo foi submetido para a revista *Computer Methods and Programs in Biomedicine*, onde encontra-se a espera do parecer de seus revisores. O capítulo também compreende os resultados de um artigo publicado pelo candidato (PEREIRA et al., 2016b).

### 4.1 Introduction

Parkinson's Disease (PD) is a chronic, progressive, and neurodegenerative disease caused by the loss of a neurotransmitter called dopamine (LEES; HARDY; REVESZ, 2009). Usually, PD is more common in the elderly population, producing alterations in gait and posture that may increase the risk of falls, the so-called "freezing of gait". PD usually impacts daily activities and reduces the quality of life concerning patients and their families (MAKI; MCILROY, 2005; MARCHETTI; WHITNEY, 2005; ZHAO et al., 2008; PRASHANTH et al., 2016).

A number of drugs have been developed to help coping with the disease, but their usage along the years might hasten neurodegeneration (FAHN et al., 2004). The main problem regarding PD concerns its detection in early stages, since it is unknown the real situations that trigger Parkinson's Disease. Therefore, researchers from different areas aim at pushing together their

skills and helping each other to better understand such illness. Due to their emerging use in a number of applications, decision-making techniques based on machine learning might be the most fruitful ones to deal with PD recognition (SAKAR et al., 2013).

(DAS, 2010), for instance, presented a comparison among some classification techniques concerning PD diagnosis, achieving around 92.2% of classification accuracy by means of Neural Networks. (SPADOTTO et al., 2010c) introduced the Optimum-Path Forest (OPF) (PAPA; FALCÃO; SUZUKI, 2009; PAPA et al., 2012) in the context of automatic PD identification, and (GHAREHCHOPOGH; MOHAMMADI, 2013b) used Artificial Neural Networks with Multi-Layer Perceptron to diagnose the effects caused by Parkinson's Disease. (SPADOTTO et al., 2010a) also considered using a meta-heuristic-driven feature selection aiming at recognizing such illness.

(MEMEDI et al., 2015) measured the disease progression in PD patients, which were asked to perform some handwritten exams at home. (LONES et al., 2014) employed evolutionary algorithms for combining classifiers aiming at the automatic identification of Parkinson's Disease. Other works, such as the one by (PAN et al., 2012b), analyzed the performance of Support Vector Machines with Radial Basis Function in order to compare the onset of tremor in patients with PD. Later on, (PEKER; SEN; DELEN, 2015) used sound-based features and complex-valued neural networks to aid PD diagnosis as well, and (HARIHARAN; POLAT; SINDHU, 2014) developed a new feature weighting method using Model-based clustering (Gaussian mixture model) in order to enrich the discriminative ability of the dysphonia-based features, thus achieving 100% of classification accuracy.

However, most works make use of audio-based datasets to cope with PD identification. Very recently, (PEREIRA et al., 2016) proposed to aid PD diagnosis by means of handwriting movements. In addition, the very same group of authors made available a dataset with hundreds of images containing handwriting drawings made by both healthy individuals and patients. Since the writing ability is affected by Parkinson's Disease, it is very usual to find such exams in hospitals and clinics, but only a few works have considered them for automatic diagnosis purposes.

Some years ago, a group of German researchers developed a very clever way to assist PD diagnosis: the so-called Biometric Smart Pen - *BiSP*<sup>®</sup> (TEAM REGENSBURG, 2002), which is essentially a pen composed of sensors that measure some information captured during handwritten exams. Although the pen has been originally designed for biometric purposes, it was further employed to aid PD diagnosis. Some years ago, (PEUKER; SCHARFENBERG; HOOK, 2011) used the signals extracted from the pen to perform PD identification, obtaining very suitable results. However, the authors extracted around 400 hand-crafted features from the signal, which were obtained by means of a sequential-driven feature selection algorithm, which may be too costly.

In this work, we proposed to learn pen-based features by means of a Convolutional Neural Network (CNN) (LECUN et al., 1989), which can process information through a set of layers, being each one in charge of learning a different and finer representation. Moreover, as far as we are concerned, we have not noticed any work that deal with automatic PD diagnosis by means of deep learning techniques, which turns out to be the main contribution of this work. Another contribution is to make available a dataset composed of the signals extracted from patients and healthy individuals through the smart pen<sup>1</sup>. Additionally, we showed how to improve PD identification by means of an ensemble of CNNs, which were trained over six different handwritten exams: (i) drawing circles on the paper, (ii) drawing circles in the air, (iii) spirals, (iv) meanders, (v) left-wrist movements and (vi) right-wrist movements.

The remainder of this paper is organized as follows. Section 4.2 presents the methodology employed in this work, as well as the proposed dataset. Section 4.3 presents the experimental results, and Section 4.4 states conclusions and future works.

## 4.2 Methodology

In this section, we present the methodology used to create the dataset, as well as the proposed approach to analyze the pen-based features (signals) using Convolutional Neural Networks.

### 4.2.1 HandPD Dataset

The writing of parkinsonian patients is often distorted and smaller (micro-graphing) than that of healthy individuals due to the tremors, reduced movement amplitudes, slowness and rigidity (GEMMERT; TEULINGS; STELMACH, 2001). Currently, it is not straightforward to pinpoint a specific exam that can identify a patient in the early stages. Also, PD can be misidentified with other brain disorders.

Recently, (PEREIRA et al., 2016) made available a dataset concerning images acquired during handwriting exams, which aim at describing an individual skill when filling a form out, as the one depicted in Figure 4.1. The idea of the form is to ask a person to perform some specific tasks that are supposed nontrivial to PD patients, including to trace some geometric forms and performing the so-called “diadochokinese test”, which is basically a test where the individual holds the pen with straight arms and perform hand-wrist movements.

From Figure 4.1, one can observe the six aforementioned handwritten exams: (i) drawing

---


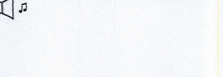

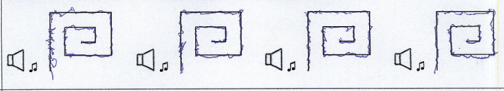
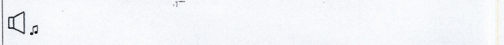
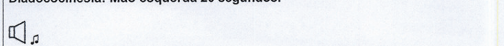
<sup>1</sup><http://www.fc.unesp.br/~papa/pub/datasets/Handpd>

22/11/2020

Field study: Unesp 2010  
University of Applied Sciences Regensburg  
Biometric Smart Pen Project  
Universidade Estadual Paulista Faculdade de Medicina (FMB),  
Botucatu

Distonia e Hiperkinesia Medicamentosa  
Tomou medicamento às 14h, agora é 15:30 Botucatu

Idade: 56 Mão dominante:  direita ( ) esquerda

|      |  |   |
|------|--|---|
| a, b | Desenhar círculo 12 vezes no mesmo lugar sem parar.<br>       | Desenhar círculo no ar 12 vezes no mesmo lugar sem parar.<br> |
| c    | Desenhar espiral após sinal sonoro, de dentro para fora.<br> |   |
| d    | Desenhar meander após sinal sonoro, de dentro para fora.<br> |   |
| e    | Diadococinesia: Mão direita 20 segundos.<br>                 |   |
| f    | Diadococinesia: Mão esquerda 20 segundos.<br>                |   |

**Figura 4.1: Form used to assess the handwritten skills of a given individual.**

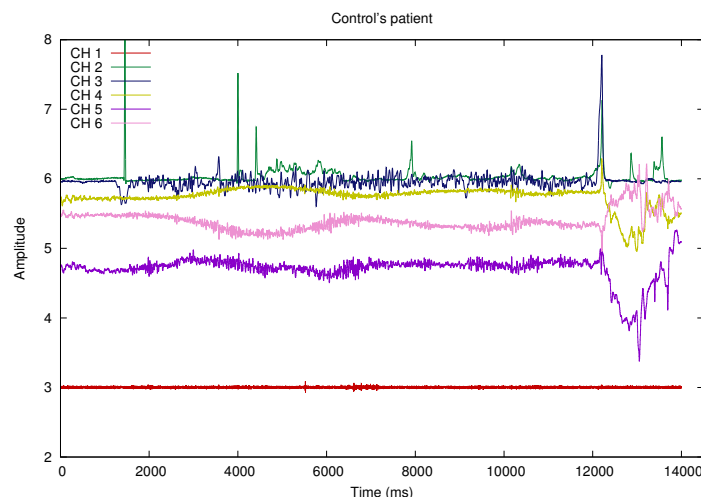
circles on the paper (exam ‘a’), (ii) drawing circles in the air (exam ‘b’), (iii) drawing spirals (exam ‘c’), (iv) drawing meanders (exam ‘d’), (v) right-wrist movements (exam ‘e’), and (vi) left-wrist movements (exam ‘f’). Notice both “spirals” and “meanders” exam are performed four times, and the individual is asked to draw the circle in the air and on the paper twelve times each.

The former HandPD dataset was collected at the Faculty of Medicine of Botucatu, São Paulo State University, Brazil, being composed of images extracted from handwriting exams of individuals divided into two groups: (i) healthy people and (ii) PD patients. The dataset comprises 92 individuals, being divided in two groups: (i) the first one contains 18 exams of healthy people, named control group, with 6 male subjects and 12 female individuals; (ii) the second group contains 74 exams of people affected with Parkinson’s disease, named patients group, having 59 male subjects and 15 female ones. The control group is composed of 16 right-handed and 2 left-handed individuals, with an average of  $44.22 \pm 16.53$  years. In regard to the patients group, we have 69 right-handed and 5 left-handed individuals with an average of  $58.75 \pm 7.51$  years.

In this work, we proposed to extend the original HandPD dataset with signals extracted from the smart pen as well, which are generated through six sensors, as described below:

- CH 1: Microphone;
- CH 2: Fingergrip;
- CH 3: Axial Pressure of ink Refill;
- CH 4: Tilt and Acceleration in “X direction”;
- CH 5: Tilt and Acceleration in “Y direction”; and
- CH 6: Tilt and Acceleration “Z direction”.

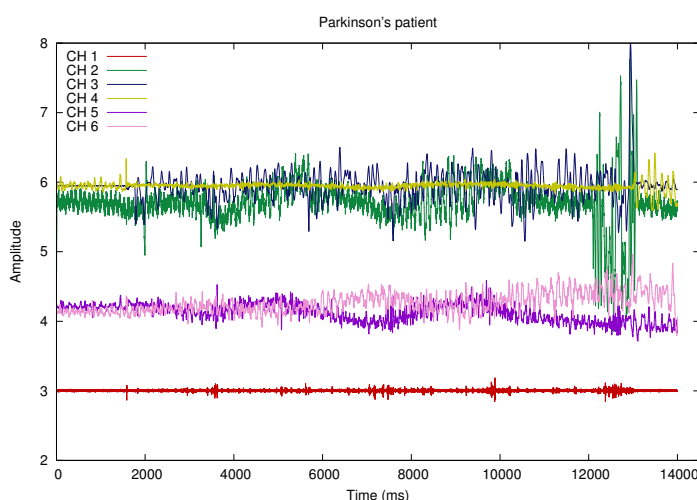
The difference between the exams of healthy individuals and patients are due to a dysfunction of movement disorders. Some parkinsonian patients, for instance, may present high levels of tremor during drawing tasks. Since each sensor outputs the whole signal acquired during the exam<sup>2</sup>, we can represent such data as a time series, as depicted in Figure 4.2, which represents the output of an exam from a healthy individual when drawing a spiral (e.g. Figure 4.5a), and each colored signal stands for a different channel. We can observe the drawing is pretty much the standard form of the image, while the signal extracted from the patient seems to be too much noisy, as displayed in Figure 4.3 (e.g. Figure 4.5b). Also, the microphone (i.e., the red channel) seems to provide little discriminative information between patients and healthy individuals. The “sounds of writing” produced a slightly different output for both types of individuals, but we included them as well.



**Figura 4.2:** Signals recorded by the pen from a control individual when drawing a spiral.

In order to build the dataset, we used signals extracted from the form tests ‘a’, ‘b’, ‘c’, ‘d’, ‘e’ and ‘f’. The new dataset comprises 34 individuals, being 14 patients (10 males and 4

<sup>2</sup>The extension of the exam is defined as the time interval between a computer beep (a start call) and the end of the drawing process.



**Figure 4.3: Signals recorded by the pen from a PD patient when drawing a spiral.**

females) and 20 control (healthy) individuals (10 males and 10 females). Each person is asked to fill the form out using the smart pen. This activity concerns the analysis of the movement provided by circles, spirals, meanders drawings and diadochokinesis; quantifying the normal motor activity in a healthy individual, as well as the dysfunction of PD patients.

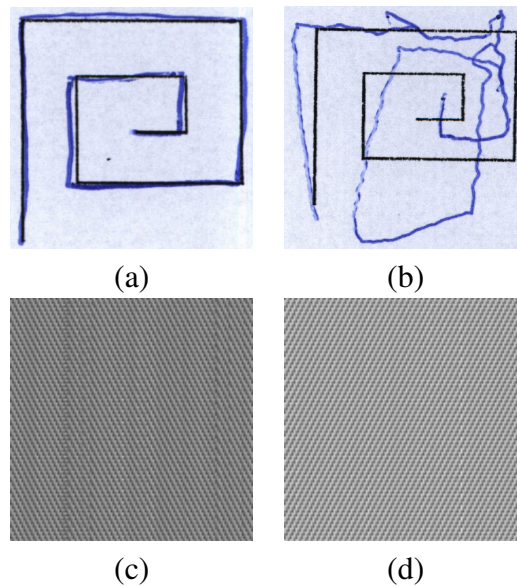
In order to facilitate the dataset organization, the form tests are divided in six exams, as follows:

- Exam 1: drawing a circle twelve times in the same place (row ‘a’ in Figure 4.1);
- Exam 2: drawing a circle twelve times in the air (row ‘b’ in Figure 4.1);
- Exam 3: drawing four spiral from inside to outside (row ‘c’ in Figure 4.1);
- Exam 4: drawing four meanders from inside to outside (row ‘d’ in Figure 4.1);
- Exam 5: diadochokinesis test with the right hand (row ‘e’ in Figure 4.1); and
- Exam 6: diadochokinesis test with the left hand (row ‘f’ in Figure 4.1).

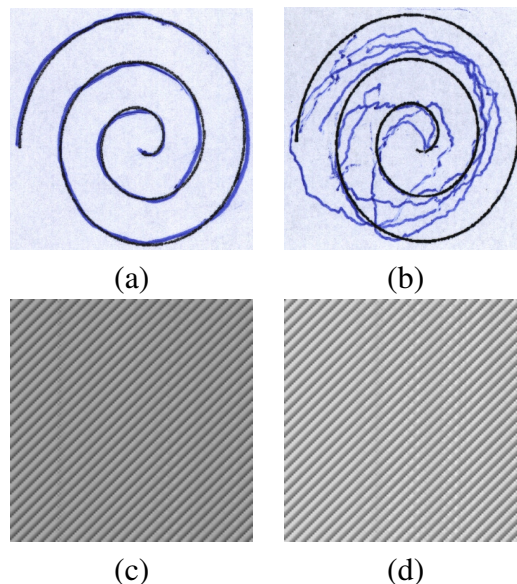
## 4.2.2 Modeling Time Series in CNNs

We propose to model the problem of distinguishing PD and control individuals as an image recognition task by means of CNNs. Roughly speaking, the signals provided by the smart pen are transformed into pictures. Each exam is composed of  $r$  rows (exam time in milliseconds) and 6 columns, which stand for the aforementioned 6 signal channels (e.g. sensors). Therefore, each exam needs to be resized to a squared matrix in order to fulfill our purposes (notice the number

of rows  $r$  may differ from each test, since a person may take longer than another to perform the exam). After rescaling, each exam-based matrix is then normalized in order to be modeled as a gray-scale image. Figures 4.4 and 4.5 illustrate some drawings and their transformed versions into time series-based images. One can observe the different patterns among the test images, as well as different patterns among the same drawings of healthy and PD patients.



**Figure 4.4:** Meander samples from: (a) control and (b) PD patient, and their respective time series-based images in (c) and (d).



**Figure 4.5:** Spiral samples from: (a) control and (b) PD patient, and their respective time series-based images in (c) and (d).

Datasets “Exam 1”, “Exam 2”, “Exam 5” and “Exam 6” contain 76 images each, being 56 from PD patients and 20 from the control group. The datasets “Exam 3” and “Exam 4” contain



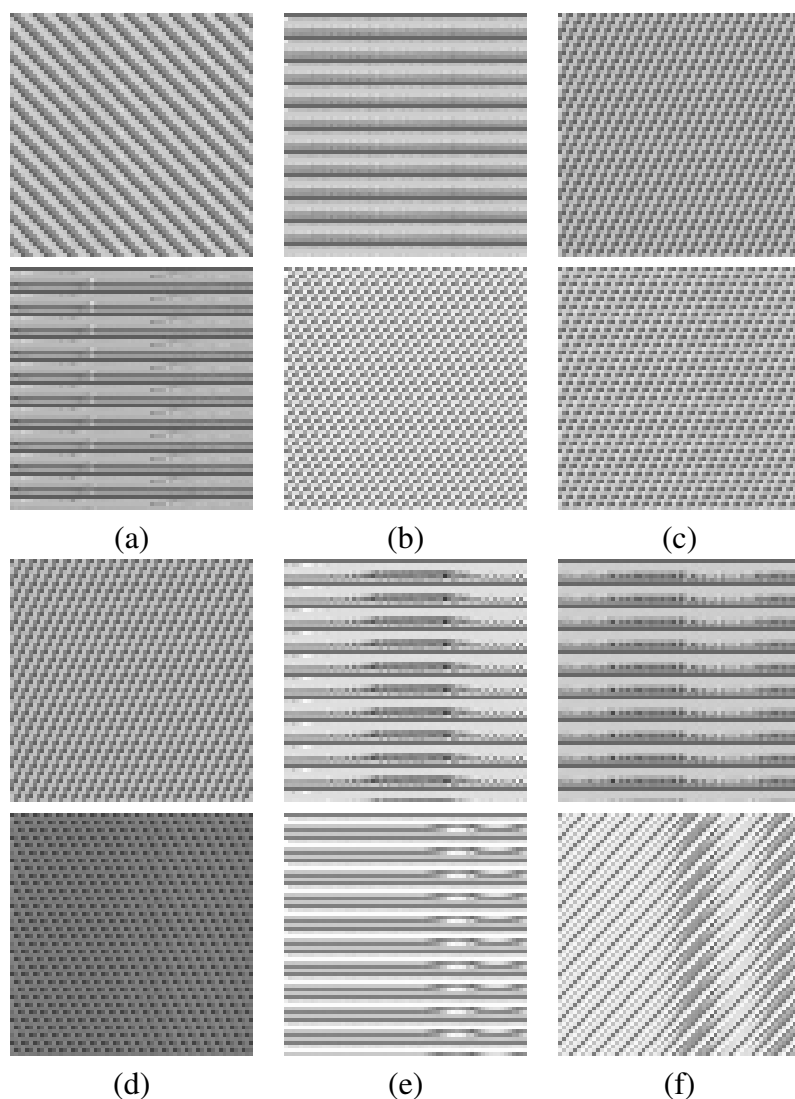
304 images each, being 224 from PD patients and 80 from the control group. The difference in the number of images concerns the fact spirals and meanders are drawn four times per exam. Additionally, for each dataset, we created two versions varying the image size: (i) datasets with images of  $64 \times 64$  pixels, and (ii) datasets with images of  $128 \times 128$  pixels. The idea is to evaluate the influence of the image resolution during the experiments.

Figure 4.6 displays the image-based dynamics of a patient and a healthy individual (control group) concerning the six exams. Clearly, one can realize the difference concerning the images from the patient (first row) and the healthy individual (second row). Since we modeled the handwritten dynamics (time series) as images, the problem now becomes to learn texture-oriented features, since they encode the tremors during the exam. It is important to notice that our dataset contains patients at the early stages of the disease (they were diagnosed later), which turns out the process more realistic and useful, since it is not pretty much interesting to diagnose a patient after the tremors have started.

Additionally, despite the time series depicted in Figure 4.6 showed to be quite important to distinguish between control individuals and patients, one can observe a considerable difference among the exams, which means they are important to capture distinct information, as further detailed in Section 4.3.3. We showed their combination is a powerful tool to enhance the automatic diagnosis concerning both the control and patient group.

### 4.2.3 Assessment Through Convolutional Neural Networks

In this section, we explain the proposed approach to assess the automatic diagnosis of Parkinson's Disease by means of Convolutional Neural Networks. Roughly speaking, we divided the experiments in two rounds: (i) Single-Assessment and (ii) Combined-Assessment. In the former experiment, we analyzed the robustness of the features learned through CNNs considering each exam individually. In regard to the second experiment, we proposed to combine the output of each CNN (i.e. each one trained over a specific exam) by means of majority voting in order to obtain the final result. Since we have six different exams, it is quite reasonable to assume each one encodes/captures a different information related to handwriting skills. Figure 4.7 depicts the aforementioned proposed combination step to assess the robustness of CNNs when modeling the problem of PD recognition by means of time series-based images.

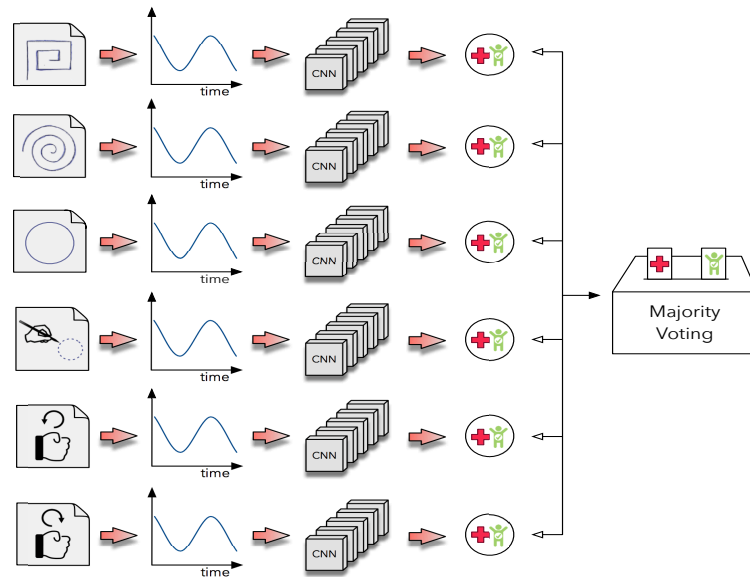


**Figura 4.6:** Time series-based images pattern considering a patient (first and third row) and a healthy individual (second and fourth row): (a) “Exam 1” (circle in the paper), (b) “Exam 2” (circle in the air), (c) “Exam 3” (spiral), (d) “Exam 4” (meander), (e) “Exam 5” (diadochokinesis with the right hand) and (f) “Exam 6” (diadochokinesis with the left hand).

## 4.3 Experiments

### 4.3.1 Experimental Setup

In this work, we used a CNN-based approach to classify the time series-based images drawn by the control group and PD patients. In order to provide more conclusive results, we also considered standard classifiers trained over the data to serve as baselines for comparison purposes: (i) Optimum-Path Forest (OPF) (PAPA; FALCÃO; SUZUKI, 2009; PAPA et al., 2012), (ii) Support Vector Machines (SVM) (CORTES; VAPNIK, 1995) and (iii) Näive-Bayes (DUDA; STORK, 2000). The reason for using such classifiers concerns the fact OPF is quite fast and parameterless, SVM



**Figure 4.7: Proposed combination approach to evaluate CNNs in the context of PD identification.**

is one of the most used techniques in the literature<sup>3</sup>, and Naïve-Bayes is considered a good alternative to achieve the gold standards. Additionally, CNN parameters were hand-tuned, i.e. the parameters were empirically chosen.

As one can observe, the images may look discriminative by texture. In order to serve as a baseline experiment, we used two texture descriptors to feed the supervised techniques addressed in this work: the gray level co-occurrence matrices (GLCM) (HARALICK; SHANMUGAM et al., 1973), and the local binary patterns (LBP) (OJALA; PIETIKÄINEN; HARWOOD, 1996). GLCM stands for the distribution of co-occurring pixels values concerning a given offset. For our purpose, we used the energy, entropy, contrast, homogeneity and correlation features computed over the matrices built upon the angles  $\theta$  as  $0^\circ$ ,  $45^\circ$ ,  $90^\circ$  and  $135^\circ$ . In regard to LBP, it recaps the local structure in an image by comparing each pixel with its neighbors. In other words, it labels the pixels by thresholding the neighborhood of each pixel and transforming them into binary numbers. Considering our approach, we used the naïve LBP with 8 neighbors and radius equals to 1.

In order to provide consistent experiments, we partitioned each dataset considering individuals and not just images. Therefore, when a given individual is selected to compose the training set, all the twelve images of that individual are used for training purposes in all six exams. Notice the same methodology is applied for the testing set. We considered using 50% of the samples to compose the training set, and the remaining 50% to be part of the testing

<sup>3</sup>Notice SVM parameters have been optimized through a grid-search procedure within the ranges  $C \in [2^{-5}, 2^{-3}, \dots, 2^{13}, 2^{15}]$  and  $\sigma \in [2^{-15}, 2^{-13}, \dots, 2^1, 2^3]$ , in which  $C$  and  $\sigma$  stand for the SVM soft-margin parameter and the Radial Basis Function (RBF) kernel variance values, respectively.

phase. Such percentages were empirically chosen, being reasonable to have the same proportion of samples for both sets. Very often, medical-dependent applications suffer from the lack of data, and it is quite usual to find works that make use of larger training sets to alleviate this problem. In this work, we decided to keep a fair distribution among the sets in order to evaluate the proposed approach. In addition, we evaluated the robustness of the experiments over two versions of the datasets: (i) the first one uses images of  $64 \times 64$  pixels, and the second one (ii) uses images of  $128 \times 128$  pixels. Since the original images have a higher resolution (they were manually cropped from the exams), we decided to evaluate the robustness of the proposed approach under different scenarios.

Aiming at evaluating the experiments by means of statistical analysis, we randomly generated 10 different training and testing sets. The statistical evaluation was carried out by means of the Wilcoxon signed-rank test with significance of 0.05 (WILCOXON, 1945a). As aforementioned, the experiments were divided into two steps: (i) the first one concerns the single assessment, where CNN, OPF, SVM and N ave-Bayes were evaluated on each exam individually (Section 4.3.2), and the second step (ii) consists the combined assessment, which considers the output of each classifier over the individual exam in a majority voting-based schema to produce the final results (Section 4.3.3).

In regard to the source-code, we used the well-known Caffe library<sup>4</sup> (JIA et al., 2014), which is developed under GPGPU (General-Purpose computing on Graphics Processor Units) platform, thus providing more efficient implementations concerning CNNs. With respect to OPF and SVM, we used the LibOPF (PAPA; SUZUKI; X, 2014) and libSVM (CHANG; LIN, 2011), respectively, and for N ave-Bayes we used our own implementation. Additionally, we considered two different CNN architectures to provide a deeper experimental analysis:

1. ImageNet: composed of 5 convolution layers, 5 pooling layers and 2 normalization layers. It is also constituted by 5 ReLU layers among the convolution ones, 2 inner product layers, 2 dropout layers, 1 softmax loss layer and 1 accuracy layer for testing purposes. The first convolutional layer uses a kernel size of  $11 \times 11$  with stride of 4, and the second convolutional layer employs a kernel size of  $5 \times 5$  with stride of 5 pixels. The next convolutional layers use kernels of size  $3 \times 3$  with stride of 1 pixel.
2. Cifar-10: a quick version is used, composed of 3 convolution layers and 3 pooling layers. It is also constituted by 3 ReLU layers among the convolution ones, 2 inner product layers, 1 softmax loss layer and 1 accuracy layer for testing intentions. All convolutional layers employ kernels of size  $5 \times 5$  with stride of 1.

---

<sup>4</sup><http://caffe.berkeleyvision.org>

Since the images used in the experiments are domain-specific, we did not employ transfer learning, i.e. we opted to train the networks using our own datasets. In addition, we used 10,000 training iterations with mini-batches of size 16 concerning CNN experiments.

### 4.3.2 Single-Assessment

This section aims at presenting the experimental results concerning the CNN-based Parkinson's Disease identification over the individual exams. As aforementioned in Section 6.3.2, we compared two distinct CNN architectures and three baseline approaches. Tables I and II present the average results regarding the single-assessment results. The most accurate results, according to Wilcoxon signed-rank test, are in bold. Table I presents the overall accuracy, while Table II presents the recognition rates per class. In regard to the overall recognition rates, we employed an accuracy measure proposed by Papa et al. (PAPA; FALCÃO; SUZUKI, 2009) that considers unbalanced datasets, which is often faced in medical diagnosis applications.

One can observe CNN-based features obtained the most accurate results for all experiments, being SVM similar to CNN-ImageNet concerning "Exam 4" dataset with  $128 \times 128$  images. Roughly speaking, the results over the images with higher resolution were slightly more accurate, but it does not seem to play a big role. The main difference when working with images with different resolution concerns CNN-Cifar10 architecture, which has been considerably affected by images with higher resolution. Since we used a "quick version" of Cifar10 architecture, i.e. a shallower network, images with higher resolution may require more neurons, and thus a deeper neural network. Therefore, we can conclude the CNN-Cifar10 network has overfitted the data. Although the images showed in Figure 4.6 seem to be texture-oriented, they do not reflect the whole dataset, which can explain the results using GLCM and LBP feature extraction algorithms. Interestingly, the raw data achieved similar results to the texture-based ones, which means the real problem is the identification of early-stage-affected patients, as discussed later on Section 4.3.4.

Additionally, "Exam 4" (i.e. meanders) has the better discriminative ability, since it obtained the best recognition rates concerning the different resolutions and architectures. Actually, a finer statistical evaluation by means of Wilcoxon test pointed out both "Exam 3" and "Exam 4" are similar to each other concerning  $64 \times 64$  images, but "Exam 4" is the sole best approach concerning  $128 \times 128$  images. However, a closer look at the recognition rates shows us a quite similar behavior among the different image resolution experiments. Therefore, without loss of generality, we can assume both "Exam 3" and "Exam 4" are similar to each other when we consider the overall (global) accuracy.

**Tabela 4.1: Average overall accuracy over the test set considering the six exams, different image resolutions and classification/feature extractor techniques**

| Classifier   | Accuracy(%) - <b>64x64</b>   |                     |                     |                     |                     |                     |
|--------------|------------------------------|---------------------|---------------------|---------------------|---------------------|---------------------|
|              | Exam 1                       | Exam 2              | Exam 3              | Exam 4              | Exam 5              | Exam 6              |
| CNN-ImageNet | <b>67.75 ± 3.86</b>          | 68.04 ± 9.02        | <b>78.02 ± 2.48</b> | <b>80.15 ± 2.91</b> | <b>72.56 ± 4.72</b> | <b>74.23 ± 5.60</b> |
| CNN-Cifar10  | <b>68.04 ± 4.17</b>          | <b>71.62 ± 4.04</b> | 73.77 ± 5.20        | <b>80.13 ± 2.54</b> | 70.93 ± 0.77        | 66.34 ± 9.98        |
| OPF-Raw      | 57.26 ± 4.71                 | 59.16 ± 2.31        | 71.79 ± 1.50        | 71.67 ± 3.41        | 61.04 ± 1.71        | <b>74.23 ± 5.60</b> |
| SVM-Raw      | 58.69 ± 3.76                 | 61.44 ± 2.00        | 74.61 ± 2.50        | 77.83 ± 5.34        | 55.49 ± 8.46        | 66.34 ± 9.98        |
| Bayes-Raw    | 54.82 ± 4.15                 | 58.11 ± 1.22        | 73.45 ± 1.76        | 73.54 ± 3.53        | 61.40 ± 4.12        | 55.64 ± 4.81        |
| OPF-GLCM     | 50.08 ± 7.62                 | 62.40 ± 8.98        | 68.76 ± 2.40        | 74.99 ± 2.98        | 54.38 ± 5.01        | 54.96 ± 7.22        |
| SVM-GLCM     | 53.18 ± 6.61                 | 51.01 ± 4.61        | 71.70 ± 4.42        | 76.25 ± 3.80        | 52.00 ± 5.77        | 54.57 ± 7.13        |
| Bayes-GLCM   | 58.00 ± 9.82                 | 51.82 ± 5.75        | 69.82 ± 4.62        | 72.63 ± 3.02        | 58.93 ± 9.89        | 55.39 ± 6.41        |
| OPF-LBP      | 56.20 ± 6.94                 | 56.17 ± 8.36        | 60.61 ± 3.93        | 58.24 ± 3.12        | 64.33 ± 4.99        | 59.43 ± 6.15        |
| SVM-LBP      | 49.40 ± 0.98                 | 50.28 ± 4.55        | 64.09 ± 7.10        | 62.29 ± 6.90        | 61.98 ± 9.89        | 59.46 ± 7.65        |
| Bayes-LBP    | 52.24 ± 6.69                 | 58.04 ± 2.96        | 64.46 ± 4.80        | 64.43 ± 3.41        | 64.58 ± 5.58        | 69.64 ± 8.04        |
| Classifier   | Accuracy(%) - <b>128x128</b> |                     |                     |                     |                     |                     |
|              | Exam 1                       | Exam 2              | Exam 3              | Exam 4              | Exam 5              | Exam 6              |
| CNN-ImageNet | <b>68.04 ± 2.96</b>          | <b>73.41 ± 3.66</b> | <b>78.26 ± 1.97</b> | <b>80.75 ± 2.08</b> | <b>73.59 ± 3.57</b> | <b>76.32 ± 5.18</b> |
| CNN-Cifar10  | 55.46 ± 3.25                 | 61.98 ± 8.52        | 52.10 ± 19.09       | 60.94 ± 14.12       | 52.05 ± 2.81        | 50.97 ± 2.17        |
| OPF-Raw      | 58.09 ± 3.13                 | 61.79 ± 2.50        | 72.83 ± 2.20        | 76.28 ± 2.91        | 59.58 ± 3.96        | 52.86 ± 4.87        |
| SVM-Raw      | 58.39 ± 7.40                 | 64.61 ± 2.50        | 77.17 ± 4.00        | <b>80.74 ± 3.22</b> | 58.21 ± 8.61        | 56.86 ± 6.39        |
| Bayes-Raw    | 57.55 ± 3.69                 | 63.45 ± 1.76        | 72.11 ± 3.33        | 74.38 ± 4.80        | 62.11 ± 3.47        | 51.79 ± 3.73        |
| OPF-GLCM     | 46.40 ± 6.47                 | 57.48 ± 7.23        | 66.59 ± 2.31        | 75.97 ± 2.34        | 55.65 ± 4.14        | 58.64 ± 3.49        |
| SVM-GLCM     | 57.11 ± 5.23                 | 53.10 ± 4.85        | 71.07 ± 3.48        | 79.46 ± 3.50        | 52.06 ± 6.06        | 58.79 ± 7.51        |
| Bayes-GLCM   | 54.42 ± 5.79                 | 53.04 ± 5.30        | 68.33 ± 3.81        | 74.15 ± 3.04        | 56.83 ± 8.66        | 54.54 ± 6.78        |
| OPF-LBP      | 54.63 ± 5.95                 | 55.71 ± 5.97        | 61.49 ± 4.00        | 66.09 ± 4.18        | 64.33 ± 9.35        | 56.68 ± 6.43        |
| SVM-LBP      | 50.42 ± 3.60                 | 48.65 ± 4.03        | 60.51 ± 6.96        | 65.65 ± 5.46        | 61.54 ± 8.84        | 63.32 ± 10.60       |
| Bayes-LBP    | 60.05 ± 5.20                 | 52.13 ± 5.73        | 63.65 ± 3.50        | 63.81 ± 4.13        | 57.01 ± 5.67        | 68.50 ± 8.11        |

Table II presents the results per class using the following format  $x(y)$ , where  $x$  and  $y$  stand for the accuracy concerning the patients and the control group, respectively. Since our dataset is not balanced, it is quite useful to provide the recognition rates per class. In general, the recognition rates are quite good, being the bottleneck of the proposed approach the recognition rates over control individuals. Although we have more control people than PD patients, a considerable number of healthy individuals were classified as patients, since the dataset comprises PD patients with exams quite close to the ones performed by healthy individuals. Texture-based and raw data information achieved reasonable recognition rates concerning the patients group, but their global accuracy were considerably affected due to the effectiveness over the control group. As aforementioned, we assume two types of problems: (i) first, the dataset is not balanced (less control group), and (ii) we have a number of early-stage patients, which means they behave similarly to healthy individuals. As a matter of fact, we observed a very few control individuals that have similar drawings to a patient one in his/her advanced state of disease. Probably, the individual was affected by another disease, he/her was nervous during the exam, or even the exam was labeled incorrectly.

The best results concerning  $64 \times 64$  images were obtained by SVM over "Exam 5" for patient identification (96.43%), and the more accurate recognition rates considering the control group were obtained by CNN-Cifar10 over "Exam 4". In regard to  $128 \times 128$  images, CNN-

Cifar10 obtained 99.30% of recognition rate concerning patients, and CNN-ImageNet obtained 70.51% of accuracy considering the control group. Roughly speaking, meanders (“Exam 4”) appear to be the most important test to identify healthy people, and “Exam 5” and “Exam 6” (right- and left-wrist movements) seemed to be the best ones to recognize PD patients. Although we can observe pretty much different exams (Figures 4.4 and 4.5) between patients and control group, the problem gets worse when we have patients at the very early stage of the disease, which may have quite close exams. However, the left- and right-wrist movements (“Exam 5” and “Exam 6”) seems to detect some subtle disorders in the motor system, thus obtaining better results.

**Tabela 4.2: Average class accuracy over the test set considering the six exams, different image resolutions and classification/feature extractor techniques**

| Classifier   | Accuracy(%) - <b>64x64</b>   |                        |                        |                               |                        |                        |
|--------------|------------------------------|------------------------|------------------------|-------------------------------|------------------------|------------------------|
|              | Exam 1                       | Exam 2                 | Exam 3                 | Exam 4                        | Exam 5                 | Exam 6                 |
| CNN-ImageNet | 81.19 ( <b>54.31</b> )       | 83.04 (53.04)          | 89.23 ( <b>67.20</b> ) | <b>88.91</b> (71.38)          | 94.10 (51.03)          | 85.57 ( <b>62.98</b> ) |
| CNN-Cifar10  | 83.68 ( <b>54.20</b> )       | 83.12 ( <b>60.12</b> ) | <b>90.69</b> (56.86)   | 85.68 ( <b>74.60</b> )        | 85.44 ( <b>56.43</b> ) | 73.43 (59.24)          |
| OPF-Raw      | 79.29 (35.24)                | 80.49 (37.84)          | 90.39 (53.20)          | 85.71 (57.62)                 | 85.71 (36.36)          | 79.29 (32.00)          |
| SVM-Raw      | 87.76 (29.52)                | 87.86 (35.02)          | <b>91.59</b> (57.64)   | <b>89.46</b> (66.19)          | <b>96.43</b> (14.55)   | 83.57 (48.00)          |
| Bayes-Raw    | 78.21 (31.43)                | 79.61 (36.63)          | 89.73 (57.18)          | 86.61 (60.48)                 | 86.43 (36.36)          | 85.00 (34.00)          |
| OPF-GLCM     | 81.06 (19.11)                | 85.71 (39.10)          | 82.05 (55.47)          | 85.43 (64.52)                 | 77.85 (30.94)          | 73.93 (36.00)          |
| SVM-GLCM     | 89.99 (16.37)                | 89.29 (12.74)          | 89.12 (54.30)          | 86.07 (66.42)                 | 90.35 (13.65)          | <b>92.15</b> (17.00)   |
| Bayes-GLCM   | 79.64 (36.38)                | 79.99 (23.66)          | 86.06 (53.58)          | 85.26 (60.01)                 | 87.86 (30.02)          | 81.79 (29.00)          |
| OPF-LBP      | 77.86 (34.57)                | 81.42 (30.93)          | 83.83 (37.39)          | 79.10 (37.40)                 | 73.23 (55.44)          | 87.86 (31.00)          |
| SVM-LBP      | <b>96.07</b> (2.73)          | <b>89.64</b> (10.92)   | 88.66 (39.53)          | 88.38 (36.19)                 | 92.14 (31.83)          | 83.92 (35.00)          |
| Bayes-LBP    | 73.56 (30.93)                | 86.07 (30.03)          | 81.06 (47.85)          | 81.24 (47.63)                 | 86.44 (42.76)          | 89.29 (50.00)          |
| Classifier   | Accuracy(%) - <b>128x128</b> |                        |                        |                               |                        |                        |
|              | Exam 1                       | Exam 2                 | Exam 3                 | Exam 4                        | Exam 5                 | Exam 6                 |
| CNN-ImageNet | 81.30 ( <b>54.78</b> )       | 82.33 ( <b>64.48</b> ) | 88.19 ( <b>68.36</b> ) | <b>90.99</b> ( <b>70.51</b> ) | 94.77 ( <b>52.41</b> ) | 92.52 ( <b>60.13</b> ) |
| CNN-Cifar10  | 89.74 (21.18)                | 84.65 (39.31)          | 84.17 (20.03)          | 72.81 (49.06)                 | <b>98.60</b> (5.50)    | <b>99.30</b> (2.64)    |
| OPF-Raw      | 74.29 (41.90)                | 82.69 (40.90)          | 82.32 (63.36)          | 88.95 (63.62)                 | 86.63 (32.73)          | 85.71 (20.00)          |
| SVM-Raw      | 88.21 (28.57)                | <b>88.46</b> (40.81)   | <b>91.74</b> (62.62)   | <b>91.46</b> ( <b>69.99</b> ) | 96.43 (20.00)          | 95.71 (22.00)          |
| Bayes-Raw    | 76.07 (39.05)                | 84.05 (42.87)          | 87.50 (56.73)          | 86.49 (62.30)                 | 87.86 (36.36)          | 83.57 (20.00)          |
| OPF-GLCM     | 76.44 (16.38)                | 76.78 (38.21)          | 84.35 (48.82)          | 86.69 (65.23)                 | 78.56 (32.75)          | 79.28 (38.00)          |
| SVM-GLCM     | 87.86 (26.37)                | <b>88.94</b> (17.29)   | 89.30 (52.86)          | 88.94 (69.99)                 | 93.21 (10.92)          | 88.57 (29.00)          |
| Bayes-GLCM   | 74.28 (34.56)                | 76.07 (30.02)          | 83.56 (53.10)          | 85.44 (62.84)                 | 88.21 (25.48)          | 81.06 (28.00)          |
| OPF-LBP      | 81.08 (28.20)                | 71.44 (40.02)          | 83.93 (39.04)          | 85.27 (46.91)                 | 83.21 (45.47)          | 80.33 (33.00)          |
| SVM-LBP      | <b>93.58</b> (7.28)          | <b>88.20</b> (9.10)    | 86.25 (34.76)          | 84.65 (46.67)                 | 90.36 (32.74)          | 94.64 (32.00)          |
| Bayes-LBP    | 74.64 (45.47)                | 76.09 (28.21)          | 82.76 (44.53)          | 79.99 (47.60)                 | 88.58 (25.48)          | 95.00 (42.00)          |

### 4.3.3 Combined-Assessment

In this section, we present the results concerning the proposed approach that considers the combination among all decisions made by the classifiers trained on each individual exam (Figure 4.7). Table 4.3 presents the overall (global) accuracy, being the best results in bold according to Wilcoxon statistical test. Clearly, we can observe the proposed approach improved the results presented in Table I considerably, confirming our hypothesis that different exams encode/model different handwritten dynamic properties. Also, CNN-ImageNet obtained the best results so far, being consistent more accurate than the compared approaches. Notice that

GLCM-based features obtained results similar to the ones achieved by CNN-ImageNet when we use the ensemble of classifiers. However, as one can further observe in Table 4.4, CNNs are more consistent to the different exams, i.e. they have been consistently the best learners for all exams, which does not happen when dealing with the texture descriptors.

**Tabela 4.3: Average overall accuracy over the test set considering the combined-assessment approach.**

| Classifier   | Accuracy(%) - Voting |                     |
|--------------|----------------------|---------------------|
|              | 64x64                | 128x128             |
| CNN-ImageNet | <b>93.42 ± 3.17</b>  | <b>95.74 ± 1.60</b> |
| CNN-Cifar10  | 90.28 ± 6.09         | 76.96 ± 21.60       |
| OPF-Raw      | 79.44 ± 2.67         | 82.44 ± 4.54        |
| SVM-Raw      | 74.80 ± 9.32         | 70.56 ± 3,56        |
| Bayes-Raw    | 85.51 ± 1.98         | 83.45 ± 3.48        |
| OPF-GLCM     | <b>93.01 ± 3.64</b>  | <b>95.21 ± 2.13</b> |
| SVM-GLCM     | 79.23 ± 8.23         | <b>95.21 ± 2.13</b> |
| Bayes-GLCM   | <b>93.05 ± 3.97</b>  | 93.48 ± 2.78        |
| OPF-LBP      | 90.21 ± 2.56         | 91.14 ± 4.56        |
| SVM-LBP      | 69.98 ± 14.43        | 75.03 ± 9.57        |
| Bayes-LBP    | 91.14 ± 2.68         | 88.17 ± 4.59        |

Table 4.4 presents the results for each class using the very same format employed in the previous section, i.e. the number in parenthesis stands for the mean accuracy concerning the control group. Once again, the ensemble of CNNs provided a considerable enhancement considering the recognition rates for both patients and control group. Also, the baseline classifiers benefited from such process, being their accuracies increased for both patients and healthy people recognition. We can conclude the best trade-off between patient and control group recognition was obtained by means of CNN-ImageNet with  $128 \times 128$  images. In this case, higher resolution images played an important role, despite the individual experiments that highlighted different image sizes are not so important to the classification process.

#### 4.3.4 Early Stage Detection

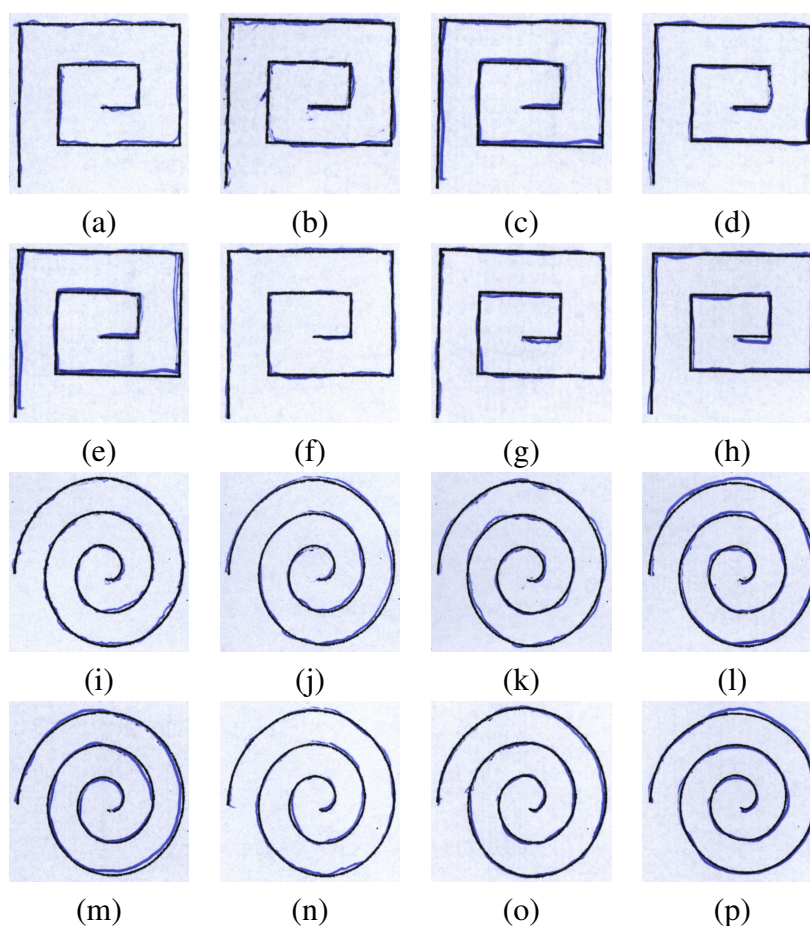
The main challenge regarding PD concerns its detection at early stages, where the symptoms are almost imperceptible. In order to evaluate the robustness of the proposed approach when identifying patients with Parkinson's Disease in its early stage, we have manually selected eight patients with very similar traces to healthy individuals. Figure 4.8 presents some images of the selected individuals. Notice these patients can perform the tasks nearly to a healthy individual.

Figure 4.9 displays some time series extracted from selected exams concerning Figure 4.8.



**Tabela 4.4: Average class accuracy over the test set considering the combined-assessment approach.**

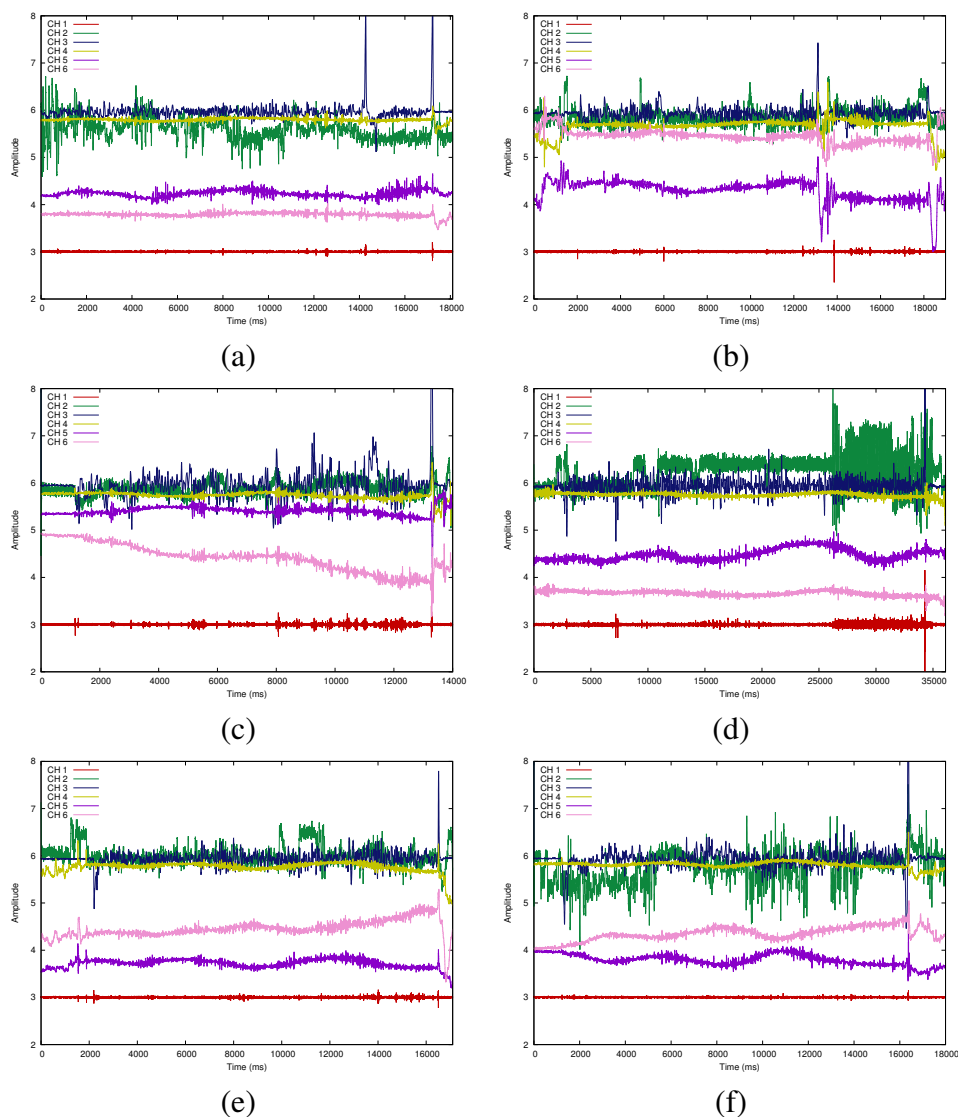
| Classifier   | Accuracy(%) - Voting   |                        |
|--------------|------------------------|------------------------|
|              | 64x64                  | 128x128                |
| CNN-ImageNet | 97.84 ( <b>89.00</b> ) | 97.48 ( <b>94.01</b> ) |
| CNN-Cifar10  | 98.56 (82.00)          | 98.92 (55.00)          |
| OPF-Raw      | <b>100.00</b> (58.87)  | <b>100.00</b> (64.33)  |
| SVM-Raw      | <b>100.00</b> (49.59)  | <b>100.00</b> (41.11)  |
| Bayes-Raw    | <b>100.00</b> (71.01)  | <b>100.00</b> (66.90)  |
| OPF-GLCM     | 98.02 (88.00)          | 98.92 (91.50)          |
| SVM-GLCM     | 94.97 (63.50)          | 98.92 (91.50)          |
| Bayes-GLCM   | 99.10 (87.00)          | 99.46 (87.50)          |
| OPF-LBP      | 98.92 (81.50)          | 99.28 (83.00)          |
| SVM-LBP      | 99.46 (40.50)          | 98.56 (51.50)          |
| Bayes-LBP    | 99.28 (83.00)          | 97.84 (78.50)          |



**Figure 4.8: Examples of meander (first and second row) and spiral (third and fourth row) images obtained by some patients in the early stages of the disease.**

Clearly, one can observe the signals extracted from those exams present a shaky behaviour, i.e., the smart pen can really capture subtle movements during the exam, which can not be observed in the handwritten exams by means of a visual inspection. The time series depicted in Figure 4.9 are pretty much similar to those presented in Figure 4.3, which shows the signals extracted from

an advanced-stage patient.



**Figure 4.9: Time series concerning the patient group: (a) Figure 4.8a, (b) Figure 4.8c, (c) Figure 4.8e, (d) Figure 4.8i, (e) Figure 4.8k, and (f) Figure 4.8m.**

For each selected patient, we computed the accuracy of both meander and spiral images considering the very same datasets generated in the previous experiments. Table 4.5 presents the accuracy concerning these selected images. Clearly, one can draw two main conclusions: (i) first, CNN-based features (Cifar10 and ImageNet) presented the highest accuracy rates compared to other approaches, and (ii) the proposed approach is robust enough to detect early-stage PD patients, since they obtained quite good recognition rates (above 94%). The high standard deviation values concerning raw and texture-based features indicate they are able to either recognize or miss the majority of early-stages PD patients.

**Tabela 4.5: Average accuracy over the early stage (selected) images.**

| Accuracy (%) <b>64x64</b>   |                     |                     |
|-----------------------------|---------------------|---------------------|
| Classifier                  | Exam 3              | Exam 4              |
| CNN-Cifar10                 | <b>95.83 ± 7.04</b> | <b>94.01 ± 6.72</b> |
| CNN-ImageNet                | <b>96.35 ± 8.08</b> | <b>94.01 ± 6.23</b> |
| Bayes-Raw                   | 52.08 ± 46.09       | 51.04 ± 48.57       |
| OPF-Raw                     | 51.04 ± 46.63       | 52.20 ± 45.49       |
| SVM-Raw                     | 50.00 ± 47.53       | 50.00 ± 47.91       |
| Bayes-GLCM                  | 52.08 ± 43.35       | 51.04 ± 50.28       |
| OPF-GLCM                    | 47.91 ± 44.93       | 50.00 ± 53.45       |
| SVM-GLCM                    | 53.15 ± 49.17       | 47.91 ± 49.75       |
| Bayes-LBP                   | 51.04 ± 47.02       | 55.20 ± 42.47       |
| OPF-LBP                     | 48.95 ± 47.02       | 54.16 ± 39.08       |
| SVM-LBP                     | 52.08 ± 47.50       | 51.04 ± 50.48       |
| Accuracy (%) <b>128x128</b> |                     |                     |
| Classifier                  | Exam 3              | Exam 4              |
| CNN-Cifar10                 | <b>95.83 ± 7.04</b> | <b>94.01 ± 6.72</b> |
| CNN-ImageNet                | <b>96.35 ± 8.08</b> | <b>94.01 ± 6.23</b> |
| Bayes-Raw                   | 47.91 ± 44.04       | 51.04 ± 46.83       |
| OPF-Raw                     | 48.95 ± 48.57       | 50.00 ± 45.74       |
| SVM-Raw                     | 50.00 ± 51.63       | 47.91 ± 49.76       |
| Bayes-GLCM                  | 54.16 ± 45.42       | 52.08 ± 51.31       |
| OPF-GLCM                    | 53.12 ± 48.37       | 53.12 ± 50.38       |
| SVM-GLCM                    | 52.08 ± 51.51       | 53.12 ± 47.96       |
| Bayes-LBP                   | 42.70 ± 40.44       | 45.83 ± 37.26       |
| OPF-LBP                     | 43.74 ± 44.09       | 43.75 ± 39.27       |
| SVM-LBP                     | 46.85 ± 44.52       | 51.04 ± 42.82       |

## 4.4 Conclusions

In this paper, we cope with the problem of PD identification by means of Convolutional Neural Networks. Basically, the idea is to model the handwritten dynamics as a time series, and to use it as an input to a CNN, which will be able to learn features that are used to distinguish healthy individuals from PD patients. The main contributions of this paper rely on three main aspects: (i) to employ a deep learning-oriented approach to aid Parkinson’s Disease diagnosis, (ii) to design a signal-based dataset composed of features related to handwritten dynamics, and (iii) to propose an ensemble of CNNs to better distinguish PD patients from control group.

The experimental section comprised different CNN architectures, as well as images with different resolutions and distinct training set sizes. The results obtained by CNNs were compared against the raw data and texture descriptors classified by means of the traditional pattern recognition techniques. These results shows to be very promising, since CNNs were able to learn important features to differentiate PD patients from healthy individuals, thus obtaining very good results over the datasets. The ensemble of CNNs depicted to be able to capture different information from each exam, thus providing considerably better results.

In regard to future works, we intend to combine the original image obtained through the exam together with the time series-based version. Also, we plan to apply Auto-encoders right after CNNs in order to reduce the dimensionality of the feature space.

# Capítulo 5

## AUXÍLIO AO DIAGNÓSTICO DA DOENÇA DE PARKINSON UTILIZANDO DINÂMICA DE ESCRITA E APRENDIZADO EM PROFUNDIDADE

---

---

Aceito para publicação na 30th Conference on Graphics, Patterns and Images - (Sibgrapi 2017), é apresentado nesta sessão o artigo *Parkinson's Disease Identification Through Deep Optimum-Path Forest Clustering*, que é voltado à identificação automática de indivíduos portadores do mal de Parkinson através de aprendizagem profunda.

### 5.1 Introduction

The cure for neurodegenerative diseases has been constantly researched by Medicine, mainly with respect to Parkinson's disease (PD), which affects nearly 1 million people only in the United States, and around 7 to 10 million people might be living with PD worldwide. Also, the number of new cases diagnosed each year ranges between 50,000 to 60,000 individuals according to the National Parkinson's Foundation (FOUNDATION, 2017). Parkinson's disease is characterized by motor dysfunctions, it is a chronic, progressive and multilesion disease caused by the loss of a neurotransmitter called *Dopamine* (LEES; HARDY; REVESZ, 2009). Such illness is usually diagnosed through a clinical exam by a neurologist with expertise in movement analysis. The PD is considered non-lethal, but people with PD have a shorter life expectancy than the general population.

More often in the elderly population, PD produces alterations in gait and posture that may increase the risk of falls and lead to mobility disabilities. As such, it impacts daily activities and reduces the quality of life concerning patients and their families (MAKI; MCILROY, 2005; MAR-

CHETTI; WHITNEY, 2005; ZHAO et al., 2008), especially because it does not have cure to date. Drugs known as dopaminergic medications and therapy are currently used to treat PD symptoms, being the *Levodopa* (L-dopa) the most widely used for such purpose. Another treatment that has been widely employed is the Deep Brain Stimulation, which is a surgical procedure that delivers electrical pulses to brain cells in order to reduce the effects of the symptoms.

The science does not measure efforts in order to make the quality of life of PD patients better. In computer science, for instance, techniques such as image processing, neural networks and others have been widely applied in the pursuit of better results in both treatment and diagnosis. Spadotto et al. (SPADOTTO et al., 2010b), for instance, introduced the Optimum-Path Forest (OPF) (PAPA; FALCÃO; SUZUKI, 2009; PAPA et al., 2012) classifier to aid the automatic identification of Parkinson's disease. Later on, the same group proposed an evolutionary-based approach to select the most discriminative set of features that helped improving PD recognition rates (SPADOTTO et al., 2011).

Most works that address automatic PD recognition deal with voice-based data. Procedures to identify voiced and unvoiced (silent) periods have been actively pursued to analyze continuous speech samples, since most techniques that quantify periodicity and regularity in voice signals are applied in the voiced regions only (SHAHBAKHI; FAR; TAHAMI, 2014). Das (DAS, 2010) presented a comparison of multiple classification methods for the diagnosis of PD, such as neural networks, regression and decision trees. Several evaluation methods were employed to calculate the performance of the classifiers, being the experiments conducted in a dataset composed of biomedical voice measurements from 31 people, in which 23 were diagnosed with Parkinson's disease. The best results were achieved by neural networks (around 92.9% of PD recognition rate).

Recently, Pereira et al. (PEREIRA et al., 2015, 2016) proposed to extract features from handwritten exams using visual features, which are learned from some drawings the patients were asked to perform, being the data used in the work made available in a dataset called "HandPD"<sup>1</sup>. Later on, Pereira et al. (PEREIRA et al., 2016b) drove its approach to a deep learning application using the signals (time series) captured by the biometric pen *BiSP*<sup>®</sup> (TEAM REGENSBURG, 2002), which were further converted to the image domain with different resolutions and used as input to a Convolutional Neural Network.

Another interesting methodology to learn discriminative features from data is related to the well-known Bag-of-words (BoW), though being quite difficult to establish the size of the bag (dictionary), as well as another open problem is how to choose the words that will compose that

---

<sup>1</sup><http://www.fc.unesp.br/~papa/pub/datasets/Handpd/>

bag. Some years ago, Afonso et al. (AFONSO et al., 2012b) proposed to use the unsupervised OPF (ROCHA; CAPPABIANCO; FALCÃO, 2009) to learn proper dictionaries since it does not require the number of words beforehand, thus becoming an useful tool for BoW purposes. Later on, Afonso et al. (AFONSO et al., 2016) presented a deep-hierarchical OPF (dOPF) clustering algorithm to make it way more efficient, and validated it in the context of seismic-geological data classification.

Although BoW usage is not new in the context of time series for biomedical purposes (WANG et al., 2013), to best of our knowledge, it has not been applied for the identification of Parkinson’s disease along with graph-based clustering algorithms so far, which turns out to be the main contribution of this work. Another main contribution is to use dOPF to learn dictionaries in a hierarchical way, where different layers of knowledge are used to compose the final dictionary. In short, the main idea of this work is to employ dOPF in the context of BoW applied for Parkinson’s disease detection using the time series data from the HandPD dataset. The remainder of this work is organized as follows: Section 5.2 describes the theoretical background related to both OPF and dOPF. Our proposed approach is detailed in Section 5.3. The experimental setup, dataset and results are presented in Section 6.4. Finally, Section 5.5 states conclusions and future works.

## 5.2 Optimum-Path Forest Clustering

The main problem in unsupervised learning is to identify clusters in a dataset  $\mathcal{L}$ , in which samples belonging to the same group should share some level of similarity. The Optimum-Path Forest clustering algorithm handles this problem as a graph partition task, where a competitive process among prototype samples (a subset from  $\mathcal{L}$ ) offers optimum-cost paths to the remaining samples in order to “conquer” them. The outcome of this competition process is a collection of trees (forest) rooted at each prototype, in which each tree represents a different cluster.

Given the dataset  $\mathcal{L}$ , we can create a graph  $(\mathcal{L}, \mathcal{A}_k)$ , where  $\mathcal{A}_k$  is a  $k$ -nearest neighbors adjacency relation, and each sample  $\mathbf{x} \in \mathcal{L}$  encodes a graph node in  $\mathfrak{R}^n$ , i.e., it basically stands for a feature vector extracted from a dataset sample. Let  $d(\mathbf{s}, \mathbf{t})$  be the distance between graph nodes  $\mathbf{s}$  and  $\mathbf{t}$ , being the edge connecting such samples (i.e.,  $(\mathbf{s}, \mathbf{t})$ ) weighted by that distance. Also, a given node  $\mathbf{s}$  is weighted by a probability density function (pdf)  $\rho(\mathbf{s})$  defined as follows:

$$\rho(\mathbf{s}) = \frac{1}{\sqrt{2\pi\sigma^2} |\mathcal{A}(\mathbf{s})|} \sum_{\forall \mathbf{t} \in \mathcal{A}(\mathbf{s})} \exp\left(\frac{-d^2(\mathbf{s}, \mathbf{t})}{2\sigma^2}\right), \quad (5.1)$$

in which  $\sigma = \frac{d_f}{3}$ , and  $d_f$  is the length of the longest edge in  $(Z, \mathcal{A}_k)$ . The choice of this parameter considers all nodes for density computation since a Gaussian function covers most samples within  $d(\mathbf{s}, \mathbf{t}) \in [0, 3\sigma]$ . The Parzen-window method is the most common method to estimate a probability density function, and is provided by Equation 5.1 based on the isotropic Gaussian kernel when the arcs are defined by  $(\mathbf{s}, \mathbf{t}) \in \mathcal{A}_k$  if  $d(\mathbf{s}, \mathbf{t}) \leq d_f$ .

This approach, however, presents some issues with the differences in scale and sample concentration, which can be solved by adaptive choices of  $d_f$  depending on the region of the feature space (COMANICIU, 2003). By choosing the best value for the  $k$ -nearest neighbors within  $[1, k_{max}]$ , for  $1 \leq k_{max} \leq |\mathcal{Z}|$ , it is possible to tackle both issues of different concentration and scale reduction. Rocha et al. (ROCHA; CAPPABIANCO; FALCÃO, 2009) proposed a solution by considering the minimum graph cut provided by clustering results for  $k \in [1, k_{max}]$ , according to a measurement suggested by Shi and Malik based on graph cuts (SHI; MALIK, 2000).

Let  $\pi_{\mathbf{t}}$  a path in  $(Z, \mathcal{A}_k)$  that can be defined as a sequence of adjacent nodes that starts in a root  $R(\mathbf{t})$  and ends at a sample  $\mathbf{t}$ , being  $\pi_{\mathbf{t}} = \langle \mathbf{t} \rangle$  a trivial path, and  $\pi_{\mathbf{s}} \cdot \langle \mathbf{s}, \mathbf{t} \rangle$  the concatenation of  $\pi_{\mathbf{s}}$  and arc  $(\mathbf{s}, \mathbf{t})$ . The main point is to find a path whose lowest density value is maximum among all possible paths  $\pi_{\mathbf{t}}$  with roots on the maxima of the pdf. Thus, each maximum should define an influence zone (cluster) by selecting samples that are more strongly connected to it than to any other maximum. Formally, this process can be defined as the maximization of  $f(\pi_{\mathbf{t}})$  for all  $\mathbf{t} \in \mathcal{Z}$ , such that

$$\begin{aligned} f(\langle \mathbf{t} \rangle) &= \begin{cases} \rho(\mathbf{t}) & \text{if } \mathbf{t} \in \mathcal{S} \\ \rho(\mathbf{t}) - \delta & \text{otherwise} \end{cases} \\ f(\langle \pi_{\mathbf{s}} \cdot \langle \mathbf{s}, \mathbf{t} \rangle \rangle) &= \min\{f(\pi_{\mathbf{s}}), \rho(\mathbf{t})\} \end{aligned} \quad (5.2)$$

for  $\delta = \min_{\forall (\mathbf{s}, \mathbf{t}) \in \mathcal{A}_k | \rho(\mathbf{t}) \neq \rho(\mathbf{s})} |\rho(\mathbf{t}) - \rho(\mathbf{s})|$  and  $\mathcal{S}$  being a root set with one element for each maximum of the pdf. High values of delta reduce the number of maxima. This work sets  $\delta = 1.0$  and scales real numbers  $\rho(t) \in [1, 1000]$ . In summary, the OPF algorithm maximizes  $f(\pi_{\mathbf{t}})$  such that the optimum paths form an optimum-path forest — a predecessor map  $P$  with no cycles that assigns to each sample  $\mathbf{t} \notin \mathcal{S}$  its predecessor  $P(\mathbf{t})$  in the optimum path from  $\mathcal{S}$  or a marker *nil* when  $\mathbf{t} \in \mathcal{S}$ .

### 5.2.1 Deep-Hierarchical Optimum-Path Forest

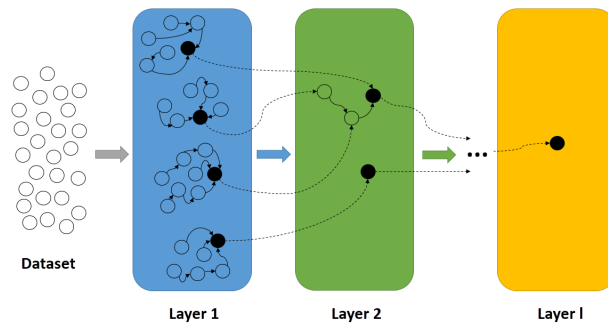
One of the main advantages of OPF concerns its capability in computing the number of clusters on-the-fly, which means such information is not required beforehand. On the other



hand, its bottleneck is to set the exact number of clusters when one knows that information. One possible solution is to consider different values for the parameter  $k_{max}$  in order to reach the desired number of clusters. However, the larger the dataset, the more costly this process will become.

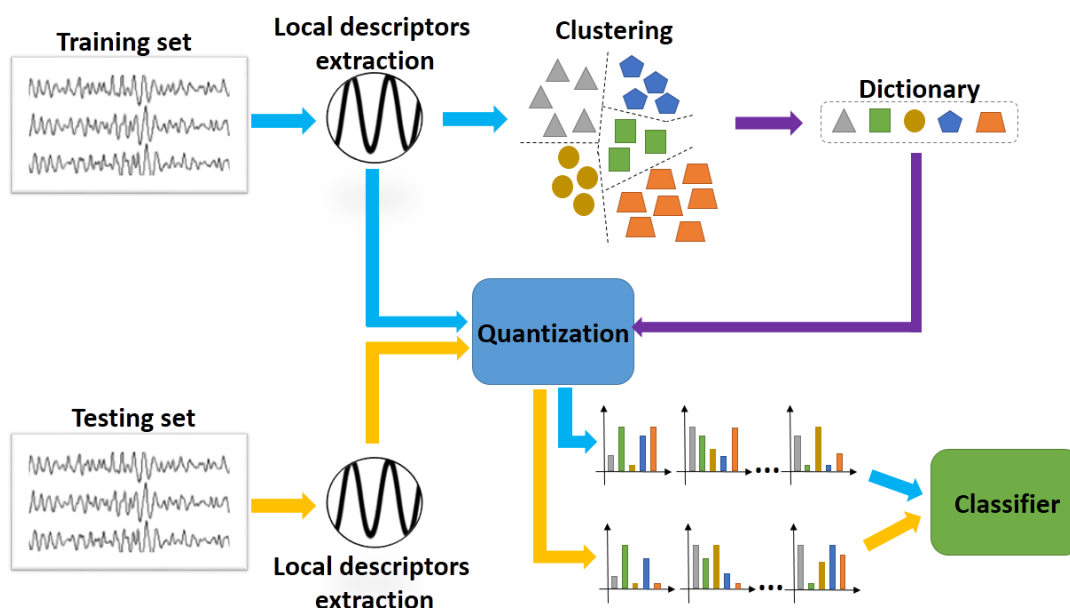
In order to overcome the aforementioned issue, Afonso et al. (AFONSO et al., 2016) proposed a multi-level clustering algorithm based on the OPF approach. Each level (layer) computes an OPF through the very same process as previously described using the roots (prototypes) from the OPF computed in the predecessor layer as new inputs. The number of layers is user-defined and set according to the number of clusters that is supposed to be reached (or close to) in the last layer. Since the prototypes are located in the highest density regions, they are very suitable to represent nearby samples, as argued in the works conducted by Castelo and Calderón-Ruiz (CASTELO-FERNÁNDEZ; CALDERÓN-RUIZ, 2015) and Afonso et al. (AFONSO et al., 2012a).

Let  $\mathcal{S}_i$  be the set of prototypes at layer  $L_i$ ,  $i = 1, 2, \dots, l$ , in which  $l$  stands for the number of layers. Since each root will be the maximum of a pdf (Equation 5.1), we have a set of samples that fall in the same optimum-path tree and are represented by the very same prototype (root of that tree) in the next layer. In summary, the higher the number of layers, the less prototypes (clusters) one shall have, i.e.,  $|\mathcal{S}_1| < |\mathcal{S}_2| < \dots < |\mathcal{S}_l| < \dots \leq 1$ . Therefore, at layer  $l$ , one shall find only one cluster when  $l \rightarrow \infty$ . Figure 5.1 displays the OPF-based architecture for deep-driven feature space representation.



**Figure 5.1: Architecture of an  $l^{\text{th}}$ -layered dOPF.**

At layer  $L_1$ , it is observed four clusters (optimum-path trees), in which the black filled nodes stand for the set of prototypes at that layer, i.e.,  $\mathcal{S}_1$ . Some of these prototypes will become new prototypes at  $L_2$ , and others not (we can observe both filled and unfilled nodes at layer 2). This process is carried out up to the  $l^{\text{th}}$  layer specified by the user. Notice at the coarsest scale, i.e.,  $L_l$ , we shall find only one cluster. Therefore, the user can halt the process as soon as the number



**Figure 5.2: Proposed approach based on BoW and dOPF for computer-aided PD diagnosis.** The main workflow is indicated by the light blue arrows: local descriptors are extracted and clustered in order to build the dictionary. The dictionary is used for the quantization of both training and testing signals that is the process of computing the feature vectors (flow indicated by purple arrows). Similarly to the training phase, testing signals have their descriptors computed and the signals are quantized (flow indicated by yellow arrows). Finally, a classifier is fed by the resulting training and testing feature vectors. Notice the two depicted dictionaries are the same.

of desired clusters (or close to it) is met.

## 5.3 Proposed Approach

This section describes all steps performed in the work to evaluate dOPF and BoW in the context of Parkinson's disease identification, as depicted in Figure 5.2.

**Data acquisition** Individuals were submitted to a series of tasks, in which they were asked to perform some hand movements and drawings using a biometric pen that contains six sensors in charge of recording hand movements (Figure 5.3) (TEAM REGENSBURG, 2002). The movements are represented by six different channels: microphone, finger grip, axial pressure of ink refill, and tilt and acceleration in the  $x$ ,  $y$  and  $z$  directions.

Figure 5.4 depicts an example of an exam containing six tasks that evaluate the hand movements and help to detect any anomalies. In the first task (exam (a) in Figure 5.4), the individual is asked to draw a circle 12 times in the same place without stopping the movement between each circle. In the second task (exam (b) in Figure 5.4), the individual performs the same mo-

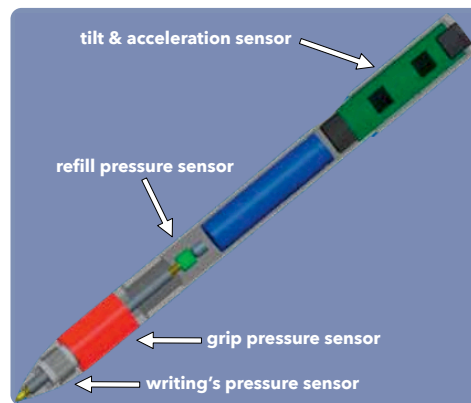


Figura 5.3: Biometric pen. Extracted from (PEREIRA et al., 2016b).

22/11/2010

Field study: Unesp 2010  
University of Applied Sciences  
Regensburg  
Biometric Smart Pen Project

Universidade Estadual Paulista  
Faculdade de Medicina (FMB),  
R. Dr. Acácio de Moraes Botucatu  
13061-900 Botucatu

Idade: 56 Mão dominante:  direita ( ) esquerda

|      |  |   |
|------|--|---|
| a, b | Desenhar círculo 12 vezes no mesmo lugar sem parar.      | Desenhar círculo no ar 12 vezes no mesmo lugar sem parar. |
| c    | Desenhar espiral após sinal sonoro, de dentro para fora. |   |
| d    | Desenhar meander após sinal sonoro, de dentro para fora. |   |
| e    | Diadococinesia: Mão direita 20 segundos.                 |   |
| f    | Diadococinesia: Mão esquerda 20 segundos.                |   |

Figura 5.4: Form used to assess the handwritten skills. Extracted from (PEREIRA et al., 2016b).

vement as in exam (a), but with its hand in the air. The third (exam (c) in Figure 5.4) and fourth (exam (d) in Figure 5.4) tasks concern drawing the spirals and meanders, respectively, over a guideline only once from the inner to the outer part. The last two tasks, i.e., exam (e) and exam (f) in Figure 5.4, stand for the diadochokines test, which is basically composed of hand-wrist movements performed with both hands. Each exam results in six different datasets, one for each task, and each sample from the dataset corresponds to an array of responses captured by each sensor in the interval of 1 ms.

**Local descriptor extraction** Given the recorded signals, the local descriptors are computed through a sliding window that goes along each of the six signals and computes a single-level Discrete Wavelet Transform (DWT) in each segment. In fact, since there are six different signals, we work with six sliding windows, in which the segments of time within each of them have always the same initial and final times as they shift along the signals. The size of the sliding window and shifting are both user-defined. The DWT is applied to each segment of time separately, and the results in each segment are concatenated in order to form the final local descriptor<sup>2</sup>.

**Dictionary formulation** The dictionary formulation aims to find the most representative “words” (descriptors) among a set of descriptors from the “bag” that are used in a later step for computing of a new sample representation. This step is usually performed by a clustering algorithm, in which the number of clusters defines the size of the dictionary, and each centroid becomes a “word” of the dictionary. It is usual to play with the size of the dictionary in order to find some trade-off between the computational cost and accuracy rate.

**The new representation** A signal can be represented by a set of descriptors, which can range from dozens to thousands. Some of these descriptors may be similar or only represent noisy information. Thus, in order to obtain a compressed and meaningful representation of the signal, the descriptors were quantized based on the dictionary computed previously. The quantization step will provide a histogram for each sample with length equals to the size of the dictionary, in which each bin will have the frequency of its closest word in the input signal. Then, the final histogram is further used as an input for machine learning algorithms.

## 5.4 Experiments and Results

The experimental setup used all data recorded from a total of 66 exams, being 35 control individuals and 31 patients. The output of the protocol discussed in the previous section results in six different datasets, one for each task. The dictionary learning step was performed by means of three different techniques: dOPF,  $k$ -means<sup>3</sup> and OPF<sup>4</sup>. The main idea is to evaluate the quality of clustering of each technique through the accuracy rate obtained in the classification phase. The architecture used by dOPF is composed of four layers, in which the values of  $k_{max}$  are: 100

---

<sup>2</sup>We used sliding windows of size 100 ms with stride of 50 ms, being such values empirically chosen.

<sup>3</sup>Our own implementation.

<sup>4</sup><https://github.com/LibOPF/LibOPF>

**Tabela 5.1: Number of descriptors extracted from the training set and number of words computed by each technique.**

| dataset (task)   | # descriptors | Deep-OPF                         | K-means | OPF   |
|------------------|---------------|----------------------------------|---------|-------|
| Circ-A exam (a)  | 18,000        | 5,682 - 2,584 - 228 - <b>68</b>  | 68      | 693   |
| Circ-B exam (b)  | 11,898        | 538 - 376 - 43 - <b>17</b>       | 17      | 33    |
| Spiral exam (c)  | 46,637        | 12,118 - 3,951 - 370 - <b>92</b> | 92      | 1,424 |
| Meander exam (d) | 41,094        | 10,865 - 3,937 - 429 - <b>99</b> | 99      | 1,591 |
| Dia-A exam (e)   | 14,608        | 666 - 480 - 95 - <b>47</b>       | 47      | 80    |
| Dia-B exam (f)   | 13,947        | 657 - 394 - 78 - <b>27</b>       | 27      | 70    |

for the first layer, 1% of the number of clusters computed in the previous layer are used as an input for the second layer, and 10% of the number of clusters computed in their respectively antecessor layers for the third and fourth layers. The value of  $k$  for  $k$ -means is always set as the number of clusters found by the fourth (last) layer of dOPF approach. Regarding the OPF algorithm, the values for  $k_{max}$  were empirically set as 2,500 for the Spiral and Meander datasets, and as 1,500 for the remaining datasets. The idea in using the same number of clusters for dOPF and  $k$ -means is to allow a fair comparison between them.

Table 5.1 presents the number of descriptors extracted from the training set of each dataset, as well as the number of words computed in each case. In the column regarding dOPF, it is shown the number of words found for each of the four layers, but only the ones computed in the last layer (bolded) are used for the quantization of both training and testing sets.

The experiments were performed using the hold-out procedure with 15 runs. Both training and testing sets were partitioned using 50% of the entire dataset each, being randomly generated in each new run. In this step, there were employed three different classifiers for comparison purposes: Bayesian Classifier (BC)<sup>5</sup>, supervised OPF (sOPF)<sup>6</sup> and SVM using a Radial Basis Function (RBF) kernel with parameter optimization (SVM-RBF) (PEDREGOSA et al., 2011).

Tables 5.2a— 5.2f present the mean recognition rates concerning all six exams, being the accuracy computed according to Papa et al. (PAPA; FALCÃO; SUZUKI, 2009). The best results are defined according to the Wilcoxon signed-rank (WILCOXON, 1945b) with significance of 0.05, which pointed out the best ones in bold for each exam. Further, we also considered the best among all exams as the underlined ones.

Let us first analyze the best results among all. The statistical evaluation pointed out [OPF, SVM-RBF] and [ $k$ -means, BC] as the best pairs of [dictionary learner, classifier] with accuracies near to 81% and 83%, respectively. Comparing that recognition rates against some previous

<sup>5</sup>Our own implementation.

<sup>6</sup><https://github.com/LibOPF/LibOPF>

works, the proposed approach showed significant gains (from 10% to 30%) against the one presented by Pereira et al. (PEREIRA et al., 2016). Despite that our results were slightly below those achieved by a further work of the same authors that makes use of deep learning techniques (PEREIRA et al., 2016b), our approach is way more efficient than using deep learning techniques taking into account a few architectures.

With respect to the best accuracies concerning each exam, dOPF obtained very much suitable results, being more accurate than naïve OPF in most cases. Supervised OPF obtained good results as well, but SVM-RBF achieved the best recognition rates in a few more situations. Additionally, we also evaluated the accuracy per class for all situations, as presented in Tables 5.3a—5.3f, whose best results are also highlighted considering the Wilcoxon signed-rank. The best results for each class are in bold, and the best among all datasets is underlined. Actually, the main improvement concerns the accuracy for the identification of healthy individuals, since Pereira et al. (PEREIRA et al., 2016b) obtained recognition rates nearly 50% over the Meander and Spirals datasets for the control class. The proposed approach increased not only the global accuracy with respect to the work by Pereira et al. (PEREIRA et al., 2016b), but also the specificity and sensitivity for most of the cases. Also, Circ-A dataset provided two out of the five best results, thus showing as a good alternative for the Parkinson’s Disease identification.

Table 5.4 presents the mean computational load required by each technique to learn the dictionary. Notice the computational burden for dOPF considers the four layers. In this context,  $k$ -means figured as the fastest one due to its simplicity. If one considers dOPF and OPF only, we can observe the former is about 78 times faster in Circ-B dataset, which is quite effective. The lowest gains can be observed in both Meander and Spiral datasets. The small differences come from the fact the value used for  $k_{max}$  in both situations is small, thus justifying the fact the dictionaries computed in these datasets have very high dimension when compared to others.

## 5.5 Conclusions

This work introduced a deep-hierarchical version of the unsupervised OPF algorithm for dictionary learning in the context of computer-aided Parkinson’s disease identification. The experiments were performed using data from handwriting dynamics, similarly to the work by Pereira et al. (PEREIRA et al., 2016b), but now handled as signals and not images.

The application of the BoW paradigm can extract more information by computing local descriptors that can enhance the overall accuracy. Also, dOPF showed satisfactory results in its first application for BoW-based Parkinson’s Disease identification. Experiments over six data-

Tabela 5.2: Overall accuracies.

(a) Circ-A dataset.

|                       | <b>BC</b>         | <b>sOPF</b>       | <b>SVM-RBF</b> |
|-----------------------|-------------------|-------------------|----------------|
| <b>dOPF</b>           | <b>82.96±2.88</b> | <b>81.71±5.12</b> | 73.87±4.58     |
| <b><i>k</i>-means</b> | <b>83.38±4.22</b> | <b>82.01±5.11</b> | 65.80±12.39    |
| <b>OPF</b>            | <b>81.06±4.36</b> | <b>81.90±4.89</b> | 76.17±6.92     |

(b) Circ-B dataset.

|                       | <b>BC</b>  | <b>sOPF</b>       | <b>SVM-RBF</b>    |
|-----------------------|------------|-------------------|-------------------|
| <b>dOPF</b>           | 68.75±7.96 | 69.14±6.95        | <b>77.31±4.45</b> |
| <b><i>k</i>-means</b> | 67.80±7.44 | 65.58±6.79        | <b>74.54±6.39</b> |
| <b>OPF</b>            | 70.81±4.62 | <b>73.08±8.96</b> | <b>76.69±5.38</b> |

(c) Spiral dataset.

|                       | <b>BC</b>         | <b>sOPF</b> | <b>SVM-RBF</b>    |
|-----------------------|-------------------|-------------|-------------------|
| <b>dOPF</b>           | <b>78.30±5.80</b> | 76.73±6.83  | 77.25±3.46        |
| <b><i>k</i>-means</b> | 73.37±5.37        | 73.11±5.31  | 78.83±2.20        |
| <b>OPF</b>            | 75.40±3.09        | 75.57±3.13  | <b>81.03±2.40</b> |

(d) Meander dataset.

|                       | <b>BC</b>  | <b>sOPF</b> | <b>SVM-RBF</b>    |
|-----------------------|------------|-------------|-------------------|
| <b>dOPF</b>           | 73.33±4.97 | 74.07±2.90  | <b>80.45±2.42</b> |
| <b><i>k</i>-means</b> | 76.07±3.31 | 76.09±2.77  | 78.26±3.91        |
| <b>OPF</b>            | 78.53±3.15 | 77.21±3.52  | <b>81.07±2.60</b> |

(e) Dia-A dataset.

|                       | <b>BC</b>         | <b>sOPF</b>       | <b>SVM-RBF</b>    |
|-----------------------|-------------------|-------------------|-------------------|
| <b>dOPF</b>           | <b>69.86±7.21</b> | <b>70.93±7.29</b> | <b>68.69±7.26</b> |
| <b><i>k</i>-means</b> | <b>72.18±7.46</b> | <b>72.43±5.81</b> | <b>73.93±8.66</b> |
| <b>OPF</b>            | <b>70.72±6.60</b> | <b>67.01±7.45</b> | <b>68.69±7.26</b> |

(f) Dia-B dataset.

|                       | <b>BC</b>         | <b>sOPF</b>       | <b>SVM-RBF</b>    |
|-----------------------|-------------------|-------------------|-------------------|
| <b>dOPF</b>           | <b>67.96±8.10</b> | 64.86±7.93        | 61.89±8.49        |
| <b><i>k</i>-means</b> | <b>72.92±8.51</b> | <b>69.84±9.03</b> | <b>67.24±9.31</b> |
| <b>OPF</b>            | 63.77±8.85        | 67.25±6.80        | <b>66.30±7.38</b> |

Tabela 5.3: Average accuracy rate for each class.

## (a) Circ-A dataset.

|         | BC         |                   |             | sOPF              |                 |            | SVM-RBF            |                   |                   |
|---------|------------|-------------------|-------------|-------------------|-----------------|------------|--------------------|-------------------|-------------------|
|         | dOPF       | <i>k</i> -means   | OPF         | dOPF              | <i>k</i> -means | OPF        | dOPF               | <i>k</i> -means   | OPF               |
| Patient | 83.33±5.62 | <u>84.17±7.79</u> | 79.17±12.19 | 77.5±10.24        | 79.58±10.15     | 80.83±8.34 | 61.67±15.10        | 70.42±12.60       | 75.42±6.87        |
| Control | 82.59±8.09 | <u>82.59±8.09</u> | 82.96±8.52  | <u>85.93±6.59</u> | 84.44±12.09     | 82.96±6.79 | <u>67.41±11.67</u> | <u>67.04±7.99</u> | <u>71.48±9.82</u> |

## (b) Circ-B dataset.

|         | BC          |                 |             | sOPF        |                 |             | SVM-RBF            |                   |             |
|---------|-------------|-----------------|-------------|-------------|-----------------|-------------|--------------------|-------------------|-------------|
|         | dOPF        | <i>k</i> -means | OPF         | dOPF        | <i>k</i> -means | OPF         | dOPF               | <i>k</i> -means   | OPF         |
| Patient | 60.83±18.32 | 61.25±11.68     | 74.58±13.39 | 63.75±13.35 | 63.75±13.35     | 54.17±13.04 | 64.58±13.24        | 68.75±14.43       | 57.92±10.07 |
| Control | 76.67±49.12 | 77.04±12.48     | 59.99±9.56  | 71.85±13.98 | 67.41±12.32     | 57.04±17.15 | <u>77.04±10.51</u> | <u>77.41±6.24</u> | 45.93±7.98  |

## (c) Spiral dataset.

|         | BC                 |                 |                   | sOPF               |                 |                   | SVM-RBF           |                   |                   |
|---------|--------------------|-----------------|-------------------|--------------------|-----------------|-------------------|-------------------|-------------------|-------------------|
|         | dOPF               | <i>k</i> -means | OPF               | dOPF               | <i>k</i> -means | OPF               | dOPF              | <i>k</i> -means   | OPF               |
| Patient | <u>74.51±10.59</u> | 65.49±10.63     | <u>72.90±6.90</u> | <u>78.04±12.07</u> | 67.06±10.14     | <u>71.61±6.27</u> | 67.81±2.17        | <u>73.59±3.67</u> | <u>74.58±0.82</u> |
| Control | 82.08±8.14         | 81.25±11.33     | 77.90±6.95        | 75.42±11.92        | 79.17±10.48     | 79.52±6.20        | <u>89.43±1.83</u> | 84.85±2.25        | 86.43±1.09        |

## (d) Meander dataset.

|         | BC                |                 |                   | sOPF              |                 |                   | SVM-RBF           |                   |            |
|---------|-------------------|-----------------|-------------------|-------------------|-----------------|-------------------|-------------------|-------------------|------------|
|         | dOPF              | <i>k</i> -means | OPF               | dOPF              | <i>k</i> -means | OPF               | dOPF              | <i>k</i> -means   | OPF        |
| Patient | <u>76.61±4.04</u> | 69.46±5.96      | <u>76.77±8.44</u> | <u>75.38±4.62</u> | 73.23±4.51      | <u>77.85±3.93</u> | 74.81±2.18        | 71.06±2.62        | 74.54±1.37 |
| Control | 73.33±4.97        | 82.67±4.88      | 80.29±4.68        | 72.76±5.47        | 78.95±4.99      | 76.57±5.47        | <u>85.80±0.89</u> | <u>84.43±3.76</u> | 87.99±0.72 |

## (e) Dia-A dataset.

|         | BC                 |                    |             | sOPF        |                    |                    | SVM-RBF     |                 |                    |
|---------|--------------------|--------------------|-------------|-------------|--------------------|--------------------|-------------|-----------------|--------------------|
|         | dOPF               | <i>k</i> -means    | OPF         | dOPF        | <i>k</i> -means    | OPF                | dOPF        | <i>k</i> -means | OPF                |
| Patient | <u>67.50±16.01</u> | <u>66.67±14.01</u> | 51.67±17.15 | 65.83±13.28 | <u>70.42±12.59</u> | <u>52.08±11.10</u> | 66.25±13.46 | 66.25±15.61     | <u>47.50±12.87</u> |
| Control | 72.22±9.51         | 75.19±5.69         | 50.74±9.70  | 78.52±8.33  | 74.44±6.97         | 55.56±12.67        | 75.19±7.55  | 67.78±12.37     | 50.00±13.46        |

## (f) Dia-B dataset.

|         | BC                 |                   |             | sOPF               |                    |             | SVM-RBF            |                    |                    |
|---------|--------------------|-------------------|-------------|--------------------|--------------------|-------------|--------------------|--------------------|--------------------|
|         | dOPF               | <i>k</i> -means   | OPF         | dOPF               | <i>k</i> -means    | OPF         | dOPF               | <i>k</i> -means    | OPF                |
| Patient | <u>63.33±12.88</u> | 60.83±11.29       | 60.00±32.18 | <u>72.50±10.89</u> | <u>67.08±13.39</u> | 47.92±10.62 | <u>71.25±11.81</u> | <u>73.75±11.23</u> | <u>52.08±15.92</u> |
| Control | 72.59±9.62         | <u>68.89±9.89</u> | 50.37±28.07 | 73.33±9.56         | <u>72.59±10.63</u> | 48.52±12.42 | <u>56.29±15.56</u> | 60.74±11.38        | <u>53.70±9.44</u>  |



**Tabela 5.4: Dictionary learning computational load [s] required by each technique.**

| <b>dataset (task)</b> | <b>dOPF</b> | <b><i>k</i>-means</b> | <b>OPF</b> |
|-----------------------|-------------|-----------------------|------------|
| Circ-A (a)            | 968.167     | 37.008                | 49,087.137 |
| Circ-B (b)            | 419.498     | 13.113                | 32,777.539 |
| Spiral (c)            | 6,063.205   | 239.859               | 6,643.906  |
| Meander (d)           | 5,003.233   | 208.443               | 5,168.819  |
| Dia-A (e)             | 613.109     | 19.878                | 41,189.133 |
| Dia-B (f)             | 569.053     | 11.025                | 39,367.844 |

sets considered dOPF against the well-known *k*-means and naïve OPF clustering for dictionary learning. Further, supervised techniques were used for classification purposes.

Future works will consider learning hierarchical BoWs, i.e., one bag for each layer in the dOPF formulation. We believe each layer can carry different information about the problem.

# Capítulo 6

## IDENTIFICAÇÃO DA DOENÇA DE PARKINSON USANDO MÁQUINAS RESTRITAS DE BOLTZMANN

---

---

Neste capítulo, é apresentada a técnica de Máquinas Restritas de Boltzmann e suas aplicações para o aprendizado automático de características de imagens para auxiliar no diagnóstico do mal de Parkinson. O capítulo compreende os resultados do artigo aceito para publicação do aluno candidato (PEREIRA et al., 2017).

### 6.1 Introduction

In the last decades, the number of people with Parkinson's disease (PD) has increased significantly worldwide. Also, research points out that approximately 60,000 Americans are diagnosed with PD (FOUNDATION, ). The disease was firstly described by the English physician James Parkinson (PARKINSON, 1817b), being more common in the elderly population and occurs when nerve cells that produce dopamine are destroyed (LEES; HARDY; REVESZ, 2009). Additionally, PD is a chronic, progressive and neuron-degenerative illness, which causes many symptoms, such as slowness of movement, freeze of gait, tremors and muscle stiffness.

One of the main problems related to PD concerns the dopamine, which is a neurotransmitter released by the brain and in charge of various tasks performed by our body, such as the movement, memory, sleep, learning and others. The absence of such substance in PD-affected individuals may trigger a number of symptoms, such as depression, sleep disturbances, memory impairment, and autonomic nervous system disorders. Also, the patient may have its speech and writing skills affected over time (BURKE, 2010b). Furthermore, despite of not being considered lethal, people with PD have a shorter life expectancy than the general population.

Although some research indicates that PD may be triggered by hereditary factors (BURKE, 2010b), the cause of the disease is still unknown. Also, the difficulty to distinguish the difference from other neurological illness as well as to detect PD in its early stages are the main barriers related to automatic identification of Parkinson's Disease. In order to assist the computer-aided PD diagnosis, systems based on machine learning techniques have been employed, showing promising results (SAKAR et al., 2013). Spadotto et al. (SPADOTTO et al., 2010b), for instance, introduced the Optimum-Path Forest (PAPA; FALCÃO; SUZUKI, 2009; PAPA et al., 2012) classifier to aid the automatic identification of Parkinson's Disease. The same group of authors proposed an evolutionary-based approach to select the most discriminative set of features that help improving PD recognition rates (SPADOTTO et al., 2011). Recently, Pereira et al. (PEREIRA et al., 2016) proposed to extract features from writing exams using image processing techniques, and later on Pereira et al. (PEREIRA et al., 2016c) introduced Convolutional Neural Networks to learn features from handwriting dynamics in the context of automatic PD identification.

Another interesting approach that has been extensively used in a number of applications, mainly in the context of deep learning-oriented applications, concerns the so-called Restricted Boltzmann Machines (RBMs), which are an undirected generative model that use a layer of hidden variables to model a distribution over visible units (LAROCHELLE; BENGIO, 2008). Therefore, given an input set of images, an RBM basically learns how to effectively reconstruct them based on a learning process that aims at learning the weights that connect the input data (image) to a hidden layer. The values of the neurons' activation at that layer can be used as the features to describe the input data.

In this paper, we introduce Restricted Boltzmann Machines in the context of feature learning for the automatic identification of Parkinson's Disease by means of images acquired from handwritten exams. Further, the features learned are then used as inputs to supervised classifiers. In this work, we considered three state-of-the-art classifiers, say that Optimum-Path Forest (OPF) (PAPA; FALCÃO; SUZUKI, 2009; PAPA et al., 2012), Naïve Bayes (NB) (DUDA; STORK, 2000) and Support Vector Machines (CORTES; VAPNIK, 1995). The experiments are conducted over the "HandPD" dataset, which is publicly available at the internet.

The reminder of this paper is organized as follows: Section 6.2 describes the theoretical background related to RBMs, and Section 6.3 presents the methodology employed in this work. The experimental results are presented in Section 6.4, conclusions and final remarks are stated in Section 6.5.

## 6.2 Restricted Boltzmann Machines

Restricted Boltzmann Machines are energy-based stochastic neural networks composed of two layers of neurons (visible and hidden), in which the learning phase is conducted by means of an unsupervised fashion. A naïve architecture of a Restricted Boltzmann Machine comprises a visible layer  $\mathbf{v}$  with  $m$  units and a hidden layer  $\mathbf{h}$  with  $n$  units. Additionally, a real-valued matrix  $\mathbf{W}_{m \times n}$  models the weights between the visible and hidden neurons, where  $w_{ij}$  stands for the weight between the visible unit  $v_i$  and the hidden unit  $h_j$ .

Let us assume both  $\mathbf{v}$  and  $\mathbf{h}$  as being binary-valued units. In other words,  $\mathbf{v} \in \{0, 1\}^m$  e  $\mathbf{h} \in \{0, 1\}^n$ . The energy function of a Restricted Boltzmann Machine is given by:

$$E(\mathbf{v}, \mathbf{h}) = - \sum_{i=1}^m a_i v_i - \sum_{j=1}^n b_j h_j - \sum_{i=1}^m \sum_{j=1}^n v_i h_j w_{ij}, \quad (6.1)$$

where  $\mathbf{a}$  e  $\mathbf{b}$  stand for the biases of visible and hidden units, respectively.

The probability of a joint configuration  $(\mathbf{v}, \mathbf{h})$  is computed as follows:

$$P(\mathbf{v}, \mathbf{h}) = \frac{1}{Z} e^{-E(\mathbf{v}, \mathbf{h})}, \quad (6.2)$$

where  $Z$  stands for the so-called partition function, which is basically a normalization factor computed over all possible configurations involving the visible and hidden units. Similarly, the marginal probability of a visible (input) vector is given by:

$$P(\mathbf{v}) = \frac{1}{Z} \sum_{\mathbf{h}} e^{-E(\mathbf{v}, \mathbf{h})}. \quad (6.3)$$

Since the RBM is a bipartite graph, the activations of both visible and hidden units are mutually independent, thus leading to the following conditional probabilities:

$$P(\mathbf{v}|\mathbf{h}) = \prod_{i=1}^m P(v_i|\mathbf{h}), \quad (6.4)$$

and

$$P(\mathbf{h}|\mathbf{v}) = \prod_{j=1}^n P(h_j|\mathbf{v}), \quad (6.5)$$

where

$$P(v_i = 1|\mathbf{h}) = \phi \left( \sum_{j=1}^n w_{ij}h_j + a_i \right), \quad (6.6)$$

and

$$P(h_j = 1|\mathbf{v}) = \phi \left( \sum_{i=1}^m w_{ij}v_i + b_j \right). \quad (6.7)$$

Note that  $\phi(\cdot)$  stands for the logistic-sigmoid function.

Let  $\theta = (W, a, b)$  be the set of parameters of an RBM, which can be learned through a training algorithm that aims at maximizing the product of probabilities given all the available training data  $\mathcal{V}$ , as follows:

$$\arg \max_{\Theta} \prod_{\mathbf{v} \in \mathcal{V}} P(\mathbf{v}). \quad (6.8)$$

One can solve the aforementioned equation using the following derivatives over the matrix of weights  $\mathbf{W}$ , and biases  $\mathbf{a}$  and  $\mathbf{b}$  at iteration  $t$  as follows:

$$\mathbf{W}^{t+1} = \mathbf{W}^t + \underbrace{\eta(P(\mathbf{h}|\mathbf{v})\mathbf{v}^T - P(\tilde{\mathbf{h}}|\tilde{\mathbf{v}})\tilde{\mathbf{v}}^T)}_{=\Delta\mathbf{W}^t} + \Phi, \quad (6.9)$$

$$\mathbf{a}^{t+1} = \mathbf{a}^t + \underbrace{\eta(\mathbf{v} - \tilde{\mathbf{v}})}_{=\Delta\mathbf{a}^t} + \alpha\Delta\mathbf{a}^{t-1} \quad (6.10)$$

and

$$\mathbf{b}^{t+1} = \mathbf{b}^t + \underbrace{\eta(P(\mathbf{h}|\mathbf{v}) - P(\tilde{\mathbf{h}}|\tilde{\mathbf{v}}))}_{=\Delta\mathbf{b}^t} + \alpha\Delta\mathbf{b}^{t-1}, \quad (6.11)$$

where  $\eta$  stands for the learning rate, and  $\lambda$  and  $\alpha$  denote the weight decay and the momentum, respectively. Notice the terms  $P(\tilde{\mathbf{h}}|\tilde{\mathbf{v}})$  and  $\tilde{\mathbf{v}}$  can be obtained by means of the Contrastive Divergence (HINTON, 2002) technique, which basically ends up performing Gibbs sampling using the training data as the visible units. Roughly speaking, Equations 6.9, 6.10 and 6.11 employ the well-known Gradient Descent as the optimization algorithm. The additional term  $\Phi$  in Equation 6.9 is used to control the values of matrix  $\mathbf{W}$  during the convergence process, and it is formulated as follows:

$$\Phi = -\lambda \mathbf{W}^t + \alpha \Delta \mathbf{W}^t^{-1}. \quad (6.12)$$

## 6.3 Methodology

In this section, we present the methodology employed to evaluate the proposed approach, as well as the datasets and the experimental setup.

### 6.3.1 Dataset

The dataset employed in this work is called “HandPD”<sup>1</sup>, being firstly presented by Pereira et al. (PEREIRA et al., 2015). Roughly speaking, the dataset comprises images drawn in a form with a template for guideline purposes (Figure 6.1), depicting exercises specifically designed to expose unique characteristics from PD patients. To create the images, the patient is aided with a digital pen *BiSP*<sup>®</sup> (TEAM REGENSBURG, 2002), which is equipped with six sensors capable of recording the hand movements during the exercises. However, differently from Pereira et al. (PEREIRA et al., 2016c) that used information from the sensors, we are considering only the visual features that can be learned from the drawing by means of RBMs.

**Figura 6.1:** Form used to assess the handwritten skills. Extracted from (PEREIRA et al., 2015).

This work makes use of two kind of images extracted from the forms: Spiral and Meander. Also, the images are classified into two classes: patients (124 images) and healthy group (56

<sup>1</sup>available in <http://www.fc.unesp.br/~papa/pub/datasets/Handpd/>

images). Furthermore, both datasets are resized in two different ways to evaluate the robustness of RBM for learning features in this context:  $64 \times 64$  and  $128 \times 128$  pixels each.

Since we are considering RBMs with binary-valued inputs, one needs to threshold the gray-scale images originally available from the dataset. In order to fulfill this task, we applied the well-known Otsu threshold (OTSU, 1979) to all images, which are finally used to feed the RBMs. After training, the images are used once more as the inputs, and the activation values at the hidden layer are used as the features for each image concerning the supervised learning methods employed in this work, i.e. OPF, SVM and Bayesian classifier.

### 6.3.2 Experimental Setup

The work employs an RBM architecture where the visible layer stands for the number of pixels from the input image, i.e. 4,096 ( $64 \times 64$  images) or 16,384 ( $128 \times 128$  images), as well as the hidden layer stands for the desirable number of features, which assume the values within the range  $J \in \{10, 100, 500, 1,000, 2,000, 4,000, 7,000\}$ <sup>2</sup>. The remaining parameters used during the RBM learning step were chosen empirically and fixed as follows:  $\eta = 0.1$  (learning rate), number of epochs = 1,000, and mini-batches of size 20. Moreover, the RBM was trained with the Contrastive Divergence (CD) (HINTON, 2002) algorithm.

Once the RBM learning process is finished, the new datasets composed of features extracted from the hidden layer units will feed three supervised learning algorithms: SVM, Bayes and the OPF. In regard to SVM, we used the Radial Basis Function kernel with parameters optimized by means of a grid search (PEDREGOSA et al., 2011). Finally, to evaluate the techniques considered in this work, a classification accuracy proposed by Papa et al. (PAPA; FALCÃO; SUZUKI, 2009) that considers unbalanced datasets has been adopted.

## 6.4 Experiments

This section presents the experimental results concerning OPF, SVM and the Bayes classifier to the task of Parkinson's Disease identification by means of features learned from handwritten forms. The evaluation is taken upon a training set with size of 50%, as well as the remaining 50% is employed for testing purposes. Tables 6.1 and 6.2 present the accuracy results concerning Meander dataset with  $64 \times 64$  and  $128 \times 128$ , respectively. The most accurate results according to the Wilcoxon signed-rank test for each number of features are in bold, and

<sup>2</sup>Notice the range values were empirically chosen

the best global results are underlined. Notice the experiments consider an average accuracy over 20 runnings.

| Number of features | OPF               | Bayes             | SVM               |
|--------------------|-------------------|-------------------|-------------------|
| <b>10</b>          | <b>53.72±0.78</b> | 53.82±0.18        | <b>55.75±1.37</b> |
| <b>100</b>         | 58.00±1.42        | 57.20±0.0         | <b>71.94±1.42</b> |
| <b>500</b>         | 62.23±4.18        | 63.21±2.32        | <b>74.38±3.02</b> |
| <b>1,000</b>       | <b>67.59±3.26</b> | <b>67.94±1.74</b> | 66.26±5.66        |
| <b>2,000</b>       | <b>64.10±1.67</b> | <b>64.07±1.30</b> | <b>62.72±8.14</b> |
| <b>4,000</b>       | 64.91±4.53        | 64.58±5.50        | <b>69.99±2.67</b> |
| <b>7,000</b>       | 62.94±3.05        | <b>64.62±3.51</b> | <b>65.34±3.57</b> |

**Tabela 6.1: Mean accuracy results considering Meander  $64 \times 64$  dataset.**

Considering the smaller-sized Meander dataset (Table 6.1), one can observe RBM can provide reasonable results with SVM classifier using only 500 features. Since the dataset is composed of 180 images only, being 90 used for training, it is expected that higher dimensional spaces (i.e., 7,000 features) will not allow good results, since the mapped space will be shrank to a lower dimensional one. This same behavior can be observed for SVM considering  $128 \times 128$  images (Table 6.2), but with OPF and Bayes obtaining the best results with 7,000 and 4,000 features, respectively.

| Number of features | OPF               | Bayes             | SVM               |
|--------------------|-------------------|-------------------|-------------------|
| <b>10</b>          | <b>55.26±4.90</b> | 50.0±0.0          | 50.0±0.00         |
| <b>100</b>         | 64.89±3.69        | <b>65.69±3.21</b> | 63.57±0.46        |
| <b>500</b>         | <b>60.63±2.24</b> | <b>61.36±2.69</b> | <b>62.94±7.13</b> |
| <b>1,000</b>       | 60.17±4.18        | 59.19±4.18        | <b>63.83±3.95</b> |
| <b>2,000</b>       | 64.23±1.38        | 66.22±0.70        | <b>68.18±1.50</b> |
| <b>4,000</b>       | 66.33± 3.15       | <b>68.18±4.51</b> | 65.05±5.23        |
| <b>7,000</b>       | <b>71.05±3.35</b> | 69.55±3.86        | 66.43±8.12        |

**Tabela 6.2: Mean accuracy results considering Meander  $128 \times 128$  dataset.**

In regard to the Spiral drawing, Table 6.3 presents the results with  $64 \times 64$  images, where the best results were obtained by SVM with 1,000 features. Also, one can observe the recognition rates were quite better than using Meanders. We believe that following the “circular” pattern of Spirals is way more difficult for those with reduced hand mobility, which turns out to be more discriminative to distinguish patients from the control group. However, the results using  $128 \times 128$  images were slightly worse, but with SVM on top of the results once more. One can observe OPF has its accuracy degraded when the number of features increases, since it uses the distance among samples for classification purposes, and it can be influenced by higher



dimensional spaces.

| Number of features | OPF        | Bayes             | SVM               |
|--------------------|------------|-------------------|-------------------|
| <b>10</b>          | 53.19±1.39 | 58.26±0.60        | <b>58.85±1.69</b> |
| <b>100</b>         | 67.75±1.60 | 67.39±5.15        | <b>73.82±2.26</b> |
| <b>500</b>         | 67.26±3.58 | 68.00±3.49        | <b>79.93±0.25</b> |
| <b>1,000</b>       | 74.59±2.99 | 74.94±2.77        | <b>83.12±2.55</b> |
| <b>2,000</b>       | 69.74±2.68 | 71.58±3.47        | <b>80.71±0.14</b> |
| <b>4,000</b>       | 68.76±3.61 | 71.31±4.55        | <b>79.49±3.81</b> |
| <b>7,000</b>       | 71.76±3.13 | <b>73.30±3.59</b> | <b>75.31±4.04</b> |

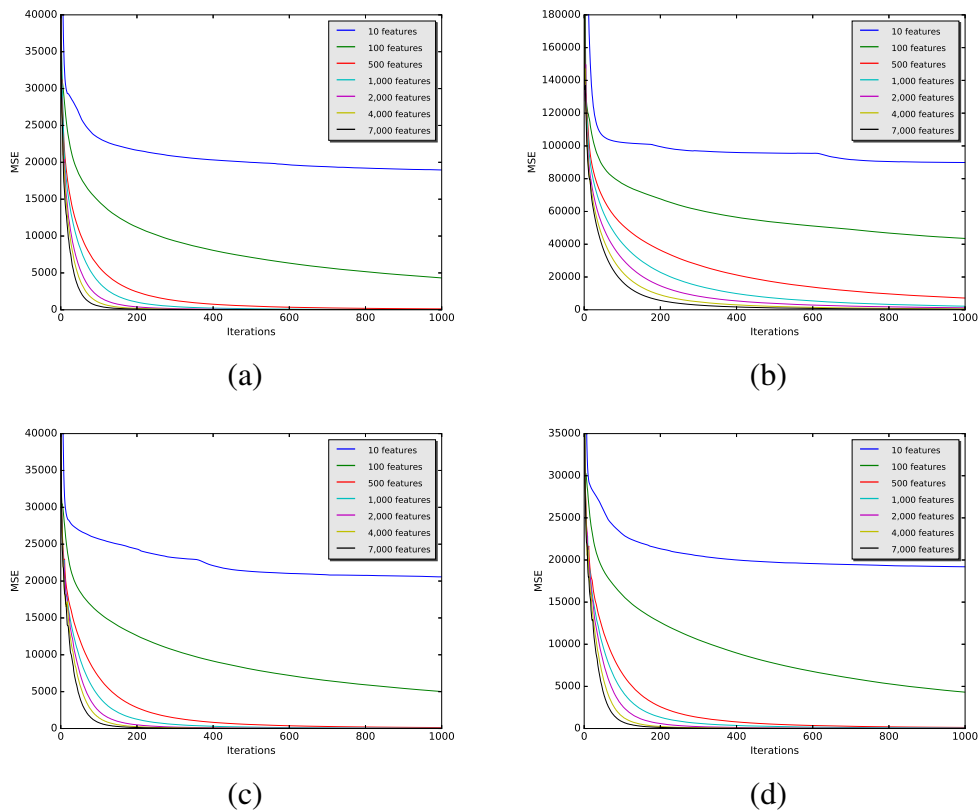
**Tabela 6.3: Mean accuracy results considering Spiral  $64 \times 64$  dataset.**

| Number of features | OPF               | Bayes             | SVM                |
|--------------------|-------------------|-------------------|--------------------|
| <b>10</b>          | 56.00±6.26        | 64.25±2.74        | <b>71.972±2.74</b> |
| <b>100</b>         | 62.47±2.33        | 63.68±3.71        | <b>73.87±1.29</b>  |
| <b>500</b>         | 67.22±1.92        | 70.43±0.81        | <b>80.29±3.19</b>  |
| <b>1,000</b>       | <b>70.17±4.25</b> | <b>69.58±2.27</b> | <b>72.69±2.49</b>  |
| <b>2,000</b>       | 74.44±3.16        | 75.02±4.41        | <b>77.92±3.61</b>  |
| <b>4,000</b>       | 71.98±3.20        | 73.32±1.80        | <b>79.73±1.19</b>  |
| <b>7,000</b>       | 67.49±4.03        | 69.70±3.80        | <b>74.91±4.64</b>  |

**Tabela 6.4: Mean accuracy results considering Spiral  $128 \times 128$  dataset**

In order to keep track of the convergence process, we analyzed the mean squared error (MSE) of the RBM during the learning step. Figure 6.2 depicts the MSE obtained during the training considering 1,000 epochs. Notice the error falls dramatically before epoch 100, and then traces a smooth curve that approaches zero as the epochs approximate 1,000 iterations for models with 500 or more hidden units. Although all approaches (i.e., different number of features) achieved similar results concerning MSE in the final of the learning step, one can observe the faster convergence during the first 200 iterations using 7,000 features. Since we have more latent variables in the hidden units, it is expected they can learn a more complex and detailed information about the input data.

In order to understand what is going on during the learning procedure of the RBM, we displayed what the network “sees” when is presented to an input image. Since each visible unit is connected to all hidden neurons, we can take all connection weights, normalize them and build an image, that is usually employed to understand what the network is learning. Figure 6.3 depicts some images from the weight matrices when Meanders and Spirals are presented to the network using 1,000 hidden units. Since all images from each dataset are somehow similar, most of the neurons are learning the shape of the drawing (i.e., spiral or meander), although



**Figure 6.2: Evolution of the Mean-Squared Error considering: (a) Meander  $64 \times 64$ , (b) Meander  $128 \times 128$ , (c) Spiral  $64 \times 64$ , and (d) Spiral  $128 \times 128$ .**

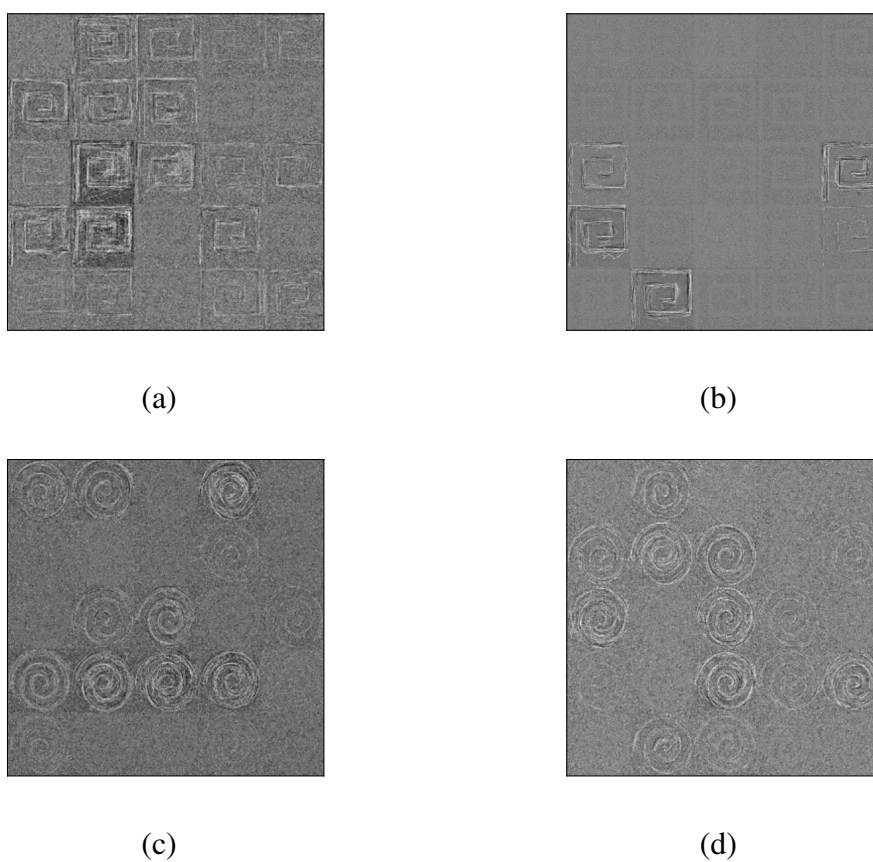
some of them did not get excited by any shape in particular.

## 6.5 Conclusions

In this work, we dealt with the problem of automatic Parkinson's Disease identification by means of features learned from Restricted Boltzmann Machines. We considered two types of drawings in two different resolutions, which were then used to feed RBM models for further supervised classification purposes.

We observed the best results were obtained with spirals at lower-resolution images, but similar results can also be obtained with  $128 \times 128$  images. Additionally, we observed that RBMs with more hidden layers allow a faster convergence during learning, but it does not necessarily imply in the better results over the test set.

With respect to future works, we aim at considering DBNs and DBMs for classification purposes, as well as to use Discriminative RBMs as the classification techniques as well.



**Figura 6.3: An “RBM’s mind”:** random weight matrices extracted from (a) Meander  $64 \times 64$ , (b) Meander  $128 \times 128$ , (c) Spiral  $64 \times 64$  and (d) Spiral  $128 \times 128$ .

# Capítulo 7

## CONCLUSÃO

---

---

A presente tese de doutorado tem como foco principal auxiliar no diagnóstico da doença do mal de Parkinson, dado que a mesma não tem cura e possui como forma mais aceitável de diagnóstico clínico o método de exclusão. Técnicas de diversas áreas da computação como aprendizado de máquina, visão computacional e inteligência artificial, dentre outras, vêm sendo aplicadas ao longo dos anos na busca de encontrar uma melhor forma de auxiliar o diagnóstico do mal de Parkinson. Uma grande dificuldade encontrada para a utilização dessas técnicas pode ser apontada como a falta de dados, pois adquirir pessoas saudáveis e portadoras da doença para o desenvolvimento de uma base de dados não é uma tarefa fácil, muito menos o desenvolvimento da mesma após a aquisição dos indivíduos.

Com base nessas informações, para este trabalho foram desenvolvidas duas bases de dados denominadas HandPD e NewHandPD, ambas contendo dados adquiridos através do preenchimento de um formulário por pacientes e pessoas saudáveis em exames realizados na Faculdade de Medicina da Universidade Estadual Paulista Júlio de Mesquita Filho - UNESP de Botucatu com uma caneta especial contendo vários sensores. Para a base de dados HandPD, após os formulários serem digitalizados, suas imagens foram recortadas para o processo de extração de características e divididas em 2 grupos (pacientes e controle), possuindo então 736 imagens de 92 indivíduos.

Ainda mais robusto e rico em informações, o conjunto de dados NewHandPD apresenta uma outra forma de aquisição de características, fazendo uso agora de uma caneta biométrica inteligente desenvolvida pelo Departamento de Matemática da Faculdade de Ciências de Regensburg - Alemanha. Através de sensores acoplados à referida caneta, características de sinais foram obtidas para a análise contando agora 792 sinais oriundos da caneta de exames realizados por 66 indivíduos, sendo os mesmos divididos em 420 sinais para pessoas saudáveis, e 372 para pessoas portadoras do mal de Parkinson.

Técnicas como classificadores Bayesianos, Floresta de Caminhos Ótimo e Máquinas de Vetores de Suporte foram utilizadas nos primeiros experimentos realizados, sendo os resultados obtidos muito satisfatório para este tipo de análise. Um fator importante a ser acrescentado dá-se ao fato a utilização de técnicas de aprendizado profundo como Redes Neurais por Convolução, aplicação inovadora para esta finalidade que obteve excelentes resultados sobre a base de dados aplicada levando em consideração as imagens possuindo diferentes resoluções. Técnicas como bag-of-words, por exemplo também foram aplicadas em análise dos sinais obtidos através dos sensores contidos na caneta, apresentando excelentes resultados.

Após, averiguar os resultados obtidos, podemos apontar para uma boa tendência a esse tipo de análise voltada para o diagnóstico da doença quando comparado aos métodos utilizados atualmente, o que nos remete a continuação dos estudos voltados à esta mesma linha de pesquisa, porém, agora como próximos trabalhos pretendemos estudar as formas e os métodos de fusão de informações fazendo uso dos dados que já obtemos pois, através da fusão, é possível um maior aproveitamento das informações contidas na base de dados que são produzidas por diferentes sensores, ou seja, combinando as características extraídas das imagens dos formulários com os sinais obtidos através da caneta inteligente.

## **7.1 Trabalhos Publicados**

Essa seção apresenta os trabalhos publicados pelo candidato que são diretamente relacionados à tese de doutorado.

- A Step Towards the Automated Diagnosis of Parkinson's Disease: Analyzing Handwriting Movements, 28th International Symposium on Computer-Based Medical Systems - (CBMS 2015) - Qualis B1 - CC;
- Deep Learning-aided Parkinson's Disease Diagnosis from Handwritten Dynamics, 29th Conference on Graphics, Patterns and Images - (Sibgrapi 2016) - Qualis B1 - CC;
- A New Computer Vision-based Approach to aid the Diagnosis of Parkinson's Disease, Computer Methods and Programs in Biomedicine - Classificação A2 - CC;
- Parkinson's Disease Identification Through Deep Optimum-Path Forest Clustering, 17th international Conference on Computer Analysis of Images and Patterns - (CAIP 2017) - Qualis B1 - CC;

- Parkinson's Disease Identification using Restricted Boltzmann Machines, 17th international Conference on Computer Analysis of Images and Patterns - (CAIP 2017) - Qualis B1 - CC;
- Parkinson's Disease Identification Through Deep Optimum-Path Forest Clustering, 30th Conference on Graphics, Patterns and Images - (Sibgrapi 2017) - Qualis B1 - CC.

## **7.2 Trabalhos em Avaliação**

Essa seção apresenta os trabalhos que estão submetidos e encontram-se em processo de avaliação no momento.

- Handwritten Dynamics Assessment Through Convolutional Neural Networks: An Application to Parkinson's Disease Identification, Computer Methods and Programs in Biomedicine - Classificação A2 - CC.
- A Survey on Computer-Assisted Parkinson's Disease Diagnosis, Computer Methods and Programs in Biomedicine - Classificação A2 - CC.

## REFERÊNCIAS

---

---

- AFONSO, L. et al. Learning to classify seismic images with deep optimum-path forest. In: *2016 29th SIBGRAPI Conference on Graphics, Patterns and Images (SIBGRAPI)*. [S.l.: s.n.], 2016. p. 401–407.
- AFONSO, L. C. et al. Automatic visual dictionary generation through optimum-path forest clustering. In: *19th IEEE International Conference on Image Processing*. [S.l.: s.n.], 2012. p. 1897–1900.
- AFONSO, L. C. S. et al. Automatic visual dictionary generation through optimum-path forest clustering. In: *2012 19th IEEE International Conference on Image Processing*. [S.l.: s.n.], 2012. p. 1897–1900.
- AHMADLOU, M.; ADELI, H. Enhanced probabilistic neural network with local decision circles: A robust classifier. *Integrated Computer-Aided Engineering*, v. 17, n. 3, p. 197–210, 2010.
- ALEKHYA, M.; CHAKRAVARTHY, V. S. A computational basal ganglia model to assess the role of stn-dbs on impulsivity in parkinson's disease. In: *International Joint Conference on Neural Networks*. [S.l.: s.n.], 2015. p. 1–8.
- ARNULFO, G. et al. Characterization of the spiking and bursting activity of the subthalamic nucleus in patients with parkinson's disease. In: *International Conference on Advances in Biomedical Engineering*. [S.l.: s.n.], 2015. p. 107–110.
- ARORA, S. et al. Detecting and monitoring the symptoms of parkinsons disease using smartphones: A pilot study. *Parkinsonism & Related Disorders*, v. 21, n. 6, p. 650 – 653, 2015.
- BAHREPOUR, M. et al. Sensor fusion-based activity recognition for parkinson patients. In: . [S.l.]: InTech, 2011. p. 171–190.
- BAI, Y. W.; CHAN, C.-C.; YU, C.-H. Design and implementation of a user interface of a smartphone for the parkinson's disease patients. In: *IEEE International Conference on Consumer Electronics*. [S.l.: s.n.], 2015. p. 257–258.
- BARRA, V.; BOIRE, J.-Y. A general framework for the fusion of anatomical and functional medical images. *NeuroImage*, v. 13, n. 3, p. 410 – 424, 2001.
- BELALCAZAR-BOLANOS, E. A. et al. Nonlinear glottal flow features in parkinson's disease detection. In: *20th Symposium on Signal Processing, Images and Computer Vision*. [S.l.: s.n.], 2015. p. 1–6.

- BHALCHANDRA, N. A. et al. Early detection of parkinson's disease through shape based features from 123i-ioflupane spect imaging. In: *IEEE 12th International Symposium on Biomedical Imaging*. [S.l.: s.n.], 2015. p. 963–966.
- BIND, S.; TIWARI, A. K.; SAHANI, A. K. Parkinson diagnosis using neural network: a survey. *International Journal of Innovative Research in Science, Engineering and Technology*, v. 2, n. 3, p. 4843–4846, 2013.
- BIND, S.; TIWARI, A. K.; SAHANI, A. K. A survey of machine learning based approaches for parkinson disease prediction. *International Journal of Computer Science and Information Technologies*, v. 6, n. 2, p. 1648–1655, Aug 2015.
- BONDY, S. C. The neurotoxicity of environmental aluminum is still an issue. *NeuroToxicology*, v. 31, n. 5, p. 575 – 581, 2010.
- BOT, B. M. et al. The mpower study, parkinson disease mobile data collected using researchkit. *Scientific Data*, Macmillan Publishers Limited SN -, v. 3, p. 160011 EP, 2016.
- BRAATZ, E. M.; COLEMAN, R. A. A mathematical model of insulin resistance in parkinson's disease. *Computational Biology and Chemistry*, v. 56, p. 84–97, 2015.
- BURKE, R. E. Evaluation of the braak staging scheme for parkinson's disease: Introduction to a panel presentation. *Movement Disorders*, v. 25, n. S1, p. S76–S77, 2010.
- BURKE, R. E. Evaluation of the braak staging scheme for parkinson's disease: Introduction to a panel presentation. *Movement Disorders*, v. 25, n. S1, p. S76–S77, 2010.
- CAMARA, C. et al. A fuzzy inference system for closed-loop deep brain stimulation in parkinson's disease. *Journal of Medical Systems*, v. 39, n. 11.
- CAMARGO, E. E. Experiência inicial com PET/CT. *Radiologia Brasileira*, v. 38, p. 0 – 0, 02 2005.
- CASTELLANOS, G. et al. Automated neuromelanin imaging as a diagnostic biomarker for parkinson's disease. *Movement Disorders*, v. 30, n. 7, p. 945–952, 2015.
- CASTELO-FERNÁNDEZ, C.; CALDERÓN-RUIZ, G. Automatic video summarization using the optimum-path forest unsupervised classifier. In: PARDO, A.; KITTLER, J. (Ed.). *Progress in Pattern Recognition, Image Analysis, Computer Vision, and Applications*. [S.l.]: Springer International Publishing, 2015, (Lecture Notes in Computer Science, v. 9423). p. 760–767. ISBN 978-3-319-25750-1.
- CHANG, C.-C.; LIN, C.-J. LIBSVM: A library for support vector machines. *ACM Transactions on Intelligent Systems and Technology*, ACM, New York, NY, USA, v. 2, n. 3, p. 1–27, 2011. ISSN 2157-6904.
- CHOMIAK, T. et al. A new quantitative method for evaluating freezing of gait and dual-attention task deficits in parkinson's disease. *Journal of Neural Transmission*, v. 122, n. 11, p. 1523–1531, 2015.
- CLARK, U. S.; NEARGARDER, S.; GOLOMB, A. C. Specific impairments in the recognition of emotional facial expressions in parkinson's disease. *Neuropsychologia*, v. 46, n. 9, p. 2300 – 2309, 2008.



- COHEN, M. J.; GLASPY, J. A.; PALMER, M. C. *UCLA Hematology/ Oncology Porter Ranch*. 2013. [Online; accessed 20-July-2016]. Disponível em: <<http://www.uclahealth.org/PRanchOncology>>.
- COMANICIU, D. An algorithm for data-driven bandwidth selection. *IEEE Transaction on Pattern Analysis and Machine Intelligence*, IEEE Computer Society, v. 25, n. 2, p. 281–288, 2003.
- CONNOLLY, A. T. et al. Guiding deep brain stimulation contact selection using local field potentials sensed by a chronically implanted device in parkinson’s disease patients. In: *7th International Conference on Neural Engineering*. [S.l.: s.n.], 2015. p. 840–843.
- COOK, D. J.; SCHMITTER-EDGECOMBE, M.; DAWADI, P. Analyzing activity behavior and movement in a naturalistic environment using smart home techniques. *IEEE Journal of Biomedical and Health Informatics*, v. 19, n. 6, p. 1882–1892, 2015.
- CORREA, C. F. *Número de Pessoas com Mal de Parkinson deve aumentar nos Próximos Anos*. 2016. [Jornal Estadão Online; accessed 24-Apr-2017]. Disponível em: <<http://vida-estilo.estadao.com.br/noticias/bem-estar,numero-de-pessoas-com-mal-de-parkinson-deve-aumentar-nos-proximos-anos,10000025586>>.
- CORTES, C.; VAPNIK, V. Support vector networks. *Machine Learning*, v. 20, p. 273–297, 1995.
- DAI, Y. et al. Detecting parkinson’s diseases via the characteristics of the intrinsic mode functions of filtered electromyograms. In: *IEEE 13th International Conference on Industrial Informatics*. [S.l.: s.n.], 2015. p. 1484–1487.
- DAS, R. A comparison of multiple classification methods for diagnosis of parkinson disease. *Expert Systems with Applications*, v. 37, n. 2, p. 1568 – 1572, 2010.
- DEFAZIO, G. et al. Assessment of voice and speech symptoms in early parkinson’s disease by the robertson dysarthria profile. *Neurological Sciences*, v. 37, n. 3, p. 443–449, 2015.
- DONG, Z. et al. Wireless body area sensor network for posture and gait monitoring of individuals with parkinson’s disease. In: *IEEE 12th International Conference on Networking, Sensing and Control*. [S.l.: s.n.], 2015. p. 81–86.
- DROTÁR, P. et al. Analysis of in-air movement in handwriting: A novel marker for parkinson’s disease. *Computer Methods and Programs in Biomedicine*, v. 117, n. 3, p. 405–411, 2014.
- DROTAR, P. et al. Contribution of different handwriting modalities to differential diagnosis of parkinson’s disease. In: *IEEE International Symposium Medical Measurements and Applications*. [S.l.: s.n.], 2015. p. 344–348.
- DUDA, P. E. H. R. O.; STORK, D. G. *Pattern Classification (2nd Edition)*. [S.l.]: Wiley-Interscience, 2000. ISBN 0471056693.
- EFTAXIAS, K. et al. Detection of parkinson’s tremor from emg signals; a singular spectrum analysis approach. In: *IEEE International Conference on Digital Signal Processing*. [S.l.: s.n.], 2015. p. 398–402.

- EICHHORN, T. E. et al. Computational analysis of open loop handwriting movements in parkinson's disease: A rapid method to detect dopamimetic effects. *Movement Disorders*, v. 11, n. 3, p. 289–297, 1996.
- EICHHORN, T. E. et al. Computational analysis of open loop handwriting movements in parkinson's disease: A rapid method to detect dopamimetic effects. *Movement Disorders*, Wiley Subscription Services, Inc., A Wiley Company, v. 11, n. 3, p. 289–297, 1996. ISSN 1531-8257. Disponível em: <<http://dx.doi.org/10.1002/mds.870110313>>.
- EKKER, M. S. et al. Neurorehabilitation for parkinson's disease: Future perspectives for behavioural adaptation. *Parkinsonism & Related Disorders*, v. 22, Supplement 1, p. S73–S77, 2016.
- ELLIS, R. J. et al. A validated smartphone-based assessment of gait and gait variability in parkinson's disease. *Public Library of Science One*, v. 10, n. 10, p. e0141694, 2015.
- FAHN, S. et al. Levodopa and the progression of parkinson's disease. *The New England journal of medicine*, v. 351, n. 24, p. 2498–2508, 2004. ISSN 0028-4793.
- FEIS, D. L. et al. Classification of symptom-side predominance in idiopathic parkinson's disease. *Nature Partner Journals Parkinson's Disease*, v. 1, p. 15018, 2015.
- FERREIRA, J. J. et al. Clinical parameters and tools for home-based assessment of parkinson's disease: Results from a delphi study. *Journal of Parkinson's Disease*, v. 5, n. 2, p. 281–290, 2015.
- FUNDATION, N. P. *The Parkinson's Foundation's Moving Day Walks Fund Local Parkinson's Programs in 2017*. 2017. <http://http://www.parkinson.org/>. [Online; accessed 08-Marc-2017]. Disponível em: <<http://www.parkinson.org/our-impact/press-room/press-releases/The-National-Parkinson-Foundations-Moving-Day-Walks-Fund-Local-Parkinsons-Programs-in-2017>>.
- FUNDATION, P. D. *Statistics on Parkinson's: Who Has Parkinson's?*
- GELDENHUYS, W. J. et al. A novel biomechanical analysis of gait changes in the MPTP mouse model of parkinson's disease. *PeerJ PeerJ Computer Science*, v. 3, p. e1175, 2015.
- GEMMERT, W. A. V.; TEULINGS, H. L.; STELMACH, G. E. Parkinsonian patients reduce their stroke size with increased processing demands. *Brain and Cognition*, Elsevier BV, v. 47, n. 3, p. 504–512, dec 2001.
- GHAREHCHOPOGH, F. S.; MOHAMMADI, P. Article: A case study of parkinsons disease diagnosis using artificial neural networks. *International Journal of Computer Applications*, v. 73, n. 19, p. 1–6, July 2013.
- GHAREHCHOPOGH, F. S.; MOHAMMADI, P. A case study of parkinsons disease diagnosis using artificial neural networks. *International Journal of Computer Applications*, v. 73, n. 19, p. 1–6, 2013.
- GILAT, M. et al. Brain activation underlying turning in parkinson's disease patients with and without freezing of gait: a virtual reality fMRI study. *Nature Partner Journals Parkinson's Disease*, v. 1, p. 15020, 2015.

- HALL, M. et al. The WEKA data mining software: An update. *ACM SIGKDD Explorations Newsletter*, v. 11, n. 1, p. 10–18, 2009.
- HALLER, S. et al. Individual detection of patients with parkinson disease using support vector machine analysis of diffusion tensor imaging data: initial results. *American Journal of Neuroradiology*, v. 33, n. 11, p. 2123–2128, 2012.
- HANDOJOSENO, A. M. A. et al. An eeg study of turning freeze in parkinson's disease patients: The alteration of brain dynamic on the motor and visual cortex. In: *IEEE 37th Annual International Conference of the Engineering in Medicine and Biology Society*. [S.l.: s.n.], 2015. p. 6618–6621.
- HARALICK, R. M.; SHANMUGAM, K. et al. Textural features for image classification. *IEEE Transactions on Systems, Man, and Cybernetics*, Ieee, n. 6, p. 610–621, 1973.
- HAREL, B.; CANNIZZARO, M.; SNYDER, P. J. Variability in fundamental frequency during speech in prodromal and incipient parkinson's disease: A longitudinal case study. *Brain and Cognition*, v. 6, n. 1, p. 24–29, 2004.
- HARIHARAN, M.; POLAT, K.; SINDHU, R. A new hybrid intelligent system for accurate detection of parkinson's disease. *Computer Methods and Programs in Biomedicine*, v. 113, n. 3, p. 904–913, 2014.
- HARMS, H. et al. Ethos: Miniature orientation sensor for wearable human motion analysis. In: *IEEE Sensors*. [S.l.: s.n.], 2010. p. 1037–1042.
- HARRIS, D. M. et al. Exergaming as a viable therapeutic tool to improve static and dynamic balance among older adults and people with idiopathic parkinson's disease: A systematic review and meta-analysis. *Frontiers in Aging Neuroscience*, v. 7, n. 167, p. 1–12, 2015.
- HEREMANS, E. et al. Amplitude manipulation evokes upper limb freezing during handwriting in patients with parkinson's disease with freezing of gait. *Public Library of Science One*, v. 10, n. 11, p. e0142874, 2015.
- HEWAVITHARANAGE, S. et al. Automatic segmentation of the rima glottidis in 4D laryngeal CT scans in parkinson's disease. In: *IEEE 37th Annual International Conference of the Engineering in Medicine and Biology Society*. [S.l.: s.n.], 2015. p. 739–742.
- HINTON, G. E. Training products of experts by minimizing contrastive divergence. *Neural Computation*, v. 14, n. 8, p. 1771–1800, 2002.
- HIRSCHAUER, T. J.; ADELI, H.; BUFORD, J. A. Computer-aided diagnosis of parkinson's disease using enhanced probabilistic neural network. *Journal of Medical Systems*, v. 39, n. 11, p. 1–12, 2015.
- HO, A. K. et al. Speech impairment in a large sample of patients with parkinson's disease. *Behavioural Neurology*, v. 3, n. 11, p. 131–137, 1998.
- IUPPARIELLO, L. et al. The effects of the vibratory stimulation of the neck muscles for the evaluation of stepping performance in parkinson's disease. In: *IEEE International Symposium on Medical Measurements and Applications*. [S.l.: s.n.], 2015. p. 606–609.

- IVKOVIC, V.; FISHER, S.; PALOSKI, W. H. Smartphone-based tactile cueing improves motor performance in parkinsons disease. *Parkinsonism & Related Disorders*, v. 22, p. 42 – 47, 2016.
- JELLISH, J. et al. A system for real-time feedback to improve gait and posture in parkinson's disease. *IEEE Journal of Biomedical and Health Informatics*, v. 19, n. 6, p. 1809–1819, 2015.
- JIA, Y. et al. Caffe: Convolutional architecture for fast feature embedding. *arXiv preprint arXiv:1408.5093*, 2014.
- KARAMINTZIOU, S. D. et al. Design of a novel closed-loop deep brain stimulation system for parkinson's disease and obsessive-compulsive disorder. In: *IEEE 7th International Conference on Neural Engineering*. [S.l.: s.n.], 2015. p. 860–863.
- KHOBRADE, N.; GRAUPE, D.; TUNINETTI, D. Towards fully automated closed-loop deep brain stimulation in parkinson's disease patients: A lamstar-based tremor predictor. In: *IEEE 37th Annual International Conference of the Engineering in Medicine and Biology Society*. [S.l.: s.n.], 2015. p. 2616–2619.
- KIM, H. et al. Unconstrained detection of freezing of gait in parkinson's disease patients using smartphone. In: *IEEE 37th Annual International Conference of the Engineering in Medicine and Biology Society*. [S.l.: s.n.], 2015. p. 3751–3754.
- KOSTIKIS, N. et al. A smartphone-based tool for assessing parkinsonian hand tremor. *IEEE Journal of Biomedical and Health Informatics*, v. 19, n. 6, p. 1835–1842, 2015.
- KRAEPELIEN, M. et al. Internet-based cognitive behavioral therapy for depression and anxiety in parkinson's disease. *Internet Interventions*, v. 2, n. 1, p. 1 – 6, 2016.
- LANCIONI, G. et al. Technology-aided leisure and communication: Opportunities for persons with advanced parkinson's disease. *Developmental Neurorehabilitation*, v. 0, n. 0, p. 1–7, 2015.
- LAROCHELLE, H.; BENGIO, Y. Classification using discriminative restricted boltzmann machines. In: *Proceedings of the 25th International Conference on Machine Learning*. [S.l.]: ACM, 2008. p. 536–543.
- LECUN, Y. et al. Backpropagation applied to handwritten zip code recognition. *Neural Computation*, MIT Press, Cambridge, MA, USA, v. 1, n. 4, p. 541–551, 1989.
- LEES, A. J.; HARDY, J.; REVESZ, T. Parkinson's disease. *The Lancet*, v. 373, n. 9680, p. 2055–2066, 2009.
- LI, B. et al. Automated segmentation and reconstruction of the subthalamic nucleus in parkinson's disease patients. *Neuromodulation: Technology at the Neural Interface*, v. 19, n. 1, p. 13–19, 2016.
- LITTLE, M. et al. Suitability of dysphonia measurements for telemonitoring of parkinson's disease. *Biomedical Engineering, IEEE Transactions on*, v. 56, n. 4, p. 1015–1022, April 2009.
- LOGEMANN, J. A. et al. Frequency and cooccurrence of vocal tract dysfunctions in the speech of a large sample of parkinson patients. *The Journal of Speech and Hearing Disorders*, Wiley, v. 43, n. 11, p. 47–57, 1978.

- LONES, M. A. et al. Evolving classifiers to recognize the movement characteristics of parkinson's disease patients. *IEEE Transactions on Evolutionary Computation*, v. 18, n. 4, p. 559–576, 2014.
- LONG, D. et al. Automatic classification of early parkinson's disease with multi-modal MR imaging. *PLoS ONE*, v. 7, n. 11, 2012.
- LORENZI, P. et al. Smart sensors for the recognition of specific human motion disorders in parkinson's disease. In: *IEEE 6th International Workshop on Advances in Sensors and Interfaces*. [S.l.: s.n.], 2015. p. 131–136.
- MAKI, B. E.; MCILROY, W. E. Change-in-support balance reactions in older persons: An emerging research area of clinical importance. *Neurologic Clinics*, Elsevier BV, v. 23, n. 3, p. 751–783, 2005.
- MANAP, H. H.; TAHIR, N. M.; YASSIN, A. I. M. Statistical analysis of parkinson disease gait classification using artificial neural network. In: *IEEE International Symposium on Signal Processing and Information Technology*. [S.l.: s.n.], 2011. p. 60–65.
- MARCHETTI, G. F.; WHITNEY, S. L. Older adults and balance dysfunction. *Neurologic Clinics*, Elsevier BV, v. 23, n. 3, p. 785–805, aug 2005.
- MAZILU, S. et al. Engineers meet clinicians: Augmenting parkinson's disease patients to gather information for gait rehabilitation. In: *Proceedings of the 4th Augmented Human International Conference*. [S.l.]: ACM, 2013. p. 124–127.
- MAZILU, S. et al. Engineers meet clinicians: Augmenting parkinson's disease patients to gather information for gait rehabilitation. In: *Proceedings of the 4th Augmented Human International Conference*. [S.l.: s.n.], 2013. p. 124–7.
- MAZILU, S.; BLANKE, U.; TRÖSTER, G. Gait, wrist, and sensors: Detecting freezing of gait in parkinson's disease from wrist movement. In: *IEEE International Conference on Pervasive Computing and Communication Workshops*. [S.l.: s.n.], 2015. p. 579–584.
- MAZILU, S. et al. Prediction of freezing of gait in parkinson's from physiological wearables: An exploratory study. *IEEE Journal of Biomedical and Health Informatics*, v. 19, n. 6, p. 1843–1854, 2015.
- MCCANDLESS, P. J. et al. Effect of three cueing devices for people with parkinson's disease with gait initiation difficulties. *Gait & Posture*, v. 44, p. 7 – 11, 2016,.
- MEKYSKA, J. et al. Assessing progress of parkinson's disease using acoustic analysis of phonation. In: *4th International Work Conference on Bioinspired Intelligence*. [S.l.: s.n.], 2015. p. 111–118.
- MEMEDI, M. et al. Validity and responsiveness of at-home touch screen assessments in advanced parkinson's disease. *IEEE Journal of Biomedical and Health Informatics*, v. 19, n. 6, p. 1829–1834, 2015.
- MEMEDI, M. et al. A web application for follow-up of results from a mobile device test battery for parkinson's disease patients. *Computer Methods and Programs in Biomedicine*, Elsevier, v. 104, n. 2, p. 219–226, 2011.

- MOHAMMED, A. et al. Patient specific parkinson's disease detection for adaptive deep brain stimulation. In: *IEEE 37th Annual International Conference of the Engineering in Medicine and Biology Society*. [S.l.: s.n.], 2015. p. 1528–1531.
- NAVAILLES, S. et al. Multisite intracerebral microdialysis to study the mechanism of l-dopa induced dopamine and serotonin release in the parkinsonian brain. *ACS Chemical Neuroscience*, v. 4, n. 5, p. 680–692, 2013.
- NAVARRO, G. P.; MAGARIÑO, I. G.; LORENTE, P. R. A kinect-based system for lower limb rehabilitation in parkinson's disease patients: a pilot study. *Journal of Medical Systems*, v. 39, n. 9, p. 1–10, 2015.
- OJALA, T.; PIETIKÄINEN, M.; HARWOOD, D. A comparative study of texture measures with classification based on featured distributions. *Pattern Recognition*, Elsevier, v. 29, n. 1, p. 51–59, 1996.
- OLSZEWSKI, M. E. et al. Quantitative measurements in geometrically correct representations of coronary vessels in 3-d and 4-d. In: *Proceedings of 4th IEEE Southwest Symposium Image Analysis and Interpretation*. [S.l.: s.n.], 2000. p. 259–263.
- OTSU, N. A threshold selection method from gray-level histograms. *IEEE Transactions on Systems, Man, and Cybernetics*, v. 9, n. 1, p. 62–66, 1979.
- OUNG, Q. W. et al. Technologies for assessment of motor disorders in parkinson's disease: A review. *Sensors*, v. 19, n. 9, p. 21710–21745, Aug 2015.
- PAN, S. et al. Parkinsons disease tremor classification, a comparison between support vector machines and neural networks. *Expert Systems with Applications*, v. 39, n. 12, p. 10764 – 10771, 2012.
- PAN, S. et al. Parkinson's disease tremor classification, a comparison between support vector machines and neural networks. *Expert Systems with Applications*, v. 39, n. 12, p. 10764–10771, 2012.
- PAPA, J. P. et al. Efficient supervised optimum-path forest classification for large datasets. *Pattern Recognition*, Elsevier Science Inc., v. 45, n. 1, p. 512–520, 2012.
- PAPA, J. P.; FALCÃO, A. X.; SUZUKI, C. T. N. Supervised pattern classification based on optimum-path forest. *International Journal of Imaging Systems and Technology*, v. 19, n. 2, p. 120–131, 2009.
- PAPA, J. P.; SUZUKI, C. T. N.; X, A. LibOPF: A library for the design of optimum-path forest classifiers. Software version 2.1 available at <http://www.ic.unicamp.br/~afalcao/libopf/index.html>. 2014.
- PAREDES, J. D. A. et al. A reliability assessment software using kinect to complement the clinical evaluation of parkinson's disease. In: *IEEE 37th Annual International Conference of the Engineering in Medicine and Biology Society*. [S.l.: s.n.], 2015. p. 6860–6863.
- PARKINSON, J. An essay on the shaking palsy. *Journal of Neuropsychiatry and Clinical Neuroscience*, v. 20, n. 4, p. 223–236, 1817.

- PARKINSON, J. An essay on the shaking palsy. *Journal of Neuropsychiatry and Clinical Neuroscience*, v. 20, n. 4, p. 223–236, 1817.
- PASLUOSTA, C. F. et al. An emerging era in the management of parkinson's disease: Wearable technologies and the internet of things. *IEEE Journal of Biomedical and Health Informatics*, p. 1873–1881, 2015.
- PEDREGOSA, F. et al. Scikit-learn: Machine learning in Python. *Journal of Machine Learning Research*, v. 12, p. 2825–2830, 2011.
- PEKER, M.; SEN, B.; DELEN, D. Computer-aided diagnosis of parkinson's disease using complex-valued neural networks and mrmr feature selection algorithm. *Journal of Healthcare Engineering*, v. 6, n. 3, p. 281–302, 2015.
- PEREIRA, C. R. et al. Parkinson's disease identification using restricted boltzmann machines. In: *17th international Conference on Computer Analysis of Images and Patterns*. [S.l.: s.n.], 2017. (accepted for publication).
- PEREIRA, C. R. et al. A new computer vision-based approach to aid the diagnosis of parkinson's disease. *Computer Methods and Programs in Biomedicine*, Elsevier North-Holland, Inc., New York, NY, USA, v. 136, p. 79–88, 2016.
- PEREIRA, C. R. et al. A step towards the automated diagnosis of parkinson's disease: Analyzing handwriting movements. In: *IEEE 28th International Symposium on Computer-Based Medical Systems*. [S.l.: s.n.], 2015. p. 171–176.
- PEREIRA, C. R. et al. A new computer vision-based approach to aid the diagnosis of parkinson's disease. *Computer Methods and Programs in Biomedicine*, 2016.
- PEREIRA, C. R. et al. Deep learning-aided parkinson's disease diagnosis from handwritten dynamics. In: *2016 29th SIBGRAPI Conference on Graphics, Patterns and Images (SIBGRAPI)*. [S.l.: s.n.], 2016. p. 340–346.
- PEREIRA, C. R. et al. Deep learning-aided parkinson's disease diagnosis from handwritten dynamics. In: *Proceedings of the 29th SIBGRAPI Conference on Graphics, Patterns and Images*. [S.l.: s.n.], 2016. p. 340–346.
- PEREIRA, J. C. et al. Residual signal auto-correlation to evaluate speech in Parkinson's disease patients. *Arquivos de Neuro-Psiquiatria*, Scielo, v. 64, n. 4, p. 912–915, 2006.
- PEUEKER, D.; SCHARFENBERG, G.; HOOK, C. Feature selection for the detection of fine motor movement disorders in parkinsons patients. In: *Advanced Research Conference 2011*. [S.l.: s.n.], 2011.
- PEUKER, D.; SCHARFENBERG, G.; HOOK, C. Feature selection for the detection of fine motor movement disorders in parkinson's patients. In: *Advanced Research Conference*. [S.l.]: Shaker Verlag, 2011. (ARC '11).
- PIELLA, G. A general framework for multiresolution image fusion: from pixels to regions. *Information Fusion*, v. 4, n. 4, p. 259–280, 2003.

- PRASHANTH, R. et al. High accuracy classification of parkinson's disease through shape analysis and surface fitting in 123i-ioflupane SPECT imaging. *IEEE Journal of Biomedical and Health Informatics*, PP, n. 99, p. 1–1, 2016.
- PROCHÁZKA, A. et al. Bayesian classification and analysis of gait disorders using image and depth sensors of microsoft kinect. *Digital Signal Processing*, v. 47, p. 169 – 177, 2015.
- QIANG, J. K.; MARRAS, C. Telemedicine in parkinson's disease: A patient perspective at a tertiary care centre. *Parkinsonism & Related Disorders*, v. 21, n. 5, p. 525 – 528, 2015.
- REINFELDER, S. et al. Timed up-and-go phase segmentation in parkinson's disease patients using unobtrusive inertial sensors. In: *IEEE 37th Annual International Conference of the Engineering in Medicine and Biology Society*. [S.l.: s.n.], 2015. p. 5171–5174.
- RESTREPO-AGUDELO, S.; ROLDÁN-VASCO, S. Time domain reconstruction of basal ganglia signals in patient with parkinson's disease. In: *20th Symposium on Signal Processing, Images and Computer Vision*. [S.l.: s.n.], 2015. p. 1–5.
- ROCHA, A. P. et al. Kinect v2 based system for parkinson's disease assessment. In: *IEEE 37th Annual International Conference of the Engineering in Medicine and Biology Society*. [S.l.: s.n.], 2015. p. 1279–1282.
- ROCHA, L. M.; CAPPABIANCO, F. A. M.; FALCÃO, A. X. Data clustering as an optimum-path forest problem with applications in image analysis. *International Journal of Imaging Systems and Technology*, Wiley Periodicals, v. 19, n. 2, p. 50–68, 2009.
- ROSENBLUM, S. et al. Handwriting as an objective tool for parkinson's disease diagnosis. *Journal of Neurology*, Springer Berlin Heidelberg, v. 260, n. 9, p. 2357–2361, 2013.
- ROSS, A. A.; JAIN, A. Information fusion in biometrics. *Pattern Recogn. Lett.*, Elsevier Science Inc., v. 24, n. 13, p. 2115–2125, set. 2003.
- RUONALA, V. et al. Autonomic nervous system response to l-dopa in patients with advanced parkinson's disease. In: *IEEE 37th Annual International Conference of the Engineering in Medicine and Biology Society*. [S.l.: s.n.], 2015. p. 6162–6165.
- SAKAR, B. E. et al. Collection and analysis of a parkinson speech dataset with multiple types of sound recordings. *IEEE Journal of Biomedical and Health Informatics*, IEEE, v. 17, p. 828–834, 2013.
- SANCHES, I. J. et al. Fusão 3d de imagens de mri/ct e termografia. *Brazilian Journal of Biomedical Engineering*, v. 29, n. 3, p. 298 – 308, 2013.
- SEGOVIA, F. et al. Parkinson's disease from atypical parkinsonian syndromes using pet data and a computer system based on support vector machines and bayesian networks. *Frontiers in Computational Neuroscience*, v. 9, n. 137, p. 1 – 8, 2015.
- SHAHBAKHI, M.; FAR, D. T.; TAHAMI, E. Speech analysis for diagnosis of parkinson's disease using genetic algorithm and support vector machine. *Journal of Biomedical Science and Engineering*, v. 07, n. 04, p. 147–156, 2014.



- SHAMIR, R. R. et al. Machine learning approach to optimizing combined stimulation and medication therapies for parkinson's disease. *Brain Stimulation*, v. 8, n. 6, p. 1025 – 1032, 2015.
- SHAO, X. et al. It is never too late: Using a computer program to treat hand contractures associated with parkinson's disease. *European Geriatric Medicine*, v. 15, n. 3, p. 153–155, 2016.
- SHI, J.; MALIK, J. Normalized cuts and image segmentation. *IEEE Transactions on Pattern Analysis and Machine Intelligence*, IEEE Computer Society, v. 22, n. 8, p. 888–905, Aug 2000.
- SINGH, G.; SAMAVEDHAM, L. Algorithm for image-based biomarker detection for differential diagnosis of parkinson's disease. *International Federation of Automatic Control - PapersOnLine*, v. 48, n. 8, p. 918 – 923, 2015.
- SINGH, G.; SAMAVEDHAM, L. Unsupervised learning based feature extraction for differential diagnosis of neurodegenerative diseases: A case study on early-stage diagnosis of parkinson disease. *Journal of Neuroscience Methods*, v. 256, p. 30 – 40, 2015.
- SMEKAL, Z. et al. Analysis of phonation in patients with parkinson's disease using empirical mode decomposition. In: *International Symposium on Signals, Circuits and Systems*. [S.l.: s.n.], 2015. p. 1–4.
- SMITH, S. L. et al. Computational approaches for understanding the diagnosis and treatment of parkinson's disease. *Institution of Engineering and Technology Systems Biology*, v. 9, n. 6, p. 226–233(7), 2015.
- SPADOTTO, A. A. et al. Improving parkinson's disease identification through evolutionary-based feature selection. In: *IEEE International Conference of the Engineering in Medicine and Biology Society*. [S.l.: s.n.], 2011. p. 7857–7860.
- SPADOTTO, A. A. et al. Improving parkinson's disease identification through evolutionary-based feature selection. In: *International Conference of the IEEE Engineering in Medicine and Biology Society*. [S.l.: s.n.], 2010. p. 7857–7860.
- SPADOTTO, A. A. et al. Parkinson's disease identification through optimum-path forest. In: *IEEE International Conference of the Engineering in Medicine and Biology Society*. [S.l.: s.n.], 2010. p. 6087–6090.
- SPADOTTO, A. A. et al. Parkinson's disease identification through optimum-path forest. In: *International Conference of the IEEE Engineering in Medicine and Biology Society*. [S.l.: s.n.], 2010. p. 6087–6090.
- STAMFORD, J. A.; SCHMIDT, P. N.; FRIEDL, K. E. What engineering technology could do for quality of life in parkinson's disease: A review of current needs and opportunities. *IEEE Journal of Biomedical and Health Informatics*, v. 19, n. 6, p. 1862–1872, 2015.
- SU, M.; CHUANG, K. S. Dynamic feature selection for detecting parkinson's disease through voice signal. In: *IEEE International Microwave Workshop Series on RF and Wireless Technologies for Biomedical and Healthcare Applications*. [S.l.: s.n.], 2015. p. 148–149.
- SUZUKI, A. et al. Disgust-specific impairment of facial expression recognition in parkinson's disease. *Brain*, v. 129, n. 3, p. 707–717, 2006.

- SZYMANSKI, A. et al. Data mining using spect can predict neurological symptom development in parkinson's patients. In: *IEEE 2nd International Conference in Cybernetics*. [S.l.: s.n.], 2015. p. 218–223.
- TAY, A. et al. Freezing of gait (FoG) detection for parkinson disease. In: *10th Asian Control Conference*. [S.l.: s.n.], 2015. p. 1–6.
- TEAM REGENSBURG, G. University of A. S. *A Novel Multisensoric System Recording and Analyzing Human Biometric Features for Biometric and Biomedical Applications*. 2002. Disponível em: <<http://www.bisp-regensburg.de/references.html>>.
- THANAWATTANO, C. et al. Temporal fluctuation analysis of tremor signal in parkinson's disease and essential tremor subjects. In: *IEEE 37th Annual International Conference of the Engineering in Medicine and Biology Society*. [S.l.: s.n.], 2015. p. 6054–6057.
- TRISTER, A. D.; DORSEY, E. R.; FRIEND, S. H. Smartphones as new tools in the management and understanding of parkinson's disease. *Npj Parkinson's Disease*, Parkinson's Disease Foundation/Macmillan Publishers Limited SN -, v. 2, p. 16006 EP, 2016.
- TROJANIELLO, D. et al. Comparative assessment of different methods for the estimation of gait temporal parameters using a single inertial sensor: application to elderly, post-stroke, parkinson's disease and huntington's disease subjects. *Gait & Posture*, v. 42, n. 3, p. 310 – 316, 2015.
- TSANAS, A. et al. Novel speech signal processing algorithms for high-accuracy classification of parkinson's disease. *IEEE Transactions on Biomedical Engineering*, v. 59, n. 5, p. 1264–1271, 2012.
- TUCKER, C. S. et al. Machine learning classification of medication adherence in patients with movement disorders using non-wearable sensors. *Computers in Biology and Medicine*, v. 66, p. 120–134, 2015.
- ÜNLÜ, A.; BRAUSE, R.; KRAKOW, K. Handwriting analysis for diagnosis and prognosis of parkinson's disease. In: *Proceedings of the 7th International Conference on Biological and Medical Data Analysis*. [S.l.]: Springer-Verlag, 2006. p. 441–450.
- VILLA-CAÑAS, T. et al. Time-frequency approach in continuous speech for detection of parkinson's disease. In: *20th Symposium on Signal Processing, Images and Computer Vision*. [S.l.: s.n.], 2015. p. 1–6.
- VOLPE, D. et al. Under water gait analysis in parkinson's disease. *Gait & Posture*, v. 2, p. S8, 2016.
- WABNEGGER, A. et al. Facial emotion recognition in parkinson's disease: An fMRI investigation. *Public Library of Science One*, v. 10, n. 8, p. 1–9, 2015.
- WAECHTER, S. M. et al. The impact of dual tasking on cognitive performance in a parkinson's disease cohort with and without freezing of gait: An eeg and behavioral based approach. In: *IEEE 7th International Conference on Neural Engineering*. [S.l.: s.n.], 2015. p. 1072–1075.
- WAHID, F. et al. Classification of parkinson's disease gait using spatial-temporal gait features. *IEEE Journal of Biomedical and Health Informatics*, v. 19, n. 6, p. 1794–1802, 2015.

- WANG, J. et al. Bag-of-words representation for biomedical time series classification. *Biomedical Signal Processing and Control*, v. 8, n. 6, p. 634 – 644, 2013. ISSN 1746-8094. Disponível em: <<http://www.sciencedirect.com/science/article/pii/S174680941300089X>>.
- WATTERS, P.; PATEL, M. A neural network model of semantic processing errors in parkinsons disease. *Neural Processing Letters*, v. 9, n. 2, p. 189–199, 1999.
- WEBER, S. A. T. et al. Classification of handwriting patterns in patients with parkinson's disease, using a biometric sensor. *Global Advanced Research Journal of Medicine and Medical Sciences*, v. 11, n. 3, p. 362–366, 2014.
- WESTIN, J. et al. A home environment test battery for status assessment in patients with advanced parkinson's disease. *Computer Methods and Programs in Biomedicine*, Elsevier, v. 98, n. 1, p. 27–35, 2010.
- WILCOXON, F. Individual comparisons by ranking methods. *Biometrics Bulletin*, v. 1, n. 6, p. 80–83, 1945.
- WILCOXON, F. Individual comparisons by ranking methods. *Biometrics Bulletin*, v. 1, n. 6, p. 80–83, 1945.
- WU, D. et al. Prediction of parkinson's disease tremor onset using radial basis function neural networks. *Expert Systems with Applications*, Pergamon Press, Inc., v. 37, n. 4, p. 2923–2928, 2010.
- WU, Y. et al. Forward autoregressive modeling for stride process analysis in patients with idiopathic parkinson's disease. In: *IEEE International Symposium on Medical Measurements and Applications*. [S.l.: s.n.], 2015. p. 349–352.
- YADAV, G.; KUMAR, Y.; SAHOO, G. Predication of parkinson's disease using data mining methods: A comparative analysis of tree, statistical, and support vector machine classifiers. *Indian Journal of Medical Sciences*, p. 231–242, 2011.
- YANG, W. C. et al. Home-based virtual reality balance training and conventional balance training in parkinson's disease: A randomized controlled trial. *Journal of the Formosan Medical Association*, p. –, 2015.
- YANG, W. C. et al. Home-based virtual reality balance training and conventional balance training in parkinson's disease: A randomized controlled trial. *Journal of the Formosan Medical Association*, p. –, 2016.
- YONEYAMA, M. et al. Ambulatory gait behavior in patients with dementia: A comparison with parkinson's disease. *IEEE Transactions on Neural Systems and Rehabilitation Engineering*, PP, n. 99, p. 1–1, 2015.
- ZHANG, L. et al. Cortical thinning and cognitive impairment in parkinson's disease without dementia. *IEEE Transactions on Computational Biology and Bioinformatics*, p. 1–1, 2015.
- ZHANG, T. Y.; SUEN, C. Y. A fast parallel algorithm for thinning digital patterns. *Commun. ACM*, ACM, New York, NY, USA, v. 27, n. 3, p. 236–239, mar. 1984. ISSN 0001-0782. Disponível em: <<http://doi.acm.org/10.1145/357994.358023>>.

ZHAO, S. et al. Automatic detection of expressed emotion in parkinson's disease. In: *IEEE International Conference on Acoustics, Speech and Signal Processing*. [S.l.: s.n.], 2014. p. 4813–4817.

ZHAO, Y. et al. E-health support in people with parkinson's disease with smart glasses: A survey of user requirements and expectations in the netherlands. *Journal of Parkinson's Disease*, v. 5, n. 2, p. 369–378, 2015.

ZHAO, Y. J. et al. Factors affecting health-related quality of life amongst asian patients with parkinson's disease. *European Journal of Neurology*, Wiley-Blackwell, v. 15, n. 7, p. 737–742, jul 2008.

ZHU, Y.-M.; COCHOFF, S. An object-oriented framework for medical image registration, fusion, and visualization. *Computer Methods and Programs in Biomedicine*, v. 82, n. 3, p. 258–267, 2006.